Novel Flexible Device Platforms Using Electrospinning Process For Sensor And Nanogenerator Applications

A Thesis Submitted to the AcSIR for the Award the Degree of

DOCTOR OF PHILOSOPHY
In
PHYSICAL SCIENCES

By

Dipti Dhakras

Registration Number: 10PP12A26081

Under the guidance of

Dr. Satishchandra Ogale

(Research Supervisor)

CSIR-NATIONAL CHEMICAL LABORATORY
PUNE – 411 008, INDIA

Certificate

This is to certify that the work incorporated in this Ph.D. thesis entitled **"Novel Flexible Device Platforms using Electrospinning Process for Sensor and Nanogenerator Applications** submitted by **Ms. Dipti Dhakras** to Academy of Scientific and Innovative Research (AcSIR) in fulfillment of the requirements for the award of the Degree of **Doctor of Philosophy in Physical Sciences,** embodies original research work under my supervision. I further certify that this work has not been submitted to any other University or Institution in part or full for the award of any degree or diploma. Research material obtained from other sources has been duly acknowledged in the thesis. Any text, illustration, table etc., used in the thesis from other sources, have been duly cited and acknowledged.

Research Student **Supervisor**

Dipti Dhakras Dr. Satishchandra Ogale

Declaration

I hereby declare that the thesis entitled **"Novel Flexible Device Platform using Electrospinning Process for Sensor and Nanogenerator Applications"** submitted for the degree **Doctor of Philosophy** in Physical Sciences to the Academy of Scientific & Innovative Research (AcSIR), has been carried out by me at the Physical and Materials Chemistry Division of National Chemical Laboratory, Pune under the guidance of **Dr. Satishchandra B. Ogale**. Such material which has been obtained by other sources has been duly acknowledged in this thesis. The work is original and has not been submitted in part or full by me for any other degree or diploma to other University.

Date: 10th August 2015 **Dipti Dhakras**

National Chemical Laboratory, (Research Student)

Pune - 411008


Dedicated to my family, friends and teachers.....

Acknowledgements

There are so many people around without whose support it is impossible to accomplish this major achievement in my life. I take this opportunity to express my deepest gratitude towards all those who have been part of this memorable journey, directly or indirectly, to make this thesis possible.

First and foremost I would like to express my gratitude to my research advisor Dr. Satishchandra Ogale. It has been a privilege to work under his able guidance and dynamic laboratory environment. He has always been a constant source of motivation and enthusiasm. He always gave me the opportunity to explore and venture into whatever I wanted to learn. He has not only nurtured my scientific and presentation skills, but also changed me to become a better human being. I am grateful to him for his critical comments, keen observations and endless support with patience during my whole tenure of PhD.

I would also like to thank Dr. Mrs. Jyoti Jog for giving me the opportunity to work in NCL. I greatly appreciate the insights she provided in various studies, particularly in the areas of polymers and their nanocomposites. I wish to express my heartfelt gratitude to her for her warm and friendly support throughout this journey.

I am grateful to Dr. Sarika Bhattacharya for accepting co-guide ship for my research work.

I would like to acknowledge various funding agencies, namely the Department of Science and Technology (DST), the Department of Information Technology (DeitY), and Council of Scientific & Industrial Research (CSIR) for research fellowships.

I wish to thank Dr. S. Sivaram, (former Director of CSIR-NCL), Dr. Saurav Pal, (former Director CSIR-NCL), Dr. Vijayamohanan Pillai (Director, NCL), Dr. Anil Kumar, HOD, Physical and Materials Chemistry Division, and the former as well as current HODs of the Polymer Science Division for the opportunity to work at CSIR-NCL and providing the infrastructure and research facilities. I sincerely thank my Doctoral Advisory Committee

(DAC) members, Dr. P.P.Wadgaonkar, Dr.Suresh Bhat and Dr.C.P.Vinod for their timely discussions, guidance, and evaluations during my course work.

The technical and non-technical staff of the Polymer Science and Engineering and Physical Materials Chemistry divisions has also been very helpful.

I take this opportunity to thank Dr. S. I. Patil, Head, Department of Physics, University of Pune for his scientific and administrative inputs and Dr. S. N. Kale, DIAT for her valuable scientific evaluations. Thanks also are due to Dr. H.H. Kumar, ARDE, Pune for providing research facilities and the scientific discussions, and Mr. Vivek Borkar and Mr.Swapnil for the technical support and useful discussions throughout this journey.

I wish to further express my thanks to Dr. Krishnamoorthy and Dr. Manjusha Shelke for their timely advice and help. My very sincere thanks are also due to the SAO office staff along with Dr.C.G.Suresh (former DAC chairman), Dr.C.J.Gadgil (DAC chairman), Mrs. Puranik, Mrs. Kolhe and Ms. Deepa for the help and co-operation throughout this period. I also greatly admire the efficiency of the Deans of AcSIR (headquarters) and their staff.

I would like to acknowledge my senior colleagues Dr. Rajesh Hyam, Dr. Tushar Jagdale, Dr.Anup Kale, Dr. Tushar Jagdale, Dr. Abhimanyu Rana, Dr.Vivek Dhas, Dr.Subas Muduli, Dr.Prasad Yadav Dr.Parvez, Dr.Mandakini, Dr.Lily, Dr.Datta, Dr.Meenal, Dr.Shruti, Dr.Abhik, Dr.Rohan, Dr.Onkar, Dr. Sarika Phadke, Anil, Aniruddha, Dhanya, Pradeep, Vishal, Satish, Satywan, Yogesh, Wahid, Umesh, Sambhaji, Nilima, Supriya, Sharddha, Mukta, Divya, Pooja, Poonam, Srashti, Ishita, Swati for their support and for creating a wonderful laboratory environment. They all have been very helpful and friendly.

I take this opportunity to thank all my teachers from my primary school till my Master's degree for imbibing good values and knowledge in me.

I wholeheartedly thank my family Aai, Baba, Kaka and Kaku (my in-laws) for their unconditional love, constant support and for allowing me to pursue my ambitions. My extended family and late grandparents have supported me with constant inspiration and blessings. I would like to take this opportunity to thank my brother Nilesh, my sister-in-law Prajakta for their love and affection. I would like thank my school and college friends –

Bhairavi, Bhargavi, Shweta and Tina for always being there for supporting and motivating me.

Lastly countless thanks to my better half, Rounak for the care, support and understanding throughout this journey. He gave me the strength and motivation in all kinds of situations. It would not have been possible to fulfill this dream without his trust and belief in me.

And finally I thank the almighty God for being with me all the way.

Dipti Dhakras

List of Abbreviations

AC	Alternating Current
AFM	Atomic force Microscopy
$BaTiO_3$	Barium Titanate
CB	Conduction Band
DC	Direct Current
DEA	Dielectric analysis
DMA	Dynamic Mechanical Analyser
ES	Electrospinning
ITO	Indium doped Tin Oxide
Jsc	Short circuit current
FET	Field Effect Transistor
FTIR	Fourier Transform Infrared Spectroscopy
LED	Light Emitting Diode
LING	Laterally Integrated nanogenerator
MEMS	Microelectromechanical systems
NEMS	Nanoelectromechanical systems
NEG	Nanocomposite electric generator
$NiCl_2.6H_2O$	Nickel chloride hexahydrate
NF	Nanofibers
NG	Nanogenerator

PAN	Polyacrylonitrile
PANI	Polyaniline
PCB	Printed Circuit Board
PDMS	Poly di-methyl siloxane
PE	Polarization Vs Electric field
PENG	Piezoelectric nanogenerator
PMN-PT	Lead magnesium niobate-lead titanate
PTFE	Polytetrafluoroethylene
PVC	Polyvinyl Chloride
PVP	Polyvinylpyrrolidone
PVDF	Polyvinylidene difluoride
P(VDF-TrFE)	Polyvinylidene Trifluoroethylene
PZT	Lead Zirconate Titanate
0D	Zero dimensional
1D	One dimensional
2D	Two dimensional
3D	Three dimensional
SEM	Scanning Electron Microscopy
SBH	Schottky Barrier Height
TENG	Triboelectric Nanogenerator
TEM	Transmission Electron Microscopy
Tg	Glass transition temperature
TIP	Titanium tetra isopropoxide

VING	Vertically integrated nanogenerator
VB	Valence Band
Voc	Open circuit voltage
WAXS	Wide angle X-ray scattering
XRD	X-ray Diffraction

Content

Section II

Section III

Abstract

Currently there is considerable research emphasis on the development of innovative, flexible or wearable device concepts in view of their portability; light weight, shock resistance, and low cost. It is further desirable that such flexible device platforms are self-powered (mechanically) or solar-powered eliminating the need for a battery or related wiring. Piezoelectric materials, which can generate electrical power locally through stress or flexing, are a great proposition in this regard. The present thesis deals with topics in this domain of interesting research. Nanomaterials based pressure and strain sensor technology is now rapidly evolving area of research, and through the related development of piezoelectric nanogenerators it has found a synergistic connection with the field of energy harvesting, a topic of great importance at this time. For the development of the self-powered nanosystems, the search for new materials within expensive processing methodologies needs to be implemented. The present work is an attempt in this direction.

A brief explanation of the methodologies used is given below in each chapter.

In the first chapter, we have discussed the effect of the addition of a hydrated salt, nickel chloride hexahydrate ($NiCl_2.6H_2O$), in a tiny amount, on the phase formation and stabilization in the PVDF system. Addition of the hydrated salt (NC) is found to enhance the desirable polar β phase by about 30%. The peak to peak piezo-voltage generated for the salted PVDF-NC material is almost 0.762 V, a factor of 3 higher than that for normal PVDF. The fiber mats exhibit a significantly enhanced dynamic strain sensor response. The voltage generated per unit micro-strain developed during the free vibration test for PVDF was 0.119 mV whereas it was 0.548 mV for PVDF NC, exhibiting a non-linearly enhanced performance vis a vis the increase in the β phase component. The power generated was also used for lighting the commercial red LED (3 mm) was lit up.

In the second chapter, we have reported the demonstration of an interesting all-organic device design comprising an electrospun P(VDF-TrFE)fiber-mat built directly on a conducting PANI film, which is also grown on a flexible PET substrate, for flexural

piezo-FET and nanogenerator applications. Orders of magnitude stronger modulation of electrical transport in PANI film is realized in this device as compared to the case of a similar device but with a uniform spin-coated P(VDF-TrFE) film. We find that in the flexural mode of operation, the interaction between the laterally modulated nanoscale strain field distributions created by the fibers and the applied coherent strain field strongly influences the carrier transport in PANI. The transport modulation is suggested to occur due to strain-induced conformational changes in P(VDF-TrFE) leading to changes in carrier localization–delocalization. We further show that the fiber-mat based device system also works as an efficient nanogenerator capable of delivering power for low power applications.

In the third chapter, we present a novel robust and durable, all-fiber nanogenerator for stretchable and wearable applications. The nanogenerator comprises of P(VDF-TrFE) nanofiber non-woven mat as piezoelectric material, directly electrospun on a conducting carbon based fabric electrode, synthesized by high temperature pyrolysis route. The intermittent porosity within the fibrous mat is later filled with another piezo-ferroelectric material i.e. $BaTiO_3$ (NF+NP mixture) which is uniformly coated onto P(VDF-TrFE) mat as room temperature paste. The device is further sealed using PDMS for the protection from dust and water etc. The hybrid device structure of [P(VDF-TrFE) + 80% BTO NF:20%BTO NP] is seen to consistently produce a peak open-circuit voltage of 6V and a peak current of 4.5μA with power density of $12\mu Wcm^{-2}$ at the applied impacts of 0.02 MPa, nearly five times higher than existing 2D structures. We further made the in-situ composites of PVDF-TrFE/BTO-NF/NP for analyzing internal confinement effect of additional interfaces to produce strong interfacial polarization. The device with 5wt% of composite structure produces highest power output of $22\mu Wcm^{-2.}$ The power generated from the device can be used to turn on the charging process of smart phone.

Chapter 1

Introduction

This present chapter commences with an overview of the current international status of energy research and the related technological advances. A discussion about the current and growing energy needs, availability of different energy resources, and future challenges in respect of clean and sustainable energy solutions is included. A comparison of the current rate of consumption of renewable and non-renewable sources is also incorporated and consequently the necessity for developing new, renewable and green energy harvesting systems is highlighted. Since this thesis primarily addresses issues related to mechanical energy various types of such mechanical energy sources are also discussed and emphasized. Towards this end the concept of Nanogenerators is introduced, which works primarily on the principle of piezoelectricity. Subsequently, the nanostructures suitable for these applications and their advantages-disadvantages are discussed. A concise review of self-powered nanosystems and the related fields such as piezotronics and piezo-phototronics is also presented. Finally, a brief discussion on the recent advances in the field of the small scale and large scale applications of mechanical energy harvesting systems is included. The chapter is concluded with the presentation of the objectives and scope of the current thesis research.

1.1 Energy: The New Research Frontier

The world energy demands have grown severely in the past few decades due to rapid developments around the globe for betterment of our lives and related technological advances. The energy consumption has increased by 39% for developed countries whereas for developing countries like India and China it has increased by 91% and 146%, respectively, particularly due to several nation building developments. Unfortunately, the pace of total energy availability does not match the demand. The figure1.1 shows the increasing energy demand in the near future. Clearly, the need for renewable energy sources and hydro power based sources will rapidly increase up to 2035. Although the dependence on coal sector, gas sector, and oil sector will grow marginally the reservoirs of such sources are rapidly depleting due to the increase in global population, urbanization and industrialization. These are polluting fuels and are hazardous to the environment.

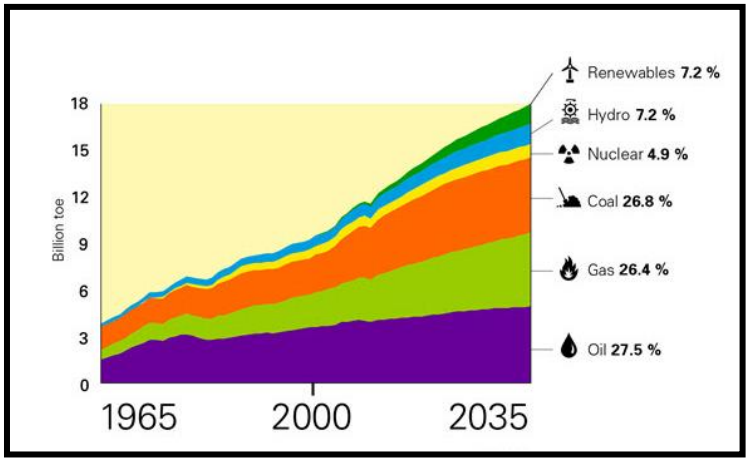

Figure: 1.1 Energy consumption and needs

http://www.bp.com/en/global/corporate/press/speeches/international-petroleum-week-2014.html

Energy sector is the main parameter controlling the global socio-economic growth. [1] Over the years every aspect of human life has been restructured by technology starting from industrial growth to medicinal diagnostics. The sector-

wise consumption of energy analysis shows that most of the energy consumption is mainly in the industrial sector which is followed by the transport sector. The domestic sector occupies 22% of total energy which mainly emphasizes on rapid urbanization as well as technology dependence of the modern living. [2]

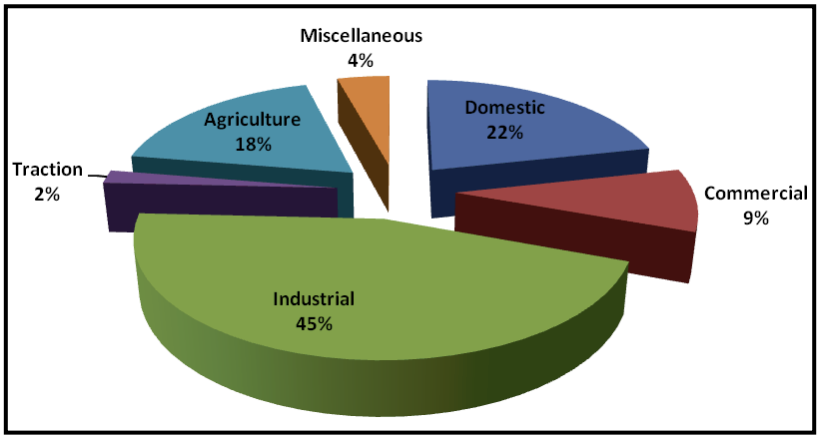

Figure: 1.2 Sector wise distribution of energy

https://electricalmania.wordpress.com/category/scenario-of-power-sector-in-india/

1.2 Energy needs for the modern world

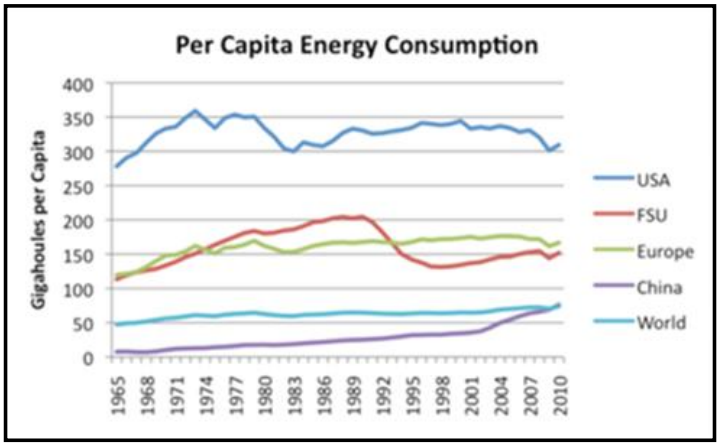

Figure: 1.3: Per capita energy consumption

http://ourfiniteworld.com/2012/03/12/world-energy-consumption-since-1820-in-charts/

The worldwide consumption of the available energy sources is also uneven. As can be seen from the per capita consumption, the USA with 4.8% of the overall world's population consumes about 21% of the energy, whereas India with 16% of the total population uses only 3.5 % of energy. [3]

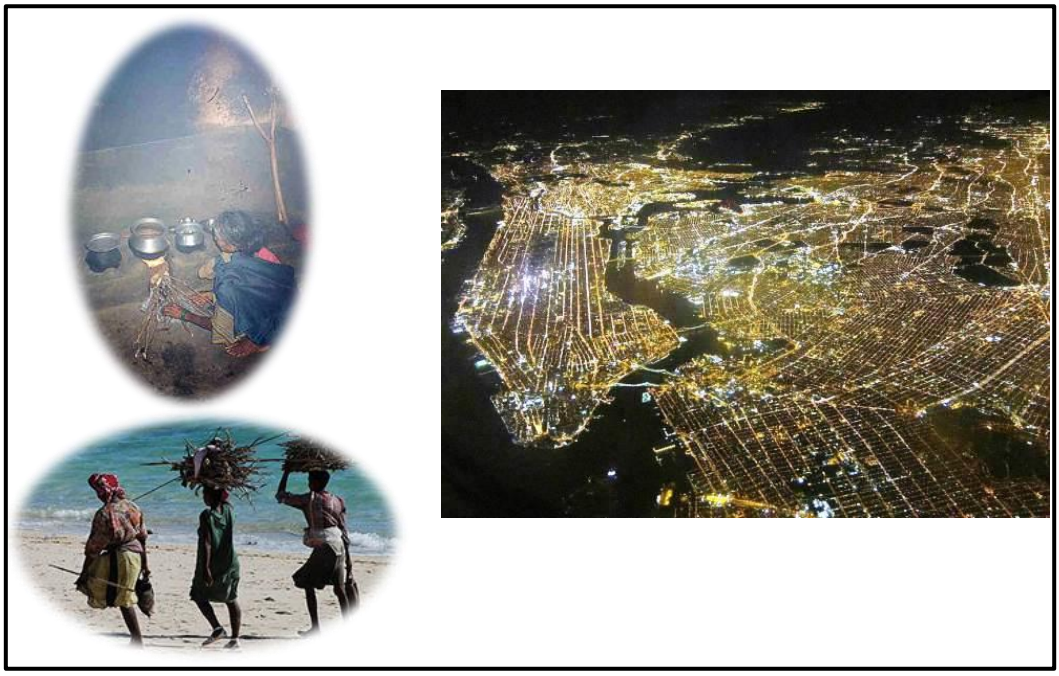

Figure 1.4: The contrast between the energy avaibility and the consumption

https://rickydeanhall.wordpress.com/tag/humanity/

Figure 1.4 aptly reflects the contrast in the present situation. Thus, in order to maintain the balance between energy supplies and consumption, alternative and environmentally safe approaches have to be followed. These energy requirements can be solved with new materials chemistry and non-conventional approaches to harvest and store energy.

1.3 Types and availability of different energy sources (Non-renewable Vs Re-newables): Need for energy harvesting

Currently, more than 80% of the global energy needs are dependent primarily on fossil fuels, namely oil, coal and natural gas. The oil is liquid form of fossil fuels which is found in reservoirs. It is mainly present in crude form which is further

refined to separate different types of fuels such as petrol, diesel and gasoline. The costs of these fuels (which are mainly required for industrial and automobile sectors) depend mainly on the crude oil prices. The recent survey by BBC shows that the current availability of oil supply can last only up to next 50 years. [4]

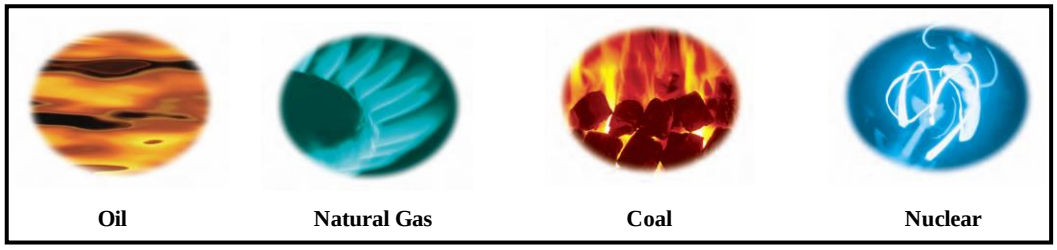

Figure: 1.5: Non-renewable energy sources

http://gnwr1.blogspot.mx/2014/09/key-world-energy-statistics-2014_23.html

Similarly the natural gas is also another very important form of fossil fuel which is essential for household energy demands. It is mainly trapped below earth surface and this is comparatively a cheaper source than coal and oil. Fuels such as coal, oil and natural gas can cause severe climate changes leading to impacts such as global warming, acid rains, deterioration of air quality etc. Figure 1.6 describes the severe effects of various pollutants on human health.

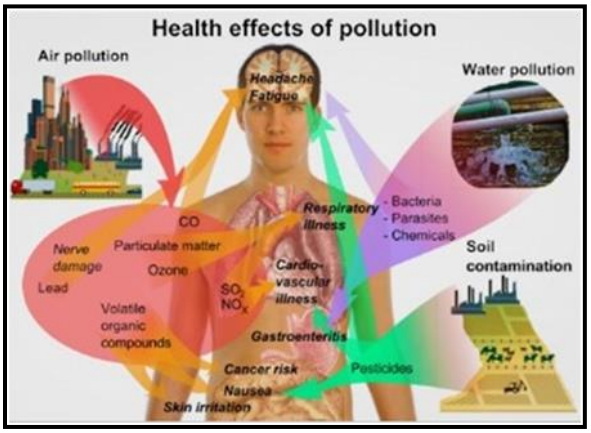

Figure: 1.6.: The hazardous health effects of burning of fossil fuels

http://webpage.pace.edu/jb44525n/page5.html

The gases released during the burning of fossil fuels such as carbon monoxide (CO), sulfur di-oxide (SO_2) nitrous oxide (NO) are toxic and mainly affects the human respiratory system. Similarly during the combustion of fossil fuels two gases namely NO_2 and NO are released which cause irritation of lungs, bronchitis, Pneumonia and decrease the immunity of respiratory system. A few other sources cause water and soil pollution which has adverse effects on gastroenteritis and increases the risk of cancer. [5]

In addition to this, nuclear energy is also an important energy source in which the electricity is generated by nuclear fission of radioactive elements in nuclear reactors. This does not pollute the atmosphere in the conventional sense but the nuclear reactors are very expensive and the nuclear waste has hazardous environmental issues. [6]

Figure: 1.7 Energy as new research frontiers

http://rakric.com/

Thus, the most urgent challenge is the efficient conversion, storage and conservation of energy. Hence major efforts are needed to find out alternative options for environmentally safe, affordable and abundant sources of the energy. [7] Significant focus and guided efforts are necessary to build up alternative robust energy harvesting systems which will substantially reduce the load on the existing

technologies with concurrent pollution control. This can be primarily achieved by developing methods and prototypes for efficient energy conversion and storage systems using knowledge of new materials physics and chemistry. This effort will also answer whether the alternative sources, i.e. renewable energy sources can really be sufficient to overcome the threatening requirements of the more energy.

Figure 1.8: Renewable energy sources

http://vectorschools.co.nz/renewable-and-non-renewable-resources

The renewable energy sources such as solar, wind, hydroelectric, geothermal and biomass are clean low cost and the sustainable energy sources which therefore need greater attention in the current scenario.[8]Sun provides abundant amount of energy in the form of light which can be effectively converted into electricity using solar cells. Thus, the tapping of this energy efficiently can be a very useful approach. Currently silicon based solar panels are highly efficient devices which can power a small village with a population of 1000. This sector is rapidly growing at the rate of 40% every year and the electricity generation cost is also rapidly decreasing. Solar thermal is another approach which harnesses the solar energy and produces thermal energy. The heat generated can be used for both

domestic and industrial purpose. The domestic hot water systems can thus be operated. The solar thermal plants rely upon use of curved mirrors for concentrating the sunlight. In addition to solar, the wind energy is also another potential route for safe and clean energy production. Wind turbines can be implanted on farms or in hilly areas to harvest the wind energy. In geothermal route the cold water is pumped below the earth surface and steams comes out; which is used for rotating turbines. Biomass is another potential energy source which can be burned in a controlled manner to produce heat and electricity. This is a long-term and sustainable source.[9] In addition to the choice of approach for energy production which will ensure clean and safe environment one has to also address the issue of short term or long term and small or large quantity of energy storage. This field of research is also being intensely pursued at the present time.

1.4 Harvesting different energy resources: The methods and consequences (Health and environment) Alternative to batteries

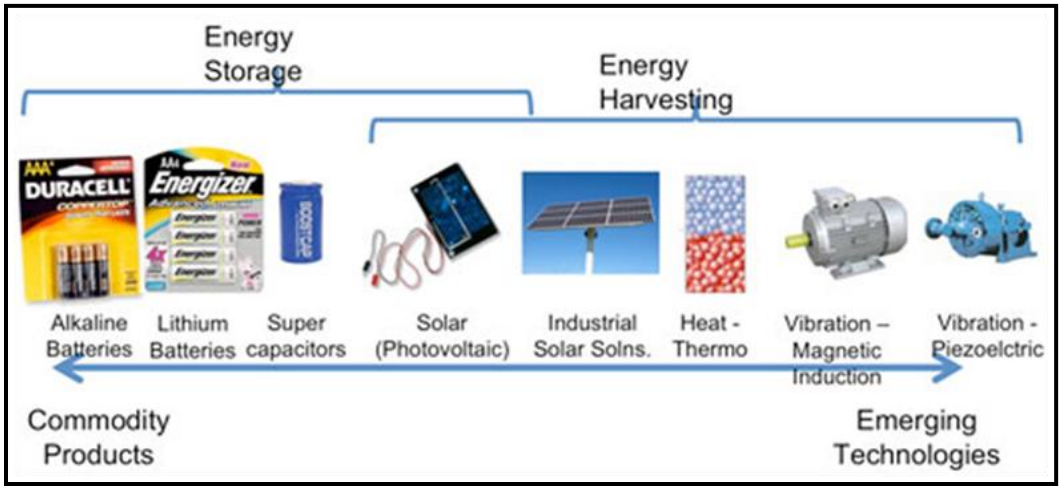

Figure 1.9: Energy Storage Vs Energy harvesting techniques

http://www.designworldonline.com/developments-in-harvesting-energy-for-wireless-sensor-networks/#

The following section briefly discusses the possible ways for efficient energy harvesting and storage[10] and the consequences for the human health and environmental factors. Energy harvesting is the process by which energy can be

captured from different sources. Solar, thermal, kinetic, nuclear, mechanical, tidal, hydrothermal etc. are some such sources of energy. All these sources are ambient energy sources.[11] Harvesting these effectively can definitely reduce the load on the existing sources which are rapidly diminishing.

1.5 Types of energy harvesting [12]

Figure 1.10: The model proposing the multiple types of energy harvesting

http://wonderfulengineering.com/german-engineer-makes-a-free-energy-harvesting-device/

1.5.1. Photovoltaic Energy Conversion

Solar energy is the clean sustainable source which is abundant and broadly distributed. Photovoltaic effect describes the conversion of (light energy) photons from sun light into electrons and holes which can be driven in external circuit to generate the useful electric current using semiconducting materials. Photovoltaic cells are best known devices in the energy harvesting regime which have wide range of applications from portable devices to large power plants. Currently silicon based solar panels which are installed on the big ground or mounted on the top roof can harvest enough energy to run building or villages. [13]

1.5.2. Mechanical Energy harvesting

The mechanical energy is the ubiquitous to us as we are surrounded by plenty of sources in terms of vibrations, human motions, and transport of vehicles etc which are otherwise wasted. Several other sources such as flow of fluid (gas or liquid,) industrial sources can also be utilized in producing vibrational energy as source.[14] This waste form of mechanical energy can be utilized further by conversion into useful electrical energy. In general, mechanical energy harvesting is identified for low power applications. With invention of nanogenerators and the self-powered nanosystems several interesting designs and approaches were developed in the last couple of years for various applications.

1.5.3. Thermal Energy Conversion

Thermoelectricity is the well-known phenomenon of converting temperature gradient/difference into electrical potential. The temperature difference causes the flow of heat in the conducting material leading to potential difference. These kinds of generators work on the principle of Seebeck effect, discovered by Seebeck in 1821. In the year 1834 Jean Peltier discovered that if the electric current is passed through the junction of two conductors it can act as heater or cooler. Both these effects are used in air coolers, heaters, generators etc.[15]

1.5.4. Radio Frequency Energy harvesting

The RF energy harvesters are currently used from radio transmitters to harvest the wireless signal available in the ambient environment. e.g. TV, mobile network, wireless systems etc. It can also be used as the wireless charging systems for the low power applications. e.g. mobile batteries. This usually works as a transducer. The energy harvested through these systems are rectified and then converted to usable DC power. [16]

1.5.5. Acoustic Energy harvesting

These kinds of systems are designed by using piezoelectric cantilever beam and Helmholtz resonator. The resonator oscillates at resonating frequency to generate the mechanical vibrations (sound) which are provided to piezoelectric material that converts sound into electric energy. This is then stored in storage device. The choice of piezoelectric material is important factor here as it has to well match with the frequency of the resonator. [17]

1.6 Energy Storage

There are different ways in which energies from different sources can be stored depending on the types and quantity. The total amount of energy stored per unit volume or mass is generally defined as the energy density. The rate at which the energy can be stored and recovered when needed is also a very important factor from the applications standpoint and defines the power density. The capabilities of different energy storage device concepts can be plotted on the so called Ragone plot shown in figure 1.11. These devices include capacitors, supercapacitors, (Electric Double layer and Pseudo capacitor, batteries and fuel cells. This chart mainly compares the performance of energy storage devices in terms of specific energy and specific power. The Y axis describes how much energy is available and X axis describes how quickly that energy can be made available. [18]

Over the last few years the energy storage concept is grabbing great attention with the successes in the development of devices such as supercapacitors and batteries. Supercapacitors are devices which store energy in chemical form and can deliver this energy with high power density when needed. These types of devices are very useful for quick charging and discharging purpose applications.[19] Batteries are well known from centuries since their invention, developing from alkaline batteries to lead acid batteries to lithium ion batteries which are more successful in recent years. Over the past few decades battery was the main source for operation of remote devices. But the main drawback of the batteries is that they

possess less capacity and their repeated replacement is essential for the operation.[20]

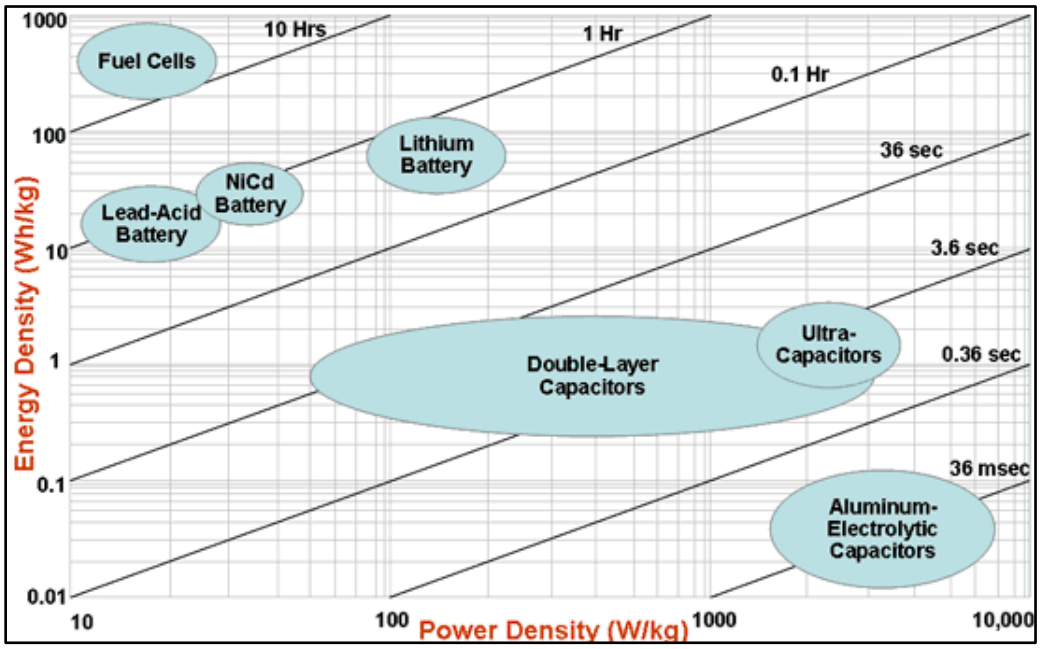

Figure: 1.11: Ragone Plot

http://www.mpoweruk.com/performance.htm

Additionally, batteries cause severe Lead pollution which leads to the critical health hazards. Electrochemical energy storage and efficient energy harvesting through solar, wind, or nuclear energy can solve the global energy need. All these energy harvesting approaches are mainly suitable for large scale energy storage which can be made available when needed. Amongst these the vibrational energy harvesting can be useful and versatile approach as it can harvest the energy from small scale to bulk scale. Vibrational energy is the most unused and rich energy source which can lead to developments of energy harvesting systems in the near future. In the current thesis we will be mainly dealing with the concept of vibrational energy harvesting units called as nanogenerators and hence the detailed approaches for vibrational energy harvesting are discussed in next section.

1.7 Types of vibrational energy harvesting systems:

Based on the physical principles, the vibrational energy harvesting systems are mainly categorized as electrostatic, piezoelectric, electromagnetic and magnetostrictive energy harvesters. [21]

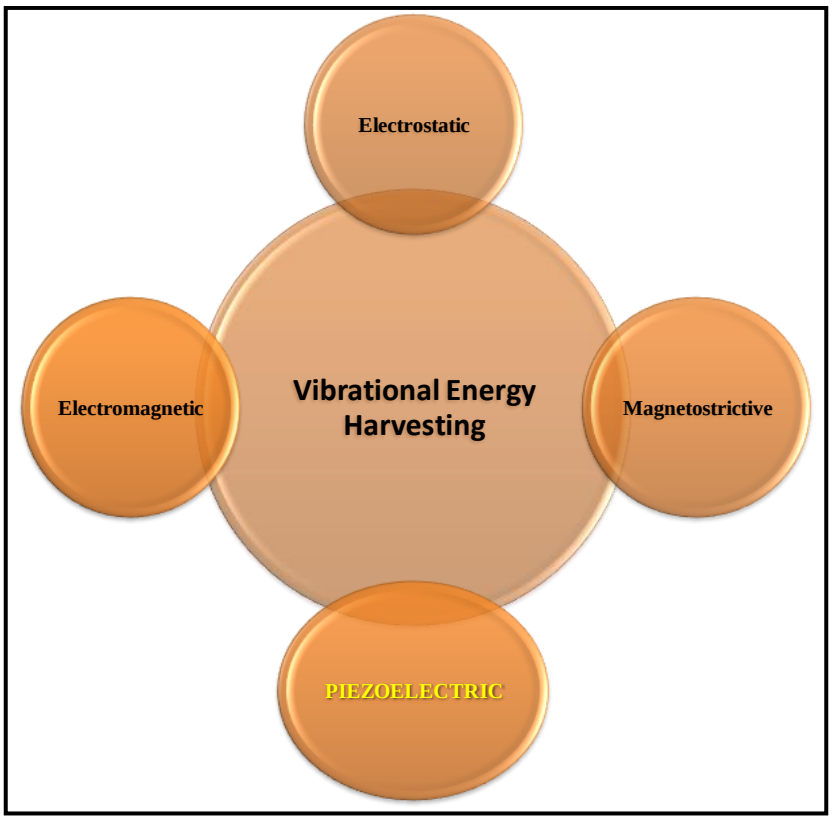

Figure 1.12: The types of vibrational energy harvesting

1.7.1 Electrostatic Harvesters

In these systems mechanical energy is coupled with vibration dependent capacitance. The variable capacitance used here stores electrical energy generated by mechanical vibrations. The displacement of the charged plates with the variable capacitance converts the mechanical energy into electrical. These systems require external power source for charging of capacitors so cannot be self-powered. [11]

1.7.2 Piezoelectric Harvesters

Piezoelectric materials generate electric potential when the mechanical strain/pressure/force is applied onto them. Mechanical energy applied in the form of pressure and force can be directly converted into electric energy. Hence the devices based on this principle are in advanced state of technology. The current devices in the market are mainly based on the cantilever beam set up where the piezoelectric material is coated on the cantilever and the force is applied on the other end of this beam. Such piezoelectric energy harvesters require no external electric bias. Moreover output voltages for such setups are relatively high. Since the discovery of piezoelectric nanogenerators the research is rapidly expanded on developing these types of energy harvesters for various applications. The design architectures of such systems make them extremely useful in integrating with MEMS devices. Variety of material classes can be considered for developing such systems as the only prerequisite is high coefficient of electromechanical coupling. Inorganic oxides and soft flexible polymer based systems can be developed which can efficiently harvest the mechanical energy and convert it into useful electric energy. [22]

1.7.3 Electromagnetic Harvesters

This type of energy harvester utilizes the fundamental law of electromagnetic induction, which states that electric current will be generated in closed circuit when magnetic flux associated with the conductor changes. This concept is mainly used in large electric grid energy storage systems. These systems do not require source of voltage but they are difficult to maintain. [23]

1.7.4 Magnetostrictive Harvesters

The phenomenon of Magnetostriction is principally observed in ferromagnetic materials. These materials undergo shape change when the magnetic field is applied onto them or vice versa. These materials possess high flexibility as well as coupling coefficients making them suitable for high frequency applications. But they show non-linear effects. [24]

1.8 Piezoelectricity:

We have worked mainly on the piezoelectric energy harvesting systems in this thesis. Piezoelectricity was discovered by Pierre and Jacques Curie in 1880. The piezoelectric effect can be defined as the dipole moment generation on the surface (of the piezoelectric material) via the application of external strain. On the other hand, when a piezoelectric material is exposed to the external electric field it changes its volume by mechanical deformation.[25, 26]

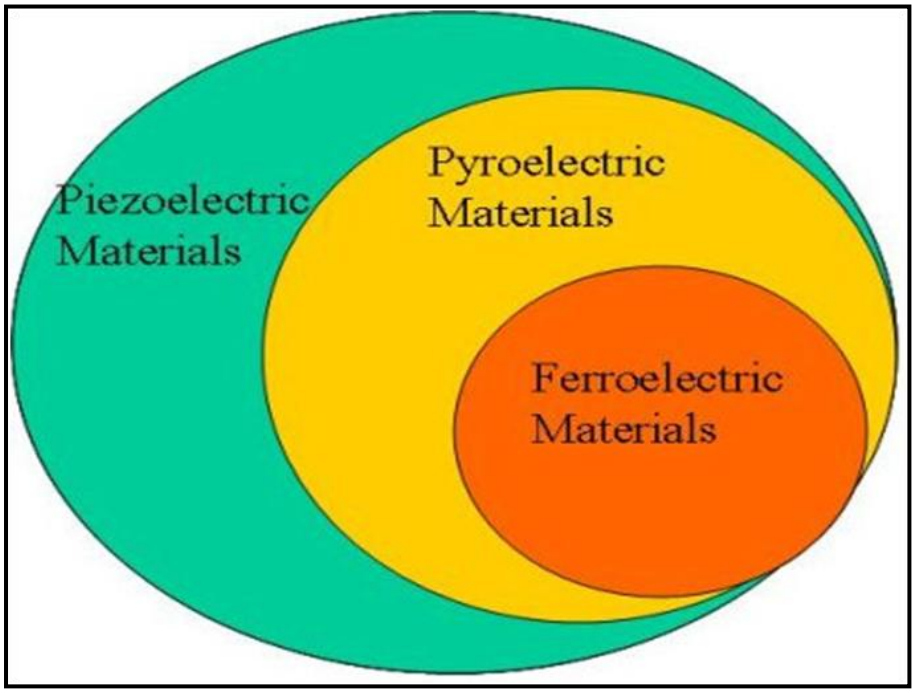

Figure 1.13: The concept of piezo, ferro and pyroelectricity

http://electrons.wikidot.com/ferroelectrics

Piezoelectricity relates electric displacement (D) (surface charges generated per unit area) induced in the material by an applied stress T. Stress is described by the applied force and the area upon which the force acts. It is thus a second rank tensor (Tij) which relates the direction of the applied stress and the electric field developed. The electric field and electric displacement are the vectors (D_i and E_j) (where i, j = 1, 2, 3 represent the three Cartesian directions) and the permittivity is represented by (ε=D/E). Thus, D is specified by

$$D = dT + \varepsilon E \ldots \quad (1)$$

and Strain S is the second rank tensor is specified by

$$S = sT + d_t E \ldots \quad (2)$$

Here, S, T and s represents the strain, stress and the elastic compliance under constant electric field respectively; whereas the E, D and ε are the electric field, electric displacement and the permittivity under constant stress. The parameter 'd' is the strain piezoelectric coefficient i.e. the charge coefficient, which can be expressed as,

$$\boldsymbol{d} = \frac{\boldsymbol{Induced\ mechanical\ strain}}{\boldsymbol{Applied\ electric\ field}} \quad \ldots (3)$$

The other coefficient is '*g'* the piezoelectric voltage coefficient, which can be expressed as

$$\boldsymbol{g} = \frac{\boldsymbol{Open\ circuit\ electric\ field\ output}}{\boldsymbol{Applied\ mechanical\ stress}} \quad \ldots (4)$$

The energy conversion efficiency obtained from the piezoelectric material strongly depends on another important coefficient '*k*' which is the electromechancial coupling coeffients, which can be expressed as

$$\boldsymbol{k} = \sqrt{\frac{\boldsymbol{Mechanical\ energy\ stored}}{\boldsymbol{Electrical\ energy\ applied}}} \ldots (5)$$

The subscripts (1, 2 and 3) associated with the above piezoelectric coefficients describe the three axes within the piezoelectric element. The orientation of these axes corresponds to the classical set of axes namely, X, Y and Z. For the charge piezoelectric coefficient 'd' the first integer (subscript) indicates the direction in which the electric field is applied whereas the second one is the direction of the induced strain. In the similar way, for the voltage coefficient 'g' the first integer indicates the direction in which the electric field is generated and the second subscript denotes the direction of the applied stress. For k, electromechanical

coefficient the first integer indicates the direction along which electric field is applied, while the second integer is the direction along which mechanical energy is stored. For the material to be piezoelectric a) the material should be non-centrosymmetric (according to the Neumann's Principle), and b) must possess at least one unique direction. Out of 32 crystal classes, 20 crystallographic classes are piezoelectric groups. [27]

1.9 Ferroelectricity and Pyroelectricity:

Out of the above mentioned 20 crystal classes, 10 class exhibit spontaneous polarization i.e. polarization is present even in the absence of applied electric field. These are termed as ferroelectrics. Ferroelectricity was discovered in 1920.[28,29] The ferroelectric materials exhibit spontaneous polarization and their polarization can be reversed under the applied external electric field. Their other important characteristic is the presence of "Curie point". For ferroelectric material, when the temperature rises above its curie point it transforms into non-polar paraelectric phase, which exhibits no ferroelectricity.

1.9.1 Pyroelectricity:

Certain crystal classes (10 out of the 20) generate voltage when they are exposed to thermal gradient, either by being heated or cooled. The change in temperature leads to atomic displacements inside the crystal and polarization takes place which produces voltage. [30]

1.10 Piezoelectric Materials

1.10.1. $BaTiO_3$

Presently, the major piezoelectric and ferroelectric materials are ceramics and polymers. The well-known piezoelectric ceramics are lead zirconate titanate (PZT) and barium titanate ($BaTiO_3$) due to their superior dielectric, ferroelectric and piezoelectric properties. Moreover their properties can be modified further with the use of doping. They possess strong piezoelectric coefficients, high dielectric constants and high operating temperatures. In view of these facts these

materials have been used for research as well as technological applications. The figure 1.14 shows the crystal structure of barium titanate.

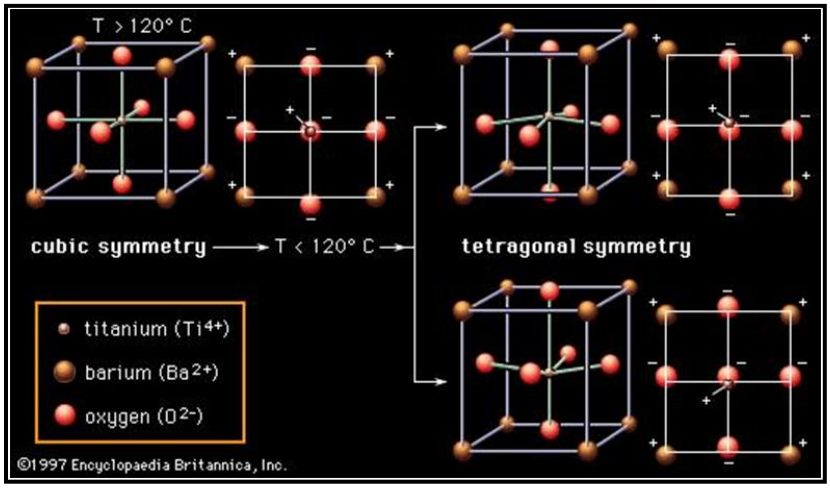

Figure 1.14: Crystal structure of $BaTiO_3$

http://www.britannica.com/science/barium-titanate/images-videos/Ferroelectric-properties-of-barium-titanate-Above-120-C-the-structure/2939

It is the best known ferroelectric material representative of oxygen octahedron group. It belongs to the family of compounds with general formula ABO_3, where A is the di or monovalent metal ion and B is the tetra or pentavalent metal ion. It is mechanically and chemically stable. It exhibits ferroelectric properties at and above the room temperature. Above the Curie temperature it has a cubic structure. In this structure, Ba^{2+} ions are situated at the corners of the cube and O^{2-} ions occupy the centers of the cube. The oxygen ion forms an octahedron at the centre where the small Ti^{4+} ion is located. When the temperature is lowered through the critical temperature of 120º C, the material becomes spontaneously polarized and at the same time structure changes from cubic to tetragonal. $BaTiO_3$ was discovered during the Second World War in 1944. [31] It belongs to the perovskite group with the similarity of the mineral formula $CaTiO_3$. The discovery of the ferroelectricity in $BaTiO_3$ was indeed a major breakthrough, as it was the first demonstration of this property in simple oxide structures. The crystal structure of the $BaTiO_3$, particularly the high temperature ferroelectric phase, was proposed

by Megaw in 1945 [32] and confirmed soon after with the work of Miyake and Vedo. [33]

Due to the attractive functional properties piezoelectric ceramics play significant role even in today's market. However, these materials have few drawbacks such as brittleness, cumbersome manufacturing process and high cost. They have high acoustic impedances leading to considerable energy loss during the signal transduction through water, ambient environments and human tissues. Ceramics possess higher elastic moduli and hence are stiffer than polymers making them less sensitive to small vibrations and more prone to stress failure. Polymers, such as Polyvinylidene difluoride (PVDF), on the other hand are flexible, and could prove more suitable for piezoelectric applications where weight of the system is an important concern.

1.10.2. PVDF:

In 1969, Kawai *et al* found piezoelectricity in PVDF for uniaxially drawn and poled films, which made it the first piezoelectric polymer discovered in the history.[34] Afterwards this property was also found in PVDF co-polymers as well as few odd numbered nylons (Nylon-11) and polyureas. Later on the other interesting aspects such as Pyro electricity and non-linear optical behaviour were discovered leading to the fact that this polymer can be used as an energy transducer. The first polarization switching and hysteresis loops were demonstrated by Furukawa which led to the establishment of this polymer for ferroelectric applications as well.[35]

In the year 1980, the existence of Curie point was observed in a co-polymer of PVDF, namely P(VDF-TrFE). To date PVDF and its co-polymers are the well-known and widely used piezoelectric and ferroelectric polymers due to their interesting properties. In polymers, molecular conformation represents the geometrical arrangement arising from the rotation about adjacent carbon-carbon single bonds. PVDF is a semi-crystalline fluoropolymer with good mechanical,

thermal and chemical stability. It is highly flexible and is well known for its piezoelectric and ferroelectric properties.

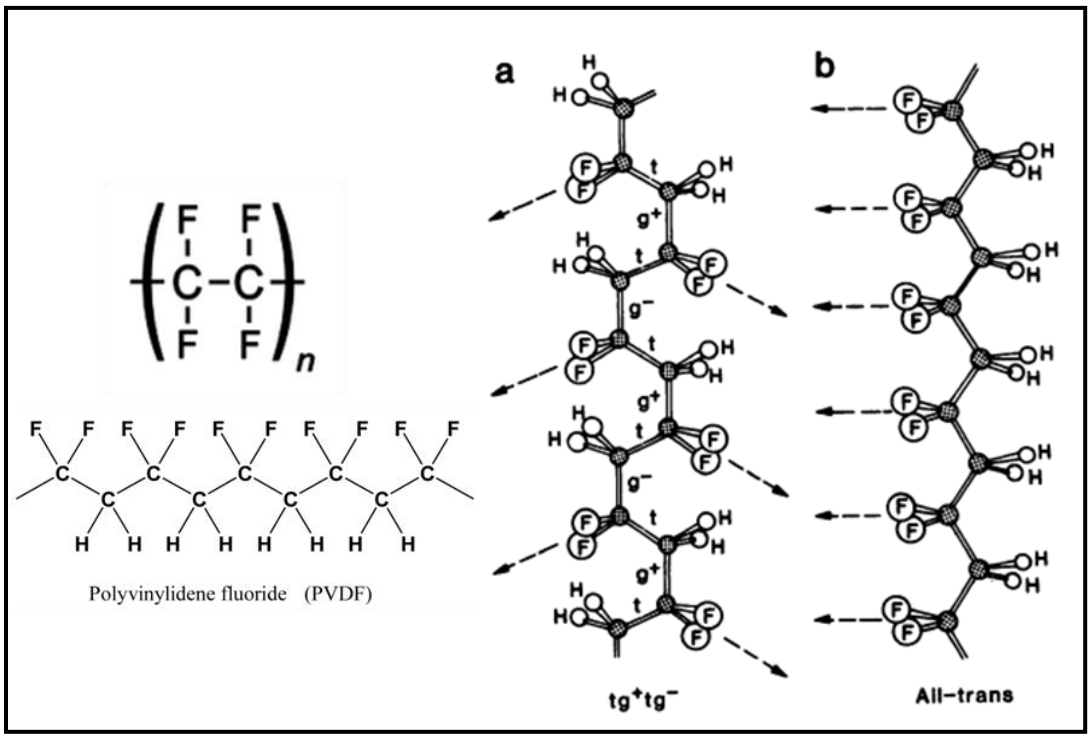

Figure 1.15: Molecular structure of PVDF[36]

Reproduced by the permission from the reference 36: *Science*, **1983**, 220 (4602): 1115–1121

PVDF has four different polymorphs namely α, β, δ and γ. All these forms are distinguished on the basis of the C-C bonding along the chain backbone. Out of these, α is the energetically stable and most common phase, which consists of trans-gauche (TGTG) conformation. There is an intermediate conformation, T_3GT_3G which favours the chain packing to generate the γ phase. The polar β phase is interesting (as it is mainly responsible for the polar i.e. piezo, ferro and pyroelectric properties), which consists of all trans (TTTT) conformations. This conformation leads to a strong polar crystal which is the origin of piezoelectricity and ferroelectricity. All these crystalline phases can be transformed into each other. Lovinger has shown a schematic of inter-conversion of these phases. [36]

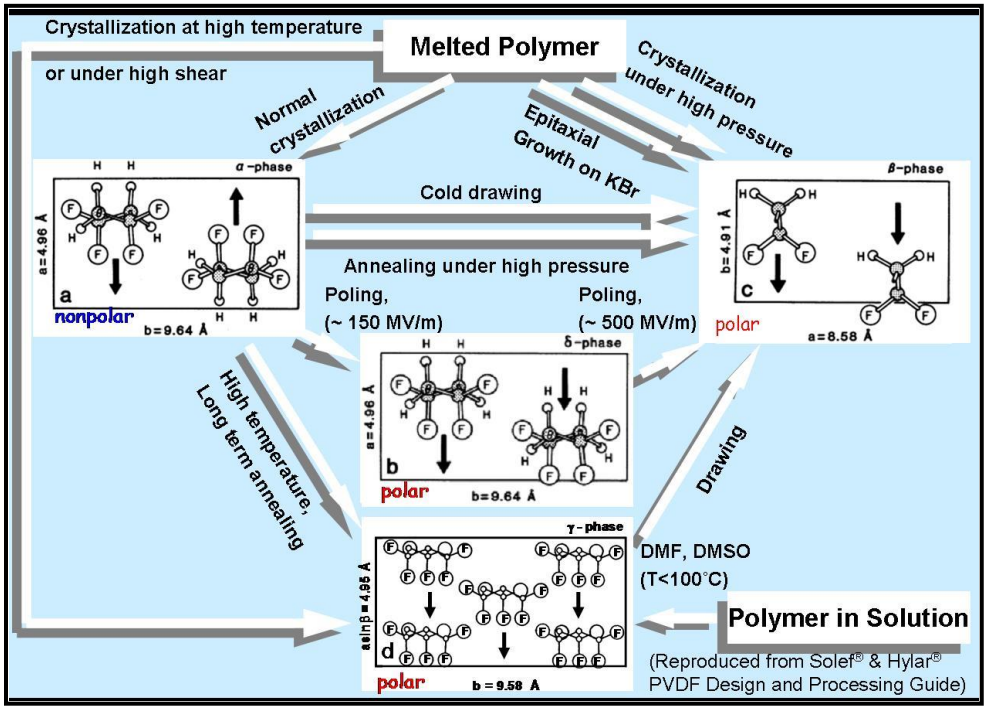

Figure 1.16: Polymorphic phases of PVDF

http://electrons.wikidot.com/direction-electric-field-dependence-of-dielectric-constant

The transformation of α phase into β phase is technically important which involves stretching of PVDF film in the temperatures below 100ºC. In this transformation, the chain unfolding process under stretching is coupled with a reduced molecular mobility that prevents chain relaxation leading to α to β phase change. Davis *et al* discovered that α phase can be converted into β phase by reorientation of crystalline plane.[37] The rich crystalline structure and polymorphic transition in PVDF may arise due to its unique structure. By inserting the CH_2 groups in between the CF_2 groups the repulsions can be compromised and balance in several locations can be achieved. Therefore it is possible to form several stable conformations.

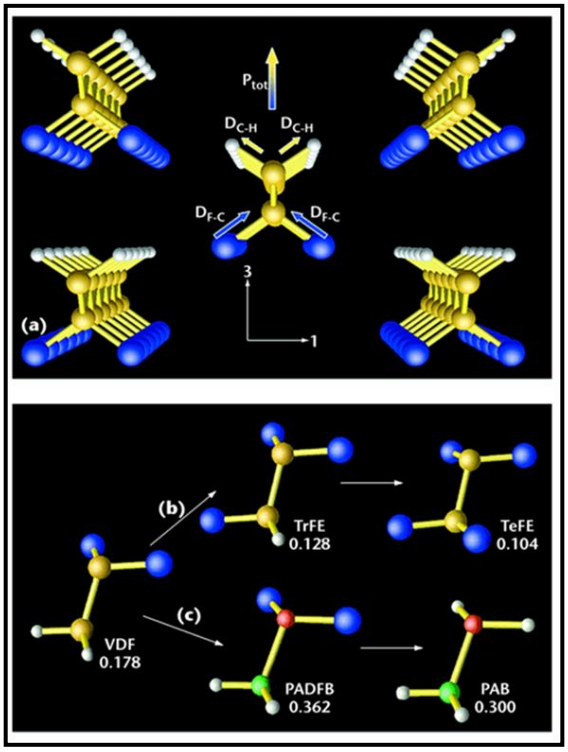

Figure 1.17: Co-polymers of PVDF:P(VDF-TrFE)and PVDF-TeFE

http://www.computer.org/csdl/mags/cs/2004/06/c6012-abs.html

The polar β phase is the most essential phase of the PVDF from the techno-commercial point of view. However as the Curie point of the PVDF is higher than its melting point it is difficult to make the phase conversions every time. Thus, researchers have improved the properties by co-polymerizing PVDF with trifluoroethylene (TrFE)-CH_2, Tetrafluoroethylene (TeFE)-CH_2, Chlorofluoroethylene (CFE) and chlorotrifluroethylene CTFE. Amongst these, P(VDF-TrFE) is the first synthetic polymer with known Curie point, and the molar content of the TrFE has important impact on the crystalline structure of P(VDF-TrFE). If the TrFE content is more than 20% the crystal phase inherently possesses β phase structure. This intentional incorporation of the extra units such as TrFE and TeFE represent defects and lower the melting and ferroelectric phase transition temperatures. This co-polymer also has slightly larger unit cell and a smaller average dipole moment than that of pure PVDF owing to the replacement of some of the hydrogen atoms by the larger fluorine atoms. The co-polymers of

the PVDF readily crystallize from melt and can be stretched and electrically polarized to improve the crystallinity. The most promising property of the P(VDF-TrFE) is the ferroelectricity, which makes it suitable for non-volatile memory applications.[38]

1.11 Piezoelectric materials for energy harvesting:

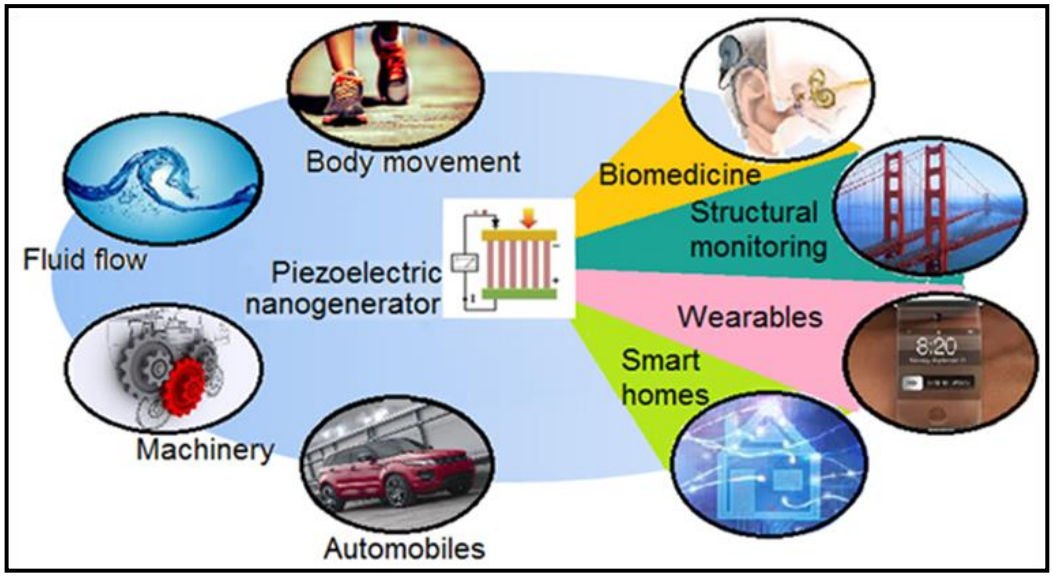

Figure 1.18: Applications of piezoelectric nanogenerators for energy harvesting

http://www.dmg.msm.cam.ac.uk/research.php?page=Nanogenerators%20and%20Sensors

Since the discovery of the piezoelectricity use of a huge number of piezoelectric materials has been demonstrated for many applications such as sensors, transducers, actuators etc. in various fields. However, research on the use of piezoelectricity for energy harvesting purposes has expanded rapidly during the last decade. These energy harvesters can be used to acquire mechanical signals even from the ambient sources from living environment.[39] Most of the studies demonstrate the use of piezoelectric-semiconducting materials from the Wurtzite family. These piezoelectric energy harvesters are commonly termed as nanogenerators. Much advancement has been made in the domain of piezoelectric

nanogenerators (PENG) recently through use of simple fabrication processes, leading to high mechanical stability and higher piezoelectric output. Numerous applications of this technology have been demonstrated such as self powered nanosystems, multiple energy harvesting systems, NG as active sensors etc. The key points for the commercialization of this technology include the development of integration of system, low cost and large scale fabrication processes as well as the power management circuits. Another useful point is the fundamental understanding of the nanoscale size effects of various piezoelectric materials on their properties.

1.12 Nanostructures for enhanced piezoelectric properties:

Apart from the inter-conversion methods for converting non polar form into polar form the morphological characteristics of the piezoelectric material also have a significant impact on their performance. Recently Fang *et al* summarized the theoretical and experimental findings for piezo-electric materials by reviewing their several nanostructures. [40]

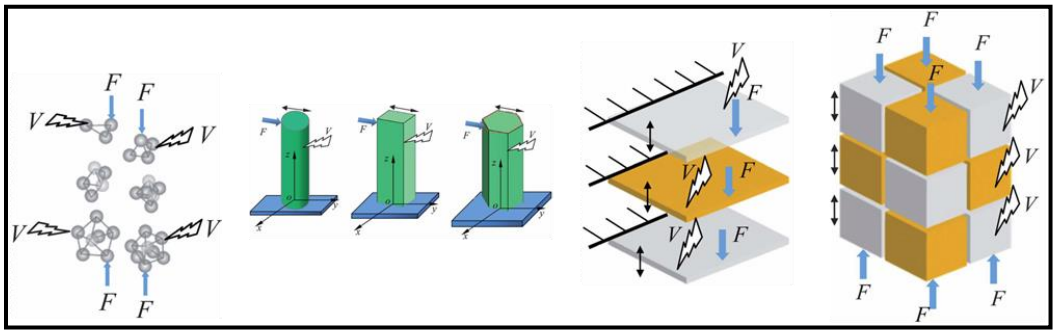

Figure 1.19: Dimensional dependence of piezoelectricity[40]

Reproduced by the permission from reference 40: *Nanoscale*, **2013**, 5, 1716

Under the applied mechanical stress, distortion takes place in piezoelectric materials and potential is generated on the sides of the surfaces. In the case of zero dimensional nanoparticles, usually the piezoelectric nanoparticles are isolated from each other. Various studies are being done in this context, to improve the dielectric, ferroelectric, and piezoelectric properties of the materials

as well as composites.[41] One dimensional nanostructures have dimensions in the range of 100 nm and length is more than 1 mm. The first work on piezoelectric nanogenerator was performed on the 1D ZnO nanowires. 1D nanostructure has additional advantage of improved charge transport over 0D nanoparticles. Particularly for piezoelectric applications, they are more sensitive to applied strain, and have higher mechanical strength and enhanced piezo properties. Up till now, 1D-nano-structures have been made which possess circular, rectangular or hexagonal cross-section.

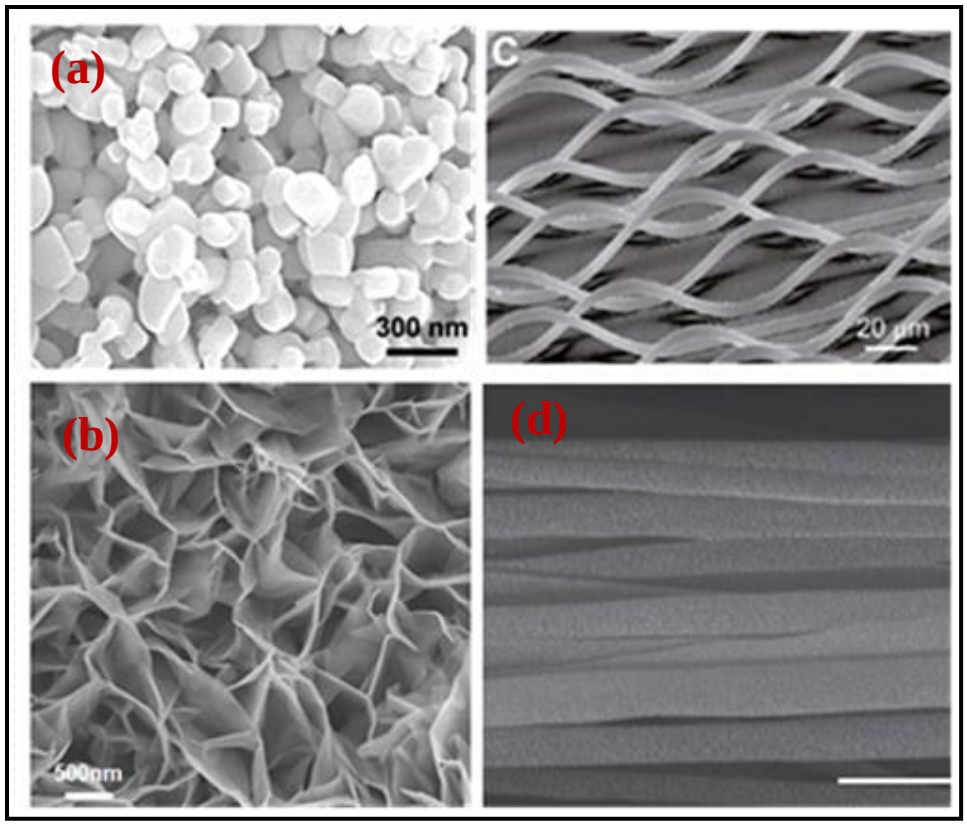

Figure 1.20: SEM images for the different piezoelectric nanostructures [42-43, 46-47]

Reproduced and reprinted by the permission of references 42-43 and 46-47.

Along with nanowires, synthesis of nanofibers and study of their properties is also a rapidly developing area for piezoelectric applications in recent years. These nanofibers possess high piezoelectric voltage coefficient, high flexibility and high

energy conversion efficiencies. [42,43] 2D nanostructures have also been used recently for piezoelectric applications. The transfer of piezoelectric nanostructures such as nanoribbons and nanofilms has been attempted by researchers in the case of PZT and $BaTiO_3$. [44-47] However such 2D nanostructures cannot sustain large deformations. Three dimensional nanostructures involve fibrous multilayers and polycrystalline materials in which 0D, 1D and 2D materials are in close proximity to form interfaces. The electro-mechanical coupling coefficients of the 3D piezoelectric nanostructures possess three independent coefficients namely d33, d13 and d15. Recently Jolandan *et al* have studied 3D piezoelectric nanostructures and have shown that they have high voltage generation than their bulk counterparts. [48] Currently, piezoelectric nanofilms, nanowires and nanofibers are regarded as the suitable candidates for energy harvesting applications, as 1) these nanostructures can tolerate the higher strains applied onto them which is the vital parameter for the generation of surface potential and piezoelectric coefficient, and 2) materials properties strongly improve due to surface/interface effects. The miniaturization of the piezoelectric structures improves the surface to volume ratio. This in turn has a pronounced effect on the surface/interface and strongly affects the mechanical properties of the nanomaterials. Simultaneously, it also affects the surface electrostatic potential. For the practical purpose, these piezoelectric nanostructures generate higher piezoelectric output. This mainly depends on the higher piezoelectric coefficients as well as the electro-elastic properties of these nanostructures. It is therefore a topic of great interest in the recent piezoelectric energy harvesting research.

1.13 Concept of nanogenerator

1.13.1 ZnO Based NG

The presence of piezoelectric potential in certain crystal classes has opened up new research opportunities in the field of energy harvesting. A piezoelectric device called “Nanogenerator” was first developed in Prof Z.L.Wang’s group at Georgia Tech. Their first work on this term got published in Science in the year

2006.[49] The figure 1.21 shows the basic concept of ZnO based piezoelectric nanogenerator.

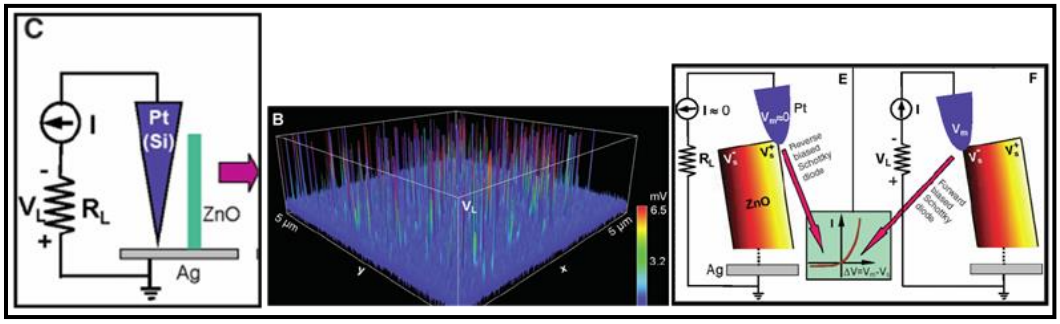

Figure 1.21: The concept of ZnO based Nanogenerator [49]

Reproduced by the permission from reference 49: *Science* 2006: 312 (5771), 242-246

The measurement of electrical transport property was studied using AFM. One end of the probe was held on the side of the ZnO NW while the other was used to push the NW from one end to other on the tensile side surface of the NW. In the case of ZnO NW, it is the relative displacement of Zn^{2+} and O^{2-} with respect to each other that generates the piezoelectric potential. This creates the potential difference at the tip of the nanowire and the bottom is grounded. The stretched portion of the nanowire experiences a positive strain while the compressed portion experiences negative strain. This leads to the band bending at the Fermi level, due to generated piezoelectric potential. The free charges flowing through the external load/circuit try to neutralize the local piezo-potential. The current is generated due to the transient flow of electrons. An AC signal is thus generated if the dynamic stress is applied along the NW.

Particularly for piezoelectric and semiconductive materials such as ZnO, CdS, GaN etc. the electrical contact plays a crucial role in pushing out the charges to the surface of the tip. The formation of Schottky contact between the electrode and the tip of the NW is essential, as the Ohmic contact neutralizes the electric potential generated at the tip of the NW. Thus to establish the Schottky contact, electron affinity must be smaller than the work function so as to create the barrier

at the interface. (e.g. in this case the E_F of the Pt = 6.1 eV and the E_{ea} for ZnO NW = 4.5 eV) Under the applied stress, once the Schottky contact is created, the electrons drive from the tip of the electrode to the bottom side electrode via the external circuit. The Schottky contact thus prevents the screening of piezo-charges generated and maintains the potential generated at the tip. The piezo-potential is then created giving a signal in positive direction.

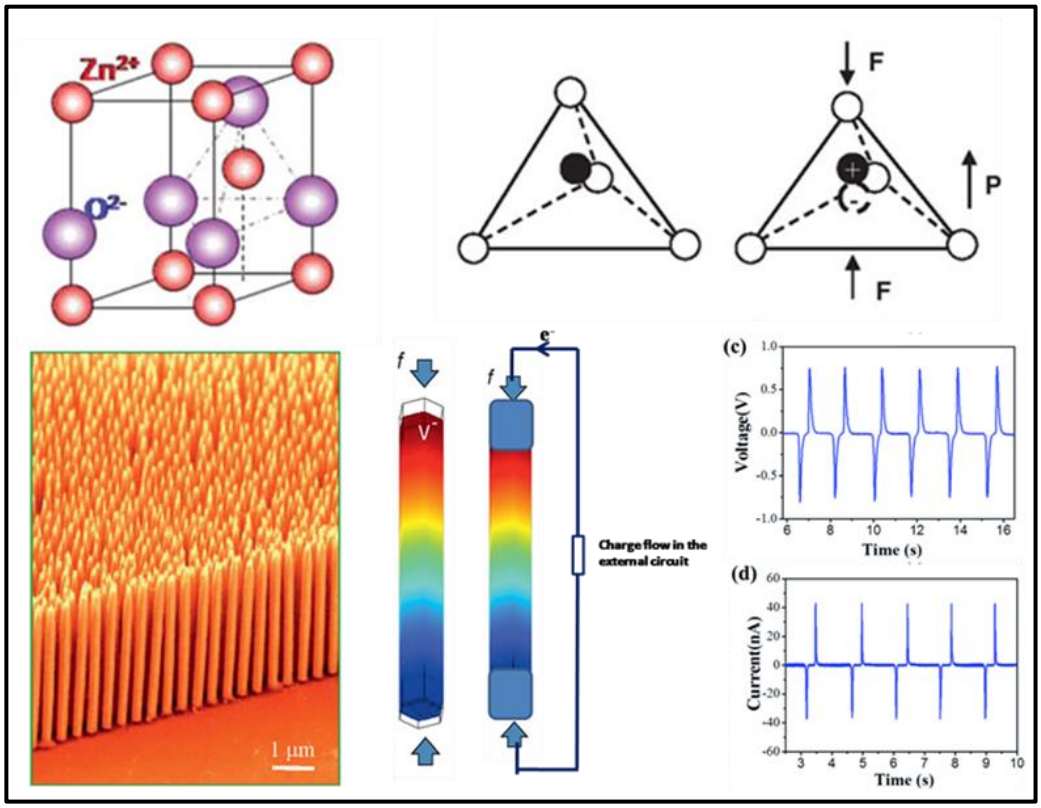

Figure 1.22: The measurement and output single ZnO NW based Nanogenerator [50]

Reproduced by the permission from reference 50: *MRS Bulletin*, volume 37, September 2012

Once the applied stress is removed, the piezoelectric potential diminishes and electron will flow back to the circuit in order to neutralize the positive potential at the tip producing the piezo-output signal in the opposite direction. An AC output signal is thus generated.

1.13.2 PVDF based NG:

Since the discovery of the first NG, different piezoelectric materials have been explored for NG applications. Initially, the piezoelectric and semiconducting structures belonging to Wurtzite family such as ZnO, CdS, GaN and InN etc. were studied. [50,51] These materials have the advantage of easy and low temperature synthesis protocol, such as hydrothermal synthesis. The orientation and crystalline growth can also be achieved using this synthesis method. Later on high piezoelectric coefficient materials such as $BaTiO_3$ have also been studied. The output was found to be 10-15 times higher than ZnO NW based NG. [45] Prof. Liwei Lin from Berkeley's Sensor and Actuator Centre has explored piezoelectric polymer PVDF for the NG application.

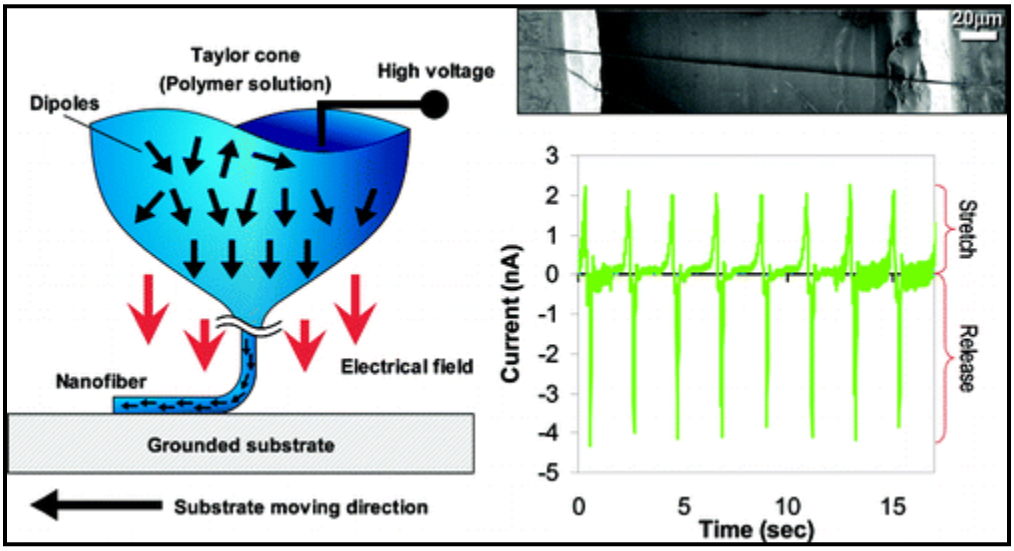

Figure 1.23: The concept of PVDF based nanogenerator [52]

Reproduced by the permission from reference 52: *Nano Letters* 2010 *10* (2), 726-731, Copyright (2010) American Chemical Society

They have used near field electrospinning process for the fabrication of the device. The nanofibers can be written directly on the flexible substrate. [52] The figure 1.23 shows the working principle of PVDF nanogenerator. When the flexible substrate is exposed to repetitive stretch and release actions, the piezoelectric power i.e. a current and a voltage are generated. During the

deformation, built-in piezoelectric potential is generated in the NG. In response to that, free electrons flow to the nanogenerator in order to counterbalance this potential. During this process the net charge also increases. At a constant strain, both the free charges as well as the potential generated reach to zero, as the built-in potential is neutralized by free charges. Once the strain is released, piezoelectric potential diminishes and the free charges flow back in the opposite direction by generating an opposite signal.

1.14 Different designs of the nanogenerator:

Most of the NGs can be categorized into three different types viz. Vertical integrated nanogenerator (VING), laterally integrated nanogenerator (LING) and nanocomposite electrical generator (NEG).

1.14.1 Vertical integrated nanogenerator (VING)

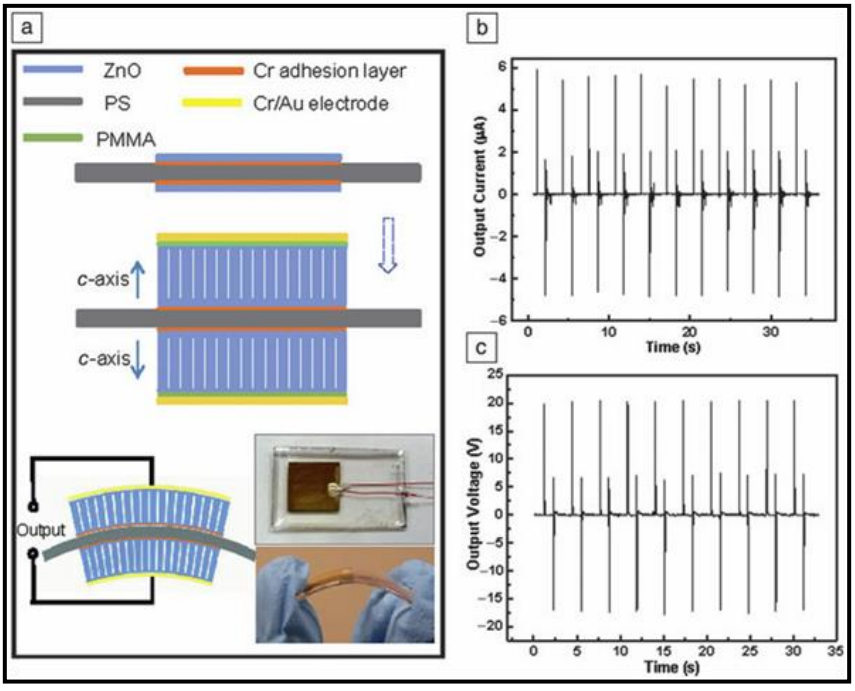

Figure 1.24: The vertically integrated ZnO NW based nanogenerator [53]

Reproduced by the permission of reference 53 *Nature Nanotechnology* **5**, 366 - 373 (2010)

After the study on single ZnO NW, well aligned NWs were used for the NG application. [53] The device structure is based on flexible Polystyrene (PS) substrate with Cr adhesion layer. After the seed layer of ZnO, thin layer of PMMA is deposited as an insulating layer, followed by a thin layer of Au as an electrode. The as-grown ZnO is aligned along its *c*-axis. As the PS substrate is deformed, the ZnO film at the top surface is under tensile strain while the bottom side is experiences a compressive strain. The resulting piezo-potential then drives the flow of electrons via an external circuit. The total power output can be improved even further by connecting the multiple NGs either in series or parallel. Such integrated nanosystems can be placed in shoes or can be attached to cloths, or rotating tires. Secondly, such systems could be useful as ambient vibration energy harvesters.

1.14.2 Laterally integrated nanogenerator (LING)

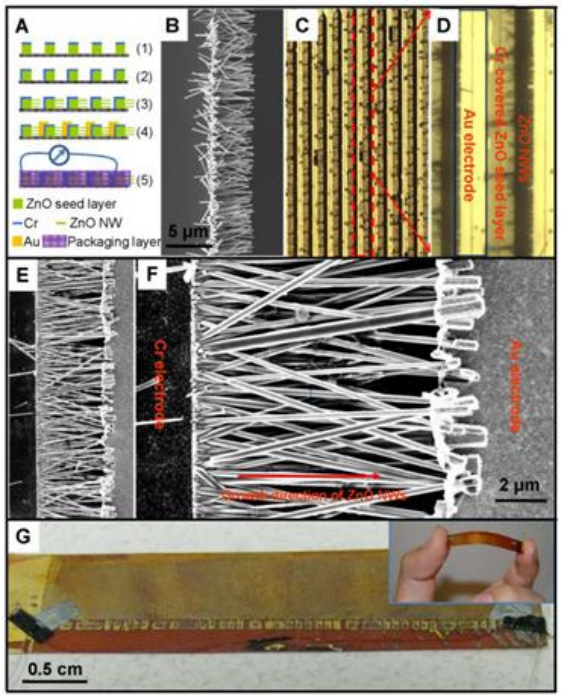

Figure 1.25: The laterally integrated ZnO NW based nanogenerator [54]

Reproduced by the permission of reference 54: *Materials Science and Engineering R* 70 (2010) 320–329

Integration of laterally grown ZnO NW's array is a key step directed towards the practical use of the NG.[54] But several factors such as non-symmetric and robust contact, crystallographic orientation of ZnO during growth as well as the synchronized mechanical deformations of the NWs have to be considered to constructively integrate laterally integrated nanogenerator (LING). The figure 1.25 shows the fabrication process of the LING device. Fig. 1.22 shows the SEM for controlled growth of ZnO NWs. The image demonstrates the flexibility of the substrates. The LING structure has proven to enhance the output potential of NGs.

1.14.3 Nanocomposite electric generator (NEG)

This type of generator consists of 3-D configuration comprising of metal plate electrodes, polymer matrix and vertically grown piezoelectric ZnO NWs. It was introduced by Momeni et al.[55]The performance of the NEG was excellent and highly sustainable as compared to only ZnO NW based systems.

1.15 Self powered nanosystems

The integration of multifunctional nanodevices with different device architectures can be operated using micro or miliwatt power output. In general the integrated system is composed of sensors such as transducers, data processing unit, and the communication units. As the size of the device is now shrinking tremendously, the power consumption also drops down to a few micro and miliwatt. In such scenarios, the self-powered nanosystems can provide an independent, sustainable and maintenance free source for the operation of personal/portable and wearable electronics, implantable biosensors and infrastructures monitoring etc. [56] The mechanical energy available in our environment is abundant but it is irregularly distributed. Additionally, the magnitude, such as wind-flow, human actions etc. mostly limit its applications for particular use. Thus, rational designs are required for the variable environment depending upon the specific needs.

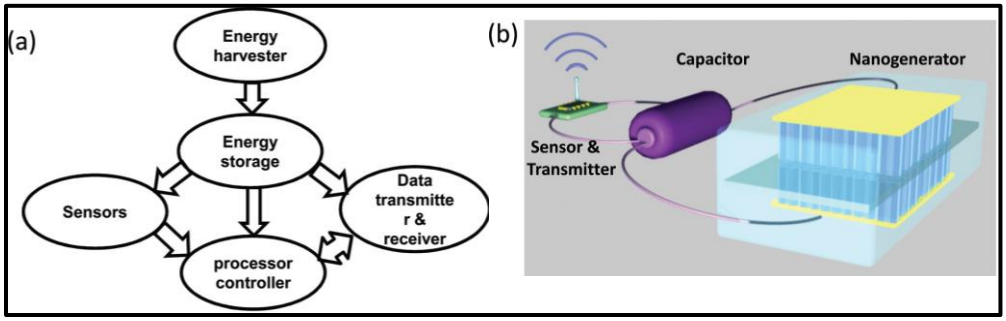

Figure 1.26: The self-powered nanosystems [56]

Reproduced by the permission from reference 56: *Adv. Mater*., **2012**, 24, 280–285

Fig. 1.23 shows the self powered system components. It mainly consists of a sensor (transmitter), energy harvesting device and a storage unit. The sensor identifies the change in the environment, and passes it to the data processor which further analyses the information received. Various demonstrations have been made afterwards such as self-powered photo-sensor [57], self powered environmental sensor and self powered pH sensor [58] .etc.

1.16 Hybrid cell for simultaneously harvesting multiple types of energies:

The ambient energy harvesters can use different forms of energies from the environment such as light, thermal, mechanical, chemical, magnetic, biological etc. For the sustainable development, energy harvesting has to fulfill the continuing energy needs. Novel design approaches have to be designed for the integration of multi-type energy harvesting simultaneously. Recently, few different strategies have been developed for simultaneously harvesting different forms of energies such as mechanical, chemical, thermal etc. The first such device harvester was demonstrated for simultaneous harvesting of solar, mechanical and thermal energies. [59] Recently, such kinds of systems have been developed for concurrently harvesting biomechanical and mechanical energies for in-vivo applications. [60] These multimode energy harvesters can utilize the energy efficiently in the environment under which the devices may operate.

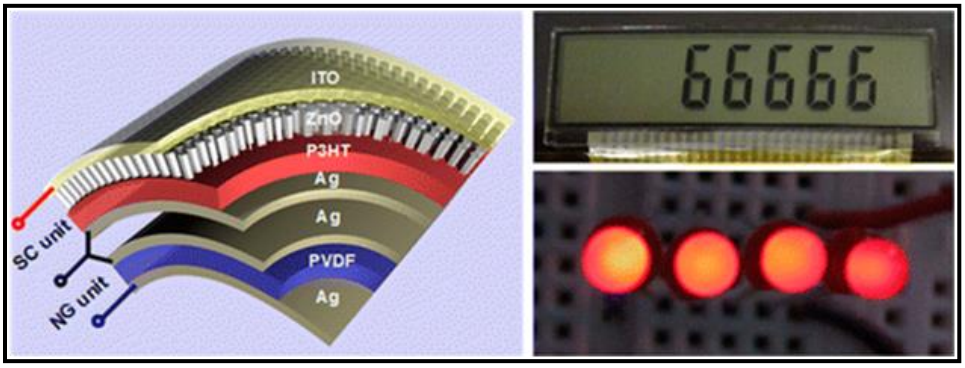

Figure 1.27: Hybrid cell for simultaneously harvesting multiple types of energies based on ZnO and PVDF [58]

Reproduced by the permission of reference 58: *ACS Nano* **2013,** 7,785-790 Copyright (2013) American Chemical Society

1.17 Nanogenerators as active sensors:

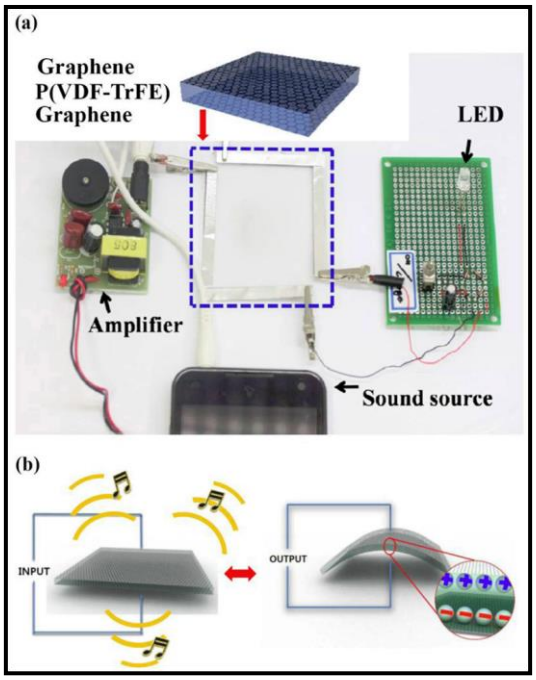

Figure 1.28: Graphene P(VDF-TrFE) based acts as actuator as well as nanogenerator [63]

Reproduced by the permission of reference 63: *ACS Nano* **2013,** 7, 3130-3138 Copyright (2013) American Chemical Society

Nanogenerators can also function as active sensors by detecting the signals generated from an electrical output. Recently, self powered sensors such as vibration sensors [61], pressure sensors [62], and strain sensors [63] have been demonstrated. In general, the mechanical deformation leads to a potential difference across the thickness of piezoelectric material and this potential is sensitive to the applied vibrations, pressure or strain. This shows that NGs can be used as active sensors for detecting applied small mechanical signals. [64]

1.18 Piezotronics and Piezo-phototronics:

The piezoelectric materials such as ZnO, CdS, and GaN are piezoelectric, and semiconducting. They have photoexcitation properties as well. Due to the three way coupling properties of these materials new fields, namely piezotronics and piezo-phototronics are born.

The piezotronic effect is the tuning/controlling the charge carrier transport by using inner crystal potential i.e. piezo potential generated under the applied strain. During the first experiment by Prof. Z.L.Wang on ZnO NW, they observed a drop in the electrical conductance of ZnO, as the bending angle increased. [65] This was due to the piezopotential drop created across the NW when it was under deformation. It was then referred to the gate effect similar to the conventional transistors. The simple FET of semiconductor wire consists of the source and drain contacts at the two ends and gate electrode is located either on the top or bottom of the substrate for applying the voltage. Thus, when the gate voltage is applied the conductance of the wire can be changed. In the similar fashion, the piezoelectric potential generated inside the semiconductor nanowire was used to control the transport of the charge carries, hence the conductance was affected. These types of devices are called as piezotronic devices which are triggered by mechanical action. The figure 1.30 shows the basic working principle of the piezoelectric FET.

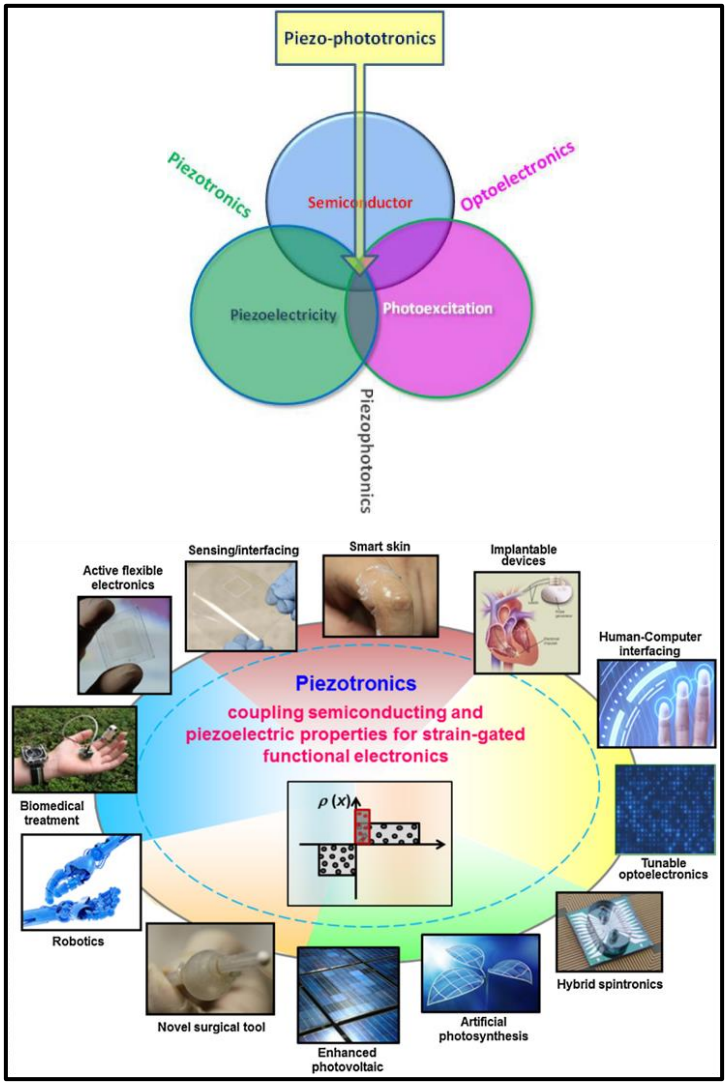

Figure 1.29: Hybrid cell for simultaneously harvesting multiple types of energies based on ZnO and PVDF [65]

Reproduced by the permission of reference 65: Piezotronics and Piezo-Phototronics Microtechnology and MEMS, 2012, pp 1-17

When the ZnO NW is strained, the two typical effects are possible, a) piezoresistance, and b) piezoelectric effect. The piezoresistance effect is the marginal change in bandgap / electrical resistance of the semiconductor due change in the conduction band. This effect is not polarity dependent i.e. no change in electric potential is observed by changing the polarity of the applied strain. Thus, it has the same effect at both the contacts of the FET. In contrast to that, the

piezoelectric polarization has dissimilar effect at both these electrical contacts of the FET. The band structure below explains the working of piezotronic FET based on ZnO NW which is laterally bonded to flexible substrate with the two electrical contacts.[50]

Initially, no strain was applied on the ZnO NW and two Schottky contacts were formed at both the electrodes with varying barrier heights namely Φ*S* and Φ*D*. (figure 1.30) The quasi-Fermi level is different at the two contacts, when the drain is forward biased. This has symmetric and non-polar effect at both the ends. Since ZnO is piezoelectric in nature; the piezo potential is generated under the applied strain.

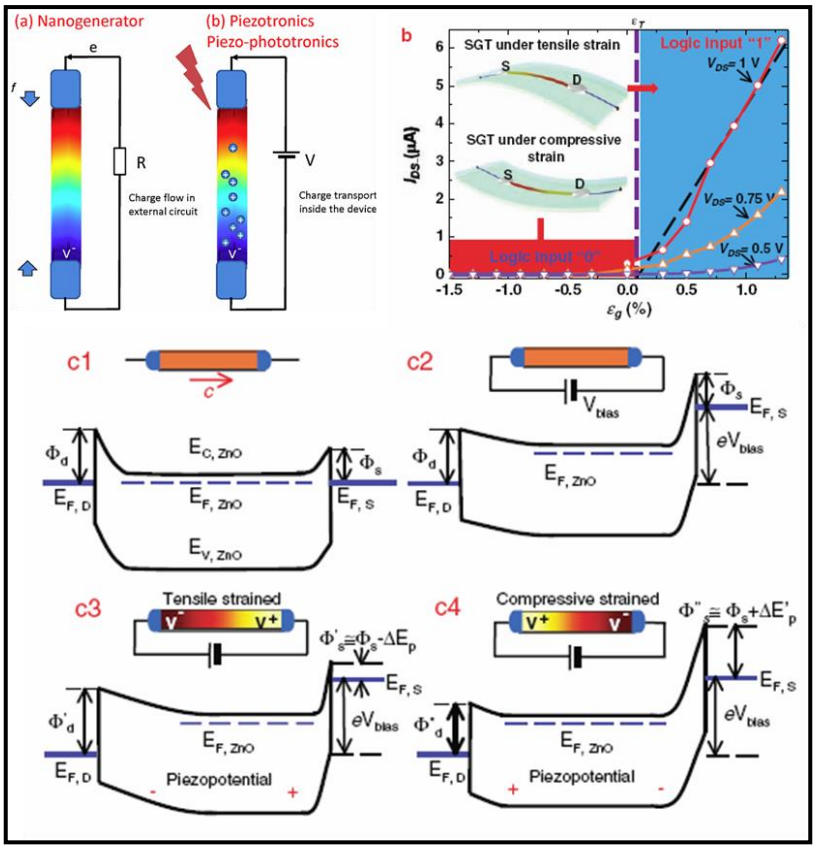

Figure 1.30: Difference between the working principle of NG and piezotronics. Band diagram for piezo-FET [66]

Reproduced by the permission from reference 66: *Adv. Mater.***2010**, 22, 4711–4715

Under the applied strain the piezoelectric potential drop is generated from V^+ to V^-. This changes the Schottky barrier height (SBH) at the source and drain electrodes. Under the tensile strain, the SBH is reduced from, $\Phi S = \Phi' S - \Delta Ep$, where ΔEp is the change arisen due to locally created piezopotential under tensile strain, resulting in increasing, the I_{ds}. On the other hand under the compressive strain, the SBH is raised from, $\Phi S = \Phi'' S + \Delta E'p$, where $\Delta E'p$ locally created piezopotential effect under compressive strain, resulting in the reduction of I_{ds}. Thus, the applied mechanical strain (tensile and compressive) can be used to effectively tune the device from "on" and "off" states via non-symmetric polar effect. This is the operating principle of strain gated FET or Piezo-FET. [66]

1.18.1 Piezotronic effect on p-n junction

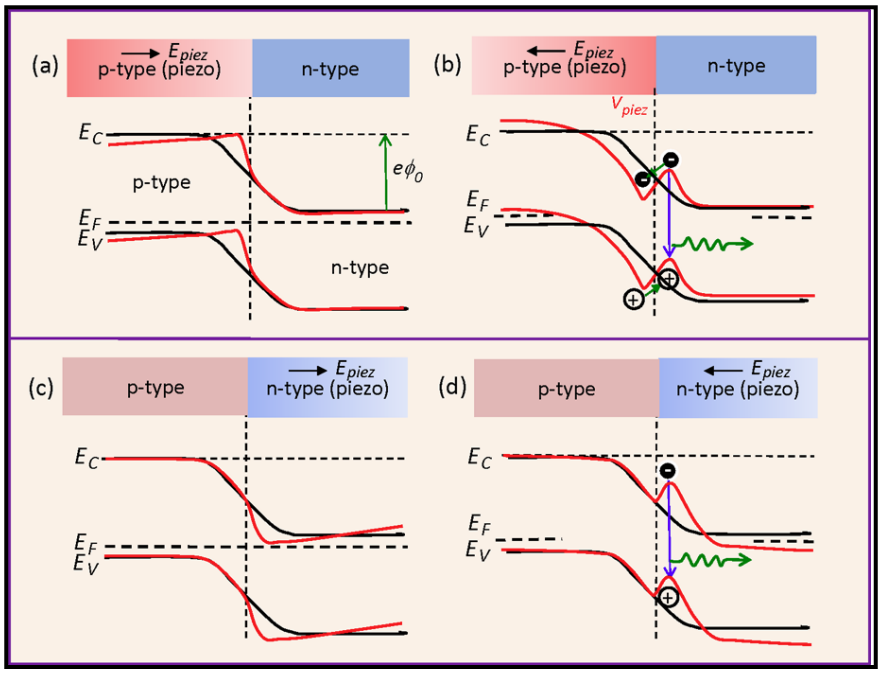

Figure 1.31: Effect of piezo-potential on p-n junction [67]

Reproduced by the permission of reference 67: Introduction of Piezotronics and Piezo-Phototronics, Z.L. Wang, Springer-Verlag Berlin, Heidelberg ,2012, pp 1-17

The piezotronic effect has been further studied with one more primary structure, i.e. p-n junctions. When p-and n-type materials establish a junction, charge depletion layer is created due to recombination and interdiffusion of the charge carriers. The strain in the structure produces piezoelectric polarization if the semiconductor is also a piezoelectric. This carrier free zone enhances the local piezoelectric effect, by avoiding the screening of the charges. The generated piezopotential can alternatively create slope and the dip in the local band depending on the sign of the applied strain. This modification in the band structure can be effectively used for trapping the holes, so that recombination rate of the charge carriers can be enhanced up to a great extent. This principle can be used for improving the efficiency of LEDs. [67]

1.19 Piezo-phototronics:

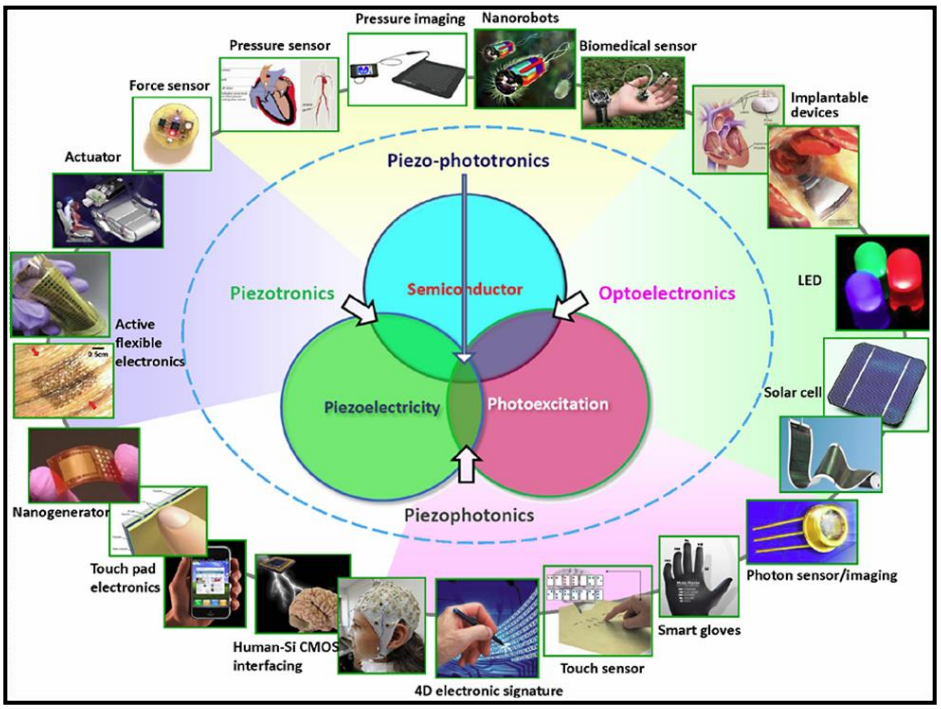

Figure 1.32: The applications for the piezotronics and piezo-phototronics [67]

Reproduced by the permission of reference 67: *Nano Today*., **2010**, 5, 540—552

This term was first coined in the year 2010.[68] It is the simultaneous coupling of the three properties of the materials namely semiconducting, piezoelectric and the

photon excitation. Besides the optoelectronic effect, the piezoelectric properties can be used to tune the charge generation as well as transport, separation or recombination at the interface/junction. The concept piezo-phototronics was used for the engineering the band structures in the devices such as, solar cells, photodetectors and LEDs.

1.19.1 Piezo-phototronics for solar cell:

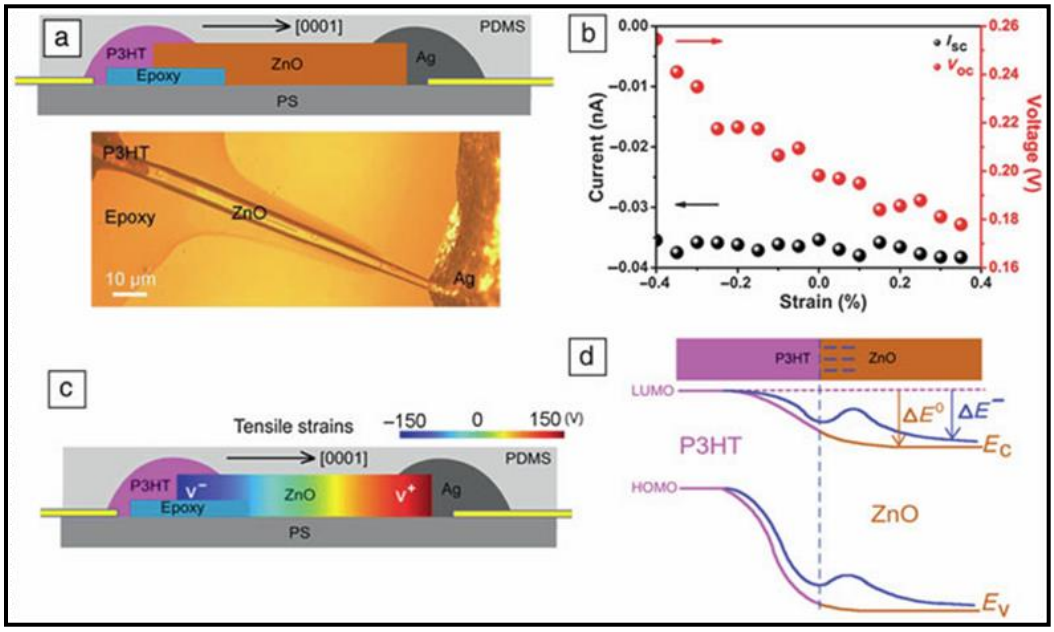

Figure 1.33: Piezo-phototronic effect for performance improvement of solar cell[69]

Reproduced by the permission of reference 69: *Nano Letters* **2011**, 11, 4812-4817 Copyright (2011) American Chemical Society

In the solar cell, the electron hole pair separation is crucial for higher efficiencies. Now, if the energy required for this process is high, then these photo generated charges cannot be separated easily. Alternatively the modification of this layer can be optimized using piezopotential, in order to align the electronic states into a favorable band structure. In the recent literature, a solar cell using the organic-inorganic hybrid such as ZnO: P3HT has been illustrated with the use of piezo-phototronic effect.[69] When the device is under applied tensile strain, P3HT is in

the vicinity of negative piezo-potential. Under the applied tensile strain, the local conduction band level raises resulting in the decrease of Voc while under the compressive strain; the local conduction band of the ZnO is lowered, therefore the Voc is increased.

1.19.2 Piezo-phototronics for photodetector

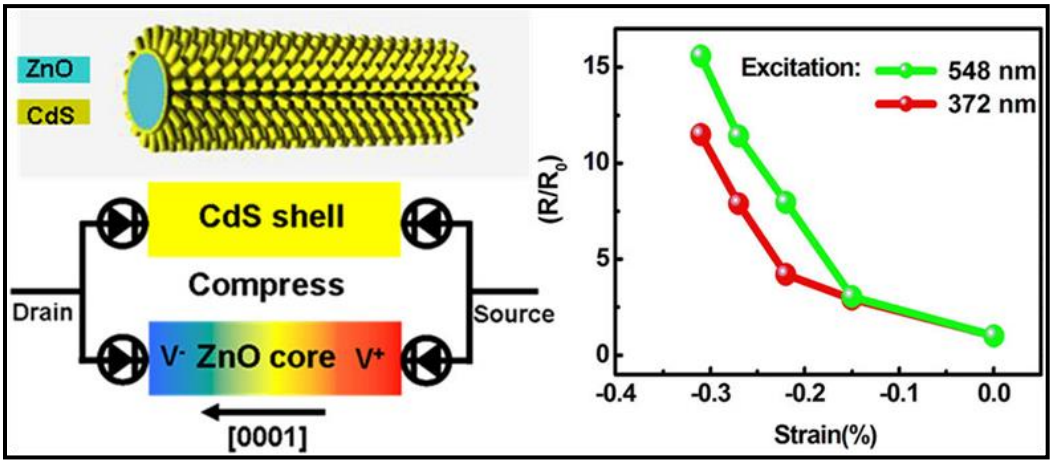

Figure 1.34: Piezo-phototronic effect for performance improvement of Photodetector[70]

Reproduced by the permission of reference 70: *ACS Nano* **2012**, 6, 9229-9236 Copyright (2012) American Chemical Society

The optoelectronic effect is the fundamental principle of the working of photodetector. Thus, excitons are created by the absorption of the light energy and the carriers are separated by p-n-junction or MS contact i.e. Schottky contact. The Schottky barrier height decides the sensitivity of the photodetector in the latter case. The sensitivity of ZnO NW towards this application has been improved, especially under the weak illumination light intensity.[70] The responsivity of the photodetector can be enhanced several times such as by over 500% for 4.1pW, 190% for 120 pW, and 15% for 180.4nW level of light illumination.

1.19.3 Piezo-phototronics for LED:

The LED works on exact opposite principle of that of solar cell i.e. the charge recombination process is necessary for LED. The first experiment on piezo-based LED was carried on n-ZnO and p-GaN based device.[71] The tensile strain was applied (normal) to the junction interface. At an applied bias of 3V, the light emission intensity and the current increased.

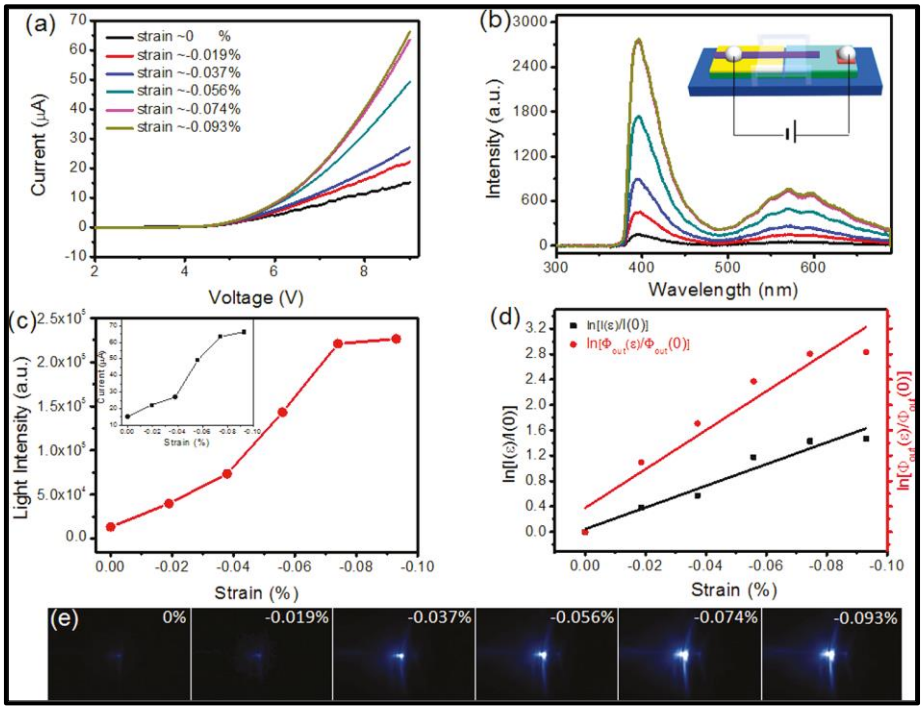

Figure 1.35: Piezo-phototronic effect for performance improvement of LED[71]

Reproduced by the permission of reference 71: *Nano Letters* **2011** *11* (9), 4012-4017

The conversion efficiency was found to be enhanced by the factor of 4 than the devices without application of strain. The data obtained was comparable to or better than the hybrid quantum well LEDs.

1.20 Development of the Nanogenerator for small scale and large scale applications:

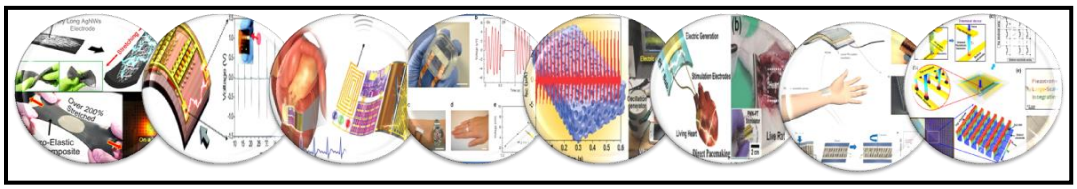

Figure 1.36: Piezo-phototronic effect for performance improvement of LED

[43, 45, 73-78,81]

Reproduced and reprinted by the permissions from references 43, 45 and 73-78, 81.

Since the first demonstration of the piezoelectric nanogenerator, the developments in the field are rapidly progressing towards various applications (figure 1.31). Besides, focusing on the global energy nanogenerator technology targets on the developing the piezoelectric energy harvesting structures for powering micro and nanosystems. Particular application domain includes personal and portable electronics, wearable technologies, implantable biomedical devices, defense technologies etc. Various materials have been used other than the ZnO, such as piezoelectric polymers, (PVDF, P(VDF-TrFE)), Ceramics ($BaTiO_3$, PMN-PT), and composite/hybrid materials for aforementioned applications. Different device designs are also being developed for the high power output.[72] Ceramic based devices are usually brittle in nature and they cannot sustain higher mechanical strain. Recently Prof.K.J.Lee has shown flexible PZT and PMN-PT based energy harvesters which can be used as implantable biomedical devices.[73,74,] Various other studies are being performed for the use of NG technology for in-vivo and in-vitro studies.[75] Transparent and flexible systems are highly recommended for flexible electronics applications.[76,77] Prof.S.W.Kim has shown the use of vertically grown ZnO on the and demonstrated the transparent and flexible nanogenerator which has applications in touch screens. Recently, Xudong Wang *et al* have shown flexible and integrable nanogenerator from PVDF based sponge kind of structures which can provide solution for self powered electric systems.

[78,79]. Composite/hybrid based systems have merits of both components rather than single material acting alone. [80] A variety of the systems have been generated using the hybrid approach for enhanced performance. Carbon based systems such as CNT, graphene, graphitic carbon etc. have been used for stretchable and piezo-elastic composites which can bear high amount of applied load. [81] The developments in the field of piezotronics and piezo-phototronics also emerged simultaneously for the self powered nanosystems and active sensors.[82] A few interesting applications include, the charging of the battery and a supercapacitor using NGs.[83,84] Furthermore, based on the concept of piezo-catalysis, Prof. X. Wang has shown interesting ways of direct mechanical to electrical energy conversion.[85] Another interesting design of NG is developed in the form of a pyroelectric nanogenerator for harvesting thermoelectric energy. These types of NGs convert the thermal energy into electric energy.

The pyroelectric effect arises in certain crystal classes, which show the spontaneous polarization as a result of temperature change. These NGs have applications in medical diagnostics, thermal imaging etc. by harvesting waste thermal energy.[86] The next level of developments in these devices relies mainly for the enhancing the sensitivity even further through enhancements in the coupling coefficients. The rapid advances currently taking place in the field of material science as well as in the designs of different device systems hold a great promise for a viable piezoelectric energy harvesting technology.

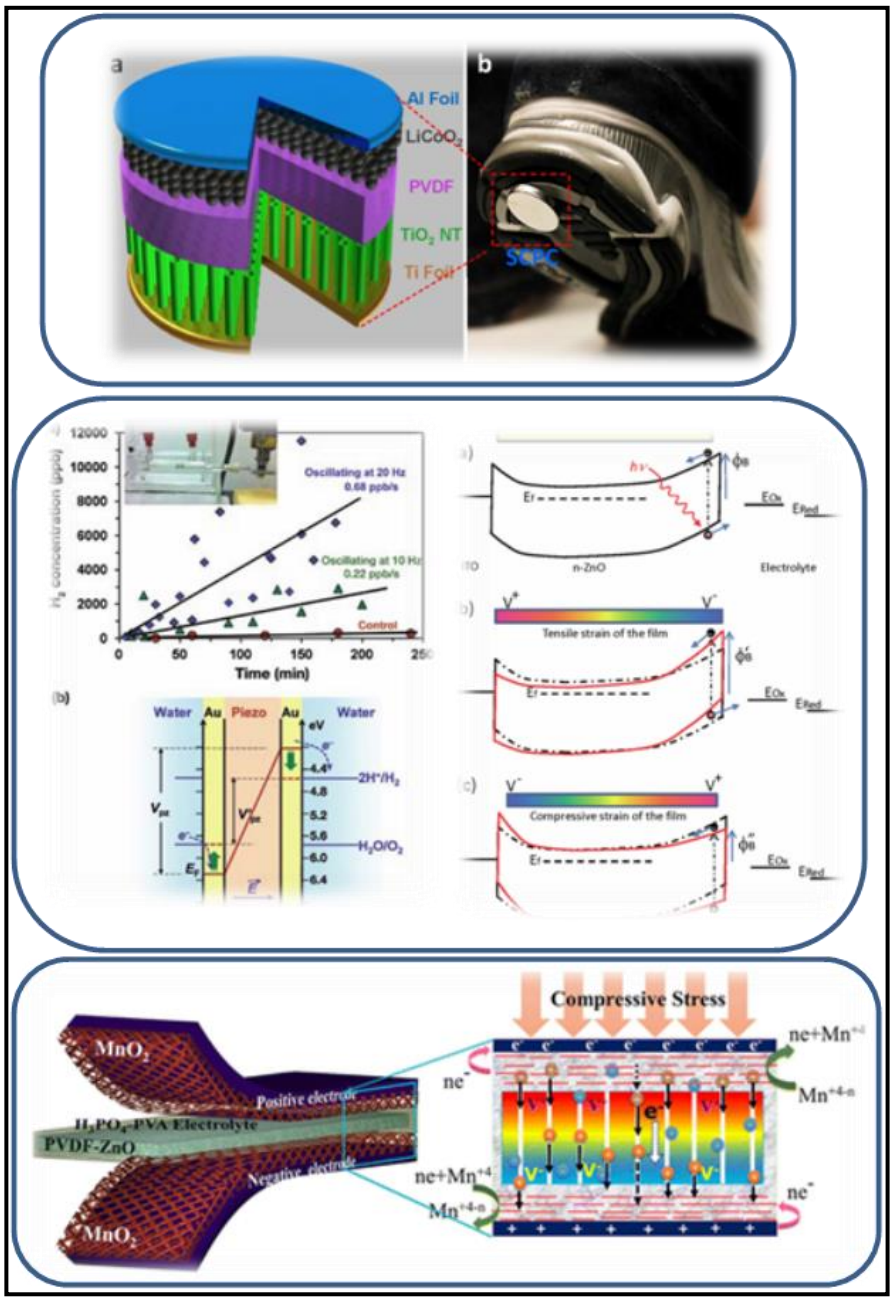

Figure 1.37: Nanogenerator applications for a) Charging of battery[83] b) piezo-catalysis for enhancing PEC performance [85] c) Charging of supercapacitor [84]

Reproduced and reprinted by the permission from references 83-85.

1.21 Triboelectric Nanogenerators:

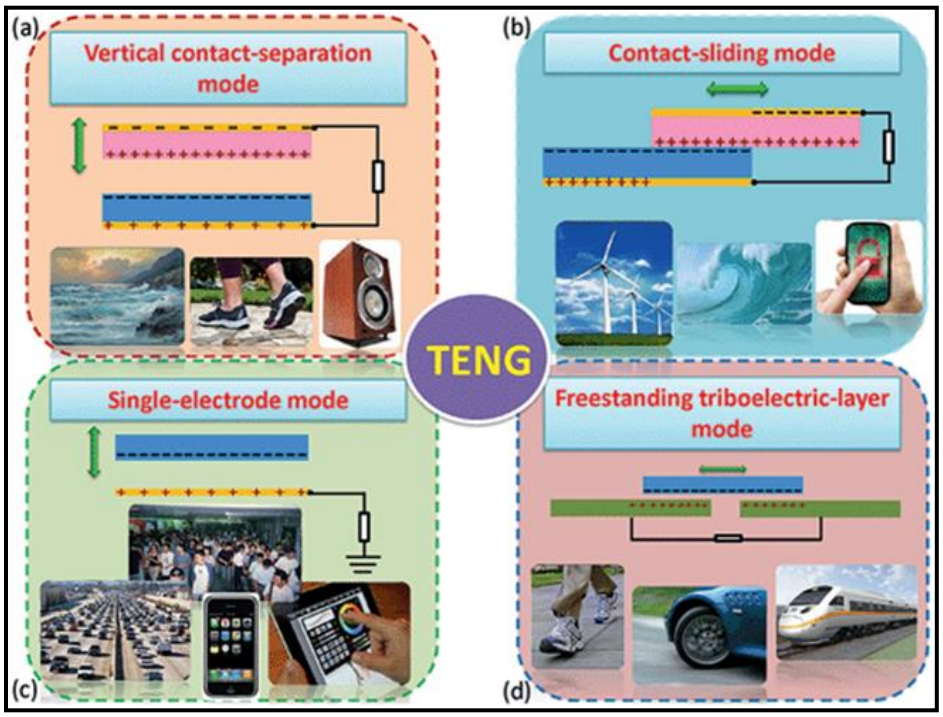

Figure 1.38: Different modes of operation of Triboelectric Nanogenerator [87]

Reproduced by the permission of reference 87: *Faraday Discussions* **2014**, 176, 447-458

For large scale mechanical energy harvesting applications, another type of nanogenerator design has been developed recently, namely triboelectric nanogenerator.[87] The triboelectric effect is well known and is a most common phenomenon around us. The Triboelectric nanogenerator (TENG) was invented using an organic material which converts the mechanical energy into electrical energy. It works on the combined principle of tribo-electrification and electrostatic induction using most of the common materials such as fabrics, paper, and few polymers such as PDMS, PVC, and PTFE etc. Typically, there are four different fundamental modes of the operation of TENG as shown in the figure 1.38. Various mechanical energy sources such as rotation energy, human motions (walking), automobile (rotating tires), wind energy, rain drops, tides or ocean waves and flowing water can be harvested using these types of nanogenerators.

The areal power density of 1200W/m^2, volume density of 490kW/$m^3$and the energy conversion efficiency of about 55-85% has been achieved through the TENGs. Thus, it offers new paradigm for the energy harvesting technologies.

1.22 Plan for the thesis:

Although, piezoelectric nanogenerator concepts and technologies are rapidly evolving, commensurate attention has not yet been given to polymer based flexible system platforms, particularly using piezoelectric electrospun nanofibers. In this thesis we have focused on such piezoelectric nanofiber based flexible systems for strain sensor, piezo-FET and wearable nanogenerator applications.

The **second** chapter presents the methods of synthesis, characterization and device fabrication used in this work, namely electrospinning, different measurements of the basic physical properties of materials, and the fabrication of nanogenerators.

The **third** chapter presents the synthesis of PVDF nanofibers (using electrospinning) with and without addition of hydrated salt i.e. $NiCl_2.6H_2O$ in various proportions, and the corresponding implications for the dynamic strain sensor application. The nanofibers with the added salt show enhanced strain sensitivity and enhanced piezo-voltage.

The **fourth** chapter presents a detailed study of an interface system based on two organic materials namely, P(VDF-TrFE) and Polyaniline. The as-fabricated device shows conductivity modulation of Polyaniline under the mechanical deformation. The device is demonstrated as piezo-FET, where the voltage generated in the P(VDF-TrFE) layer under applied strain acts as the gate voltage for Polyaniline layer. A detailed study of various parameters is performed and presented.

The **fifth** chapter presents an interesting case study of an organic-inorganic hybrid piezoelectric nanogenerator for wearable applications. The composite of P(VDF-TrFE) and $BaTiO_3$ nanofibers deposited directly on a conducting cloth with the $BaTiO_3$ nanofiber-nanoparticle overlayer is shown to produce an impressive

power output of 22μW/cm^2. The power generated is used further to turn on the charging process of a smart phone.

The **sixth** chapter presents the conclusions of the work presented in this thesis and the future scope for further work.

1.23 References

1. World Energy Resources 2013 Survey , Published 2013 by: World Energy Council Registered in England and Wales https://www.worldenergy.org/wp-content/uploads/2013/09/Complete_WER_2013_Survey.pdf
2. World energy consumption. *Wikipedia, The Free Encyclopedia*. https://en.wikipedia.org/w/index.php?title=World_energy_consumption&oldid=669551246
3. World Energy Consumption https://en.wikipedia.org/wiki/World_energy_consumption
4. BBC News http://www.bbc.co.uk/schools/gcsebitesize/geography/energy_resources/energy_rev1.shtml
5. Dana Huggins, Judy Tangata and Rachel Segal http://webpage.pace.edu/jb44525n/page1.html
6. Key World Energy Statistics 2014, http://gnwr1.blogspot.mx/2014/09/key-world-energy-statistics-2014_23.html
7. Energy Statistics 2013 Ministry of Statistics and Programme Implementation , Government of India, New Delhi http://mospi.nic.in/mospi_new/upload/Energy_Statistics_2013.pdf
8. Renewable Energy https://en.wikipedia.org/wiki/Renewable_energy
9. Advanced Materials for Our Energy Future https://mrs.org/advanced-online/
10. IDTechEx, October 2010, Energy Harvesting and Storage for Electronic Devices 2010-2020,
11. Energy Harvesting Technologies, Shashank Priya, Daniel J. Inman http://link.springer.com/book/10.1007%2F978-0-387-76464-1
12. Types of energy harvesting materials http://www.iop.org/resources/energy/
13. A Survey of Energy Harvesting Sources for Embedded Systems, Chalasani, S.,Conrad,J.M.,IEEE-Southeastcon-2008, http://ieeexplore.ieee.org/xpl/articleDetails.jsp?arnumber=4494336
14. Development of Energy Harvesting Sources for Remote Applications as Mechatronic system. Hadas, Z., Vechet, S., Ondrusek, C., Singule, V., Microsyst Technol (2012) 18:1003-1014.
15. Thermoelectric Energy Harvesting, Paul, D.J., School of Engineering, University of Glasgow. http://www.nipslab.org/files/Paul.pdf.

16. Overview of Energy Harvesting Systems (for low-power electronics), Park, G., Engineering Sciences & Applications Los Alamos National Laboratory, http://institutes.lanl.gov/ei/_docs/Annual_Workshops/Overview_of_energy_harvesting_systemsLA-UR_8296.pdf.
17. Acoustic energy harvesting using quarter-wavelength straight-tube generator, Li, B., Laviage, A. J, Proceedings of the ASME 2012 International Mechanical Engineering Congress & Exposition.
18. Ragone plot energy storage https://en.wikipedia.org/wiki/Ragone_chart
19. Guoping Wang, Lei Zhang and Jiujun Zhang, Chem. Soc. Rev., 2012,41, 797-828
20. John B. Goodenough and Kyu-Sung Park, J. Am. Chem. Soc., 2013, *135* (4), pp 1167–1176
21. Marek Matak, Peter Šolek, American Journal of Mechanical Engineering, 2013, Vol. 1, No. 7, 438-442
22. Introduction to Vibration energy harvesting, Cottone, F, NiPS, Energy Harvesting Summer School August 1-5, 2011
23. Vibration energy harvesting for Civil Infrastructure Monitoring Jia, Y., Mair, R., Yan, J., Soga, K., Seshia, A., Department of Engineering, University of Cambridge, http://eh-network.org/events/eh2013/speakers/2.1.pdf.
24. Magnetostrictive Energy Harvesters and Applications (Energy Harvesting and StorageUSA2012):IDTechEx http://www.idtechex.com/events/presentations/magnetostrictive-energy-harvesters-and-applications-003554.asp
25. Curie, Jacques and Curie, Pierre (1880). Bulletin de la Societe de Minerologique de France, 3: 90-93.
26. Curie, Jacques, and Curie, Pierre (1881). Comptes Rendus 93: 1137-1140.
27. A. L. Kholkin, N. A. Pertsev, A. V. Goltsev Piezoelectric and Acoustic Materials for Transducer Applications 2008, pp 17-38
28. J. Valasek (1920). Physical Review 15: 537.
29. J. Valasek (1921). Physical Review 17 (4): 475
30. Brewster, David (1824). The Edinburgh Journal of Science **1**: 208–215.

31. History of the First Ferroelectric Oxide, $BaTiO_3$ C.A. Randall, R.E. Newnham, and L.E. Cross
32. H.D. Megaw, Nature 155 484 (1945)
33. S. Miyake and R. Ueda, J. Phys. Soc. Jap. 1 32 (1946)
34. Kawai, Heiji (1969). Japanese Journal of Applied Physics **8** (7): 975.
35. T. Furukawa, in Phase Transitions, Vol. 18, pp. 143–211 (1989).
36. Lovinger, A.J. (1983). Science, 220 (4602): 1115–1121.
37. Davis, G. T., McKinney, J. E., Broudhurst, M. G. & Roth, S. C. J. Appl. Phys. 49, 4998–5002 (1978).
38. Nalwa, H. (1995). , New York: Marcel Dekker,
39. Micro Energy Harvesting Danick Briand, Eric Yeatman, Shad Roundy John Wiley & Sons, 21-Apr-2015 - Technology & Engineering
40. Xue-Qian Fang, Jin-Xi Liu and Vijay Gupta, Nanoscale, 2013, 5, 1716
41. Dragan Damjanovic 1998 Rep. Prog. Phys. 61 1267
42. Chang, Jiyoung, Dommer, Michael, Chang, Chieh, Lin, Liwei Nano Energy, Volume 1, 3, 2012,356–371
43. Luana Persano, Canan Dagdeviren, Yewang Su, Yihui Zhang, Salvatore Girardo, Dario Pisignano, Yonggang Huang& John A. Rogers Nature Communications 4, Article number:1633
44. Yi Qi, Jihoon Kim, Thanh D. Nguyen, Bozhena Lisko, Prashant K. Purohit, and Michael C. McAlpine Nano Letters 2011 11 (3), 1331-1336
45. Kwi-Il Park, Sheng Xu, Ying Liu, Geon-Tae Hwang, Suk-Joong L. Kang, Zhong Lin Wang, and Keon Jae Lee Nano Letters 2010 10 (12), 4939-4943
46. Sung-Ho Shin, Young-Hwan Kim, Joo-Yun Jung, Min Hyung Lee and Junghyo Nah, Nanotechnology, 2014, 25, 485401.
47. Kwon-Ho Kim , Brijesh Kumar , Keun Young Lee , Hyun-KyuPark , Ju-Hyuck Lee , Hyun Hwi Lee, Hoin Jun , Dongyun Lee , Sang-Woo Kim, Scientific Reports 3, Article number:2017
48. M. Minary-Jolandan, R. A. Bernal, I. Kuljanishvili, V. Parpoil and H. D. Espinosa, Nano Lett., 2012, 12, 970

49. Zhong Lin Wang and Jinhui Song. Science 14 April 2006: 312 (5771), 242-246.
50. Zhong Lin Wang, MRS BULLETIN • VOLUME 37 • SEPTEMBER 2012
51. Piezotronics and piezo-phototronics: fundamentals and applications Zhong Lin Wang and Wenzhuo Wu, National Science Review 1: 62–90, 2014
52. Chieh Chang, Van H. Tran, Junbo Wang, Yiin-KuenFuh, and Liwei Lin Nano Letters 2010 10 (2), 726-731
53. Sheng Xu, Yong Qin, Chen Xu, Yaguang Wei, Rusen Yang & Zhong Lin Wang Nature Nanotechnology 5, 366 - 373 (2010)
54. Zhong Lin Wang , Rusen Yang, Jun Zhou, Yong Qin, Chen Xu, Youfan Hu, Sheng Xu Materials Science and Engineering R 70 (2010) 320–329
55. Momeni, K.; Odegard, G. M.; Yassar, R. S. (2010). Journal of Applied Physics 108 (11): 114303.
56. Zhong Lin Wang, Adv. Mater. 2012, 24, 280–285
57. Shengnan Lu, Junjie Qi, Shuo Liu, Zheng Zhang, Zengze Wang, Pei Lin, Qingliang Liao, Qijie Liang, and Yue Zhang ACS Applied Materials & Interfaces 2014 6 (16), 14116-14122
58. Balasubramaniam Saravanakumar, Shin Soyoon, and Sang-Jae Kim ACS Applied Materials & Interfaces 2014 6 (16), 13716-13723
59. Ya Yang, Hulin Zhang, Guang Zhu, Sangmin Lee, Zong-Hong Lin, and Z hong Lin Wang ACS Nano 2013 7 (1), 785-790
60. Benjamin J. Hansen, Ying Liu, Rusen Yang, and Zhong Lin Wang ACS Nano 2010 4 (7), 3647-3652
61. Yu, Aifang , Jiang, Peng, Lin Wang, Zhong , Nano Energy, Volume 1, Issue 3, May 2012, Pages 418–423
62. Dipankar Mandal, Sun Yoon and KapJin Kim Macromolecular Rapid Communications, Volume 32, Issue 11, pages 831–837, June 1, 2011
63. Jun Zhou, Yudong Gu, Peng Fei, Wenjie Mai, Yifan Gao, Rusen Yang, Gang Bao, and Zhong Lin Wang Nano Letters 2008 8 (9), 3035-3040

64. Sang-Hoon Bae, Orhan Kahya, Bhupendra K. Sharma, Junggou Kwon, Hyoung J. Cho, Barbaros Özyilmaz, and Jong-Hyun Ahn ACS Nano 2013 7 (4), 3130-3138
65. Xudong Wang, American Ceramic Society Bulletin, Vol. 92, No. 6
66. Wenzhuo Wu, Yaguang Wei , and Zhong Lin Wang, Adv. Mater. 2010, 22, 4711–4715.
67. Introduction of Piezotronics and Piezo-Phototronics, Z.L. Wang, Piezotronics and Piezo-Phototronics, Microtechnology and MEMS, Springer-Verlag Berlin, Heidelberg 2012, pp 1-17
68. Zhong Lin Wang, Nano Today., (2010) 5, 540—552.
69. Ya Yang, Wenxi Guo, Yan Zhang, Yong Ding, Xue Wang, and Zhong Lin Wang Nano Letters 2011 11 (11), 4812-4817
70. Fang Zhang, Yong Ding, Yan Zhang, Xiaoling Zhang, and Zhong Lin Wang ACS Nano 2012 6 (10), 9229-9236
71. Qing Yang, Wenhui Wang, Sheng Xu, and Zhong Lin Wang *Nano Letters* **2011** *11* (9), 4012-4017
72. Youfan Hu, Zhong Lin Wang, Nano Energy, Volume 14, May 2015, Pages 3–14
73. G. Hwang, H. Park, J. Lee, S. Oh, K. Park, M. Byun, H. Park, G. Ahn, C. Jeong, K. No, H. Kwon, S. Lee, B. Joung, K. Lee, Adv. Mater., 26, 4880, 2014,
74. Seung Hyun Lee , Chang Kyu Jeong, Geon-Tae Hwang, Keon Jae Lee Seung Hyun Lee , Chang Kyu Jeong, Nano Energy (2015) 14, 111–125
75. Z Li, G Zhu, R Yang, AC Wang, ZL Wang - Advanced Materials, 2010, 22, 2534–2537.
76. Changhyun Pang, Gil-Yong Lee,Tae-il Kim,Sang Moon Kim,Hong Nam Kim,Sung-Hoon Ahn & Kahp-Yang Suh Nature Materials11,795–801, (2012)
77. Wenzhuo Wu, Xiaonan Wen, and Zhong Lin Wang Science 24 May 2013: 340 (6135), 952-957.

78. Yanchao Mao, Ping Zhao, Geoffrey McConohy, Hao Yang, Yexiang Tong and Xudong Wang Advanced Energy Materials Volume 4, Issue 7, May 13, 2014
79. Min-Yeol Choi, Dukhyun Choi, Mi-JinJin, Insoo Kim, Sang-Hyeob Kim, Jae-Young Choi, Sang Yoon Lee, Jong Min Kim, and Sang-Woo Kim, Adv. Mater. 2009, 21, 2185–2189
80. Minbaek Lee, Chih-Yen Chen, Sihong Wang, Seung Nam Cha, Yong Jun Park, Jong Min Kim, Li-Jen Chou, Zhong Lin Wang Volume 24, Issue 13 April 3, 2012 Pages 1759–1764
81. Chang KyuJeong, Jinhwan Lee, Seungyong Han, Jungho Ryu, Geon-Tae Hwang, Dae Yong Park, Jung Hwan Park, Seung Seob Lee, Myunghwan Byun, Seung Hwan Ko, Keon Jae Lee Volume 27, Issue 18 May 13, 2015Pages 2866–2875, Advanced Materials
82. Z.L.Wang ,Nano Today, Volume 5, Issue 6, December 2010, Pages 540–552
83. Xinyu Xue, Sihong Wang, Wenxi Guo, Yan Zhang, and Zhong Lin Wang Nano Letters 2012 12 (9), 5048-5054
84. Ananthakumar Ramadoss, Balasubramaniam Saravanakumar, Seung Woo Lee, Young-Soo Kim, Sang Jae Kim, and Zhong Lin Wang ACS Nano 2015 9 (4), 4337-4345
85. M.B. Starr, X.D. Wang, Scientifc Reports, 3, 2160 (2013).
86. Ya Yang, WenxiGuo, Ken C. Pradel, Guang Zhu, Yusheng Zhou, Yan Zhang, Youfan Hu, Long Lin, and Zhong Lin Wang Nano Letters 2012 12 (6), 2833-2838
87. Zhong Lin Wang, Faraday Discussions 2014, 176, 447.

Chapter 2

Experimental Methods, Characterization Techniques and Device Fabrication

This chapter presents the synthesis techniques, characterization tools, device fabrication and device testing protocols used in this thesis. Firstly, the process of electrospinning is discussed at length. The effect of internal and external factors on this process is also discussed. Further characterization tools used for elucidation of the structure, composition and piezoelectric, dielectric and ferroelectric properties are covered in details. The nanogenerator (NG) device fabrication protocol and testing of the corresponding quality factors such as output voltage, output current, and the power output per unit area is also included.

Introduction: This chapter covers the experimental methods, materials characterization techniques and device fabrication protocol used in this thesis. As this thesis is mainly based on electrospun nanofibers (NFs) the details of electrospinning are covered initially. Further the characterization tools used for compositional property analysis and surface morphology are covered at length. Towards this end we have given the details of nanogenerator fabrication part along with its testing protocols.

Section I

2.1 The Electrospinning Technique:

One dimensional NFs of polymer based materials, metal oxides; metal chalcogenides can be easily synthesized through various routes such as template directed synthesis, solution processible routes such as the solvothermal techniques, vapour phase growth approach, solution based growth using various capping agents, self-assembly and electrospinning. Amongst these approaches, electrospinning is considered to be a very popular route in research as well as the industrial context. This technique allows bulk scale as well lab scale synthesis of one dimensional NFs. The brief history, working mechanism, and various aspects of electrospinning are discussed in details in the following paragraphs.

2.2: Electrospinning:

Electrospinning has been a technologically viable manufacturing process, especially since last decade. It is a versatile and simple method for producing continuous one dimensional nanofibers (NFs). It has captured the attention of the research community as well as industries covering a range of applications such as tissue engineering, energy storage, photovoltaic, catalysis, gas/water filtration membranes and flexible electronics. [1] It can produce NFs with diameters in the range of few nanometers to micron. This method can be used for natural, synthetic polymers as well for mixed polymer blends and composites with nanoparticles of metal oxides/sulfides and various inorganic ceramics.

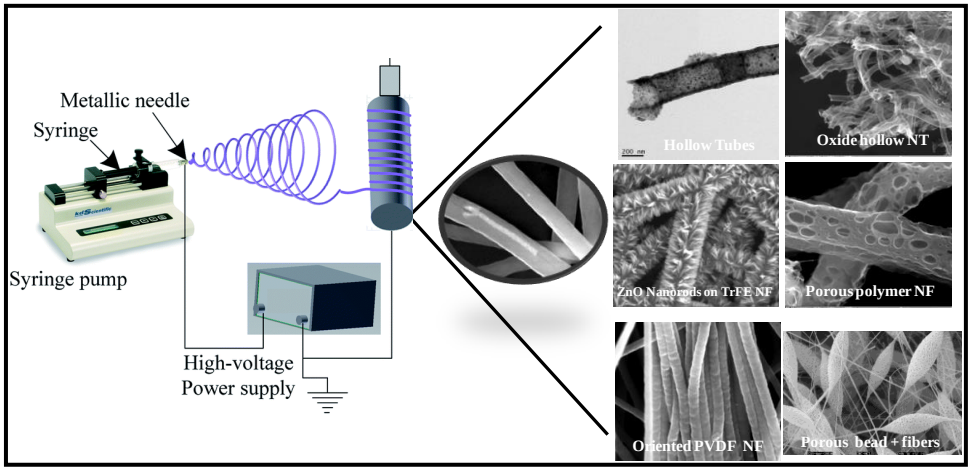

Figure 2.1: Electrospinning set up and SEM for various morphologies obtained using electrospinning

Interestingly, using this technique single nanofiber or well aligned mesh of NFs can be prepared on large scale. The figure 2.2 shows the process of formation of NFs. These NFs are having even thinner diameters than human hair and possess high specific surface area, which makes them suitable for many applications.

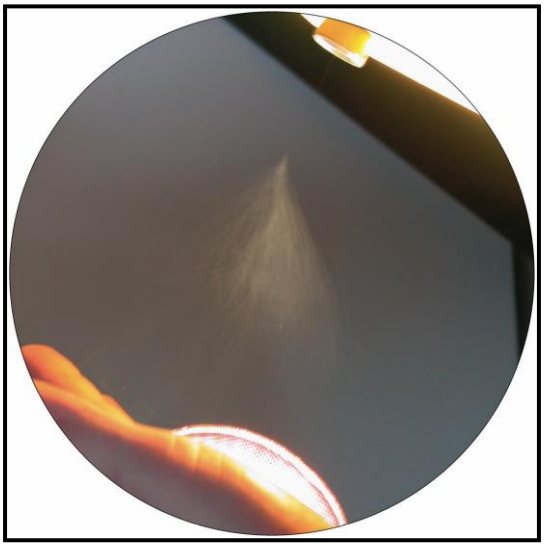

Figure: 2.2 The electrospinning jet and NF formed on collector [2]

Reproduced by the permission from reference 2: *Angewandte Chemie,* **2007**, 46 (30) 5670-5703.

2.2.1 History of Electrospinning:

The tools for the weaving and the spinning have been used since many centuries. Especially, the origin for different textile based spinning has been found in various countries. Earlier, particularly in India, the mechanical spinning was used as main tool for making fabrics. [2] Electrospinning is rather new technique which has its basis in the year 1745. It was also known as electrostatic spinning at that time. [3] After the earlier experiments, around 1902, Cooley and Morton, used a device to spray the liquids with applied electric field. [4,5] In the year 1934, this technique got the first patent reported by Anton Formhals. [6] Simm *et al.* discovered and patented the procedure for obtaining fibers with less than 1 μm diameter. [7] The first commercialized application of this technique was in the filtration membrane domain. [8] Later on the technique was established and many more contributions were made for various applications. The substantial number of patents and research publications reflects the versatility and advantages of this technique in rapid development in different fields.

2.2.2 Electrospinning process & working mechanism:

The electrospinning set up usually consists of,

a. High voltage power supply
b. Syringe pump
c. Syringe with needle tip to which positive electrode is connected
d. Collector

The conventional electrospinning set up uses either vertical or horizontal arrangement. The bore diameter of the needle used for spinning primarily decides the NF diameter. The voltage applied is in the range of kilovolts from 10-50kV. The typical distance between needle tip and collector is 10-20 cm. The nanofiber formation process mainly occurs due to stretching of polymer solution in the presence of applied electric field. The polymer solution of approximately 5-10 wt% is homogeneously prepared. The, solution is feeded using syringe pump. When the drop experiences the applied electric field, the surface tension quickly

changes and it results in cone formation due to stretching. This cone is called as Taylor cone as shown in the figure 2.2. At higher voltages, the electric field exceeds the surface tension of the drop and the jet of elongated NFs is deposited on to the collector. Depending on the polymer solution properties, at sufficiently higher potentials, the ejected jet begins to whip in the presence of electric field towards the collector plate. During this process due to sudden elongation the surface area of polymer fibers is increased which results in effective evaporation of solvent. This results in NF formation. The as synthesized NFs are mainly randomly oriented and form the self-supporting fiber mat.

2.2.3 Methods for alignment of the electrospun NFs

The alignment of the NFs has always been a challenge for the researchers. Usually, randomly oriented fibers/mats are deposited on the collector plate. Efforts have been taken to sort out this issue by using, rotating cylindrical collectors, including, drums, circular disks etc. The Boland et al first used the rotating collector while electrospinning process. [9] Later on various other modifications have also been explored for the fiber alignment. Later the variation in the applied electric field has been used to obtain continuous aligned NF. Li *et al* demonstrated that, two electrodes with a gap (separation) in between can be put on the collector, to align the fibers in between the gap. [10] Apart from this, more recently, the near field i.e. very short electrode-collector distance (in micrometer range) arrangement has also shown successful alignment of NFs.[11] Further another interesting approach of making core shell NFs for various applications is also shown in recent years. Core shell NFs are produced using co-axial syringes. The figure 2.3 (a and b) below shows the set up for the co-axial electrospinning.

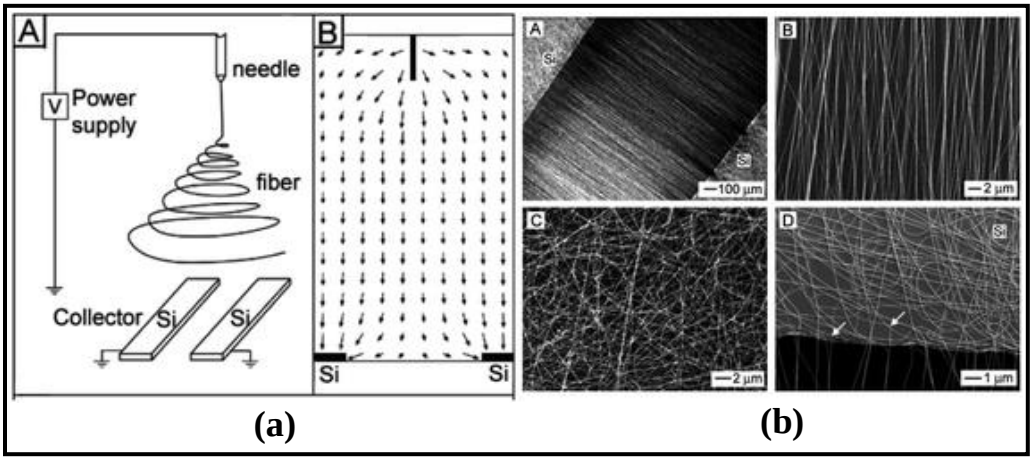

Figure: 2.3 a) A) Electrospinning set up for the formation of aligned NF and B) electric field vectors in the region between needle and collector. b) The SEM images orientation of PVP NF with varying gap distance [10]

Reprinted with permission from reference 10 (*Nano Letters* **2003,** 3 (8), (1167-1171). Copyright (2003) American Chemical Society

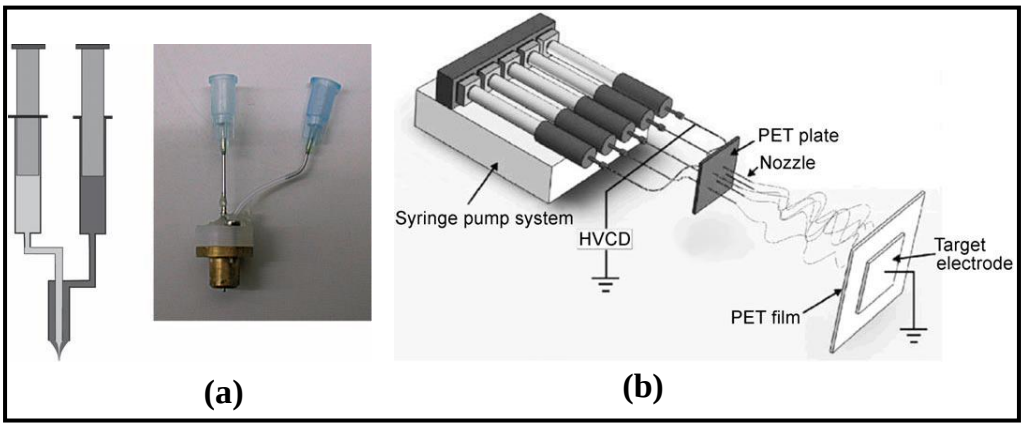

Figure: 2.4 a) An experimental set up for coaxial electrospinning b) An experimental set up for multijet electrospinning [2]

Reproduced by the permission of reference 2: *Angewandte Chemie*, **2007**, 46 (30) 5670-5703.

It consists of two nozzles, which are concentrically connected. The applied voltage is same for both the electrodes. The applied voltage deforms the drop of individual polymer jet form core and sheath to produce core-shell NF. Variety of

materials can form core-shell NFs using co-axial electrospinning. [12] Interestingly, this approach can be used for variety of applications. e.g. for the insertion of biologically active different drugs in core fibers as well in shell fibers.[13] Few additional efforts have also been taken to produce hollow core-shell NFs using co-axial electrospinning. [14] Other than, co-axial, multijet electrospinning technique also has number of applications, which use multiple syringes connected in parallel arrangement. It is particularly used for tissue engineering applications. [15]

2.2.4 Types of Electrospinning:

2.2.5 Near field electrospinning

The method used for controlling the nanofiber alignment is called as near field electrospinning**.** In this method, the needle to collector distance is just in few microns, i.e. less than millimeter and the applied voltage is also in the range of 1-3 kV. In initial experiments, dip pen kind of approach was demonstrated. Later on near field electrospinning technique was developed using normal syringes, in order to deposit continuous NF by feeding polymer solution. [11] It has advantage over conventional electrospinning set up, as it possess more control on fiber deposition and alignment. Thus, these methods can be used to fabricate aligned NFs on flexible substrate as large arrays mainly for NG applications. [16]

2.2.6 Conventional Far field electrospinning:

During electrospinning process, when the high voltage is applied to polymer solution, the drop elongates and forms cone called as Taylor cone. If the tip to collector distance is far away, e.g.10-20 cm, the drop experiences swirling and deposits in a random fashion on the collector. This is the mechanism for the conventional, far-field electrospinning. The fibers diameter produced by this type of electrospinning is usually in the range of few hundreds of nanometers and the applied field is 10-40 kilovolts. Interestingly, this process has been further modified by using rotating collector drums, disks etc. for various applications.

2.2.7 Factors affecting electrospinning

There are mainly two prime parameters responsible for smooth nanofiber formation, namely internal and external parameters. Internal parameters include the polymer solution properties such as conductivity, viscosity, polymer concentration. In addition to this, surface tension, molecular weight of polymer and solvent boiling point are also important factors. By considering the above parameters the basic criteria include the choice of appropriate solvent for the polymer dissolution. The complete polymer chain entanglement has to take place in order to form homogenous and uniform solution. The solvent should preferably possess lesser boiling point, for the quick solvent evaporation during electrospinning. The polymer molecular weight also plays an important role, as high molecular weight polymer structures entangle due to their long chain structures. The chain entanglement is a critical parameter for stabilizing the jet during bending and stretching of polymer liquid drop in electric field. Thus, the molecular weight should be optimum in order to control the flow of the polymer solution. The viscosity and polymer concentration also affects the fiber formation in the similar manner. The conductivity of the solution is also important parameter which critically decides the fiber formation process. Under the applied electric field, the solution with higher conductivity experiences more elongation; this reduces the fiber diameter as well as bead formation, if any. The surface tension also controls the fiber formation, by eliminating the beads in the fibers.

The external parameters also have impact on the electrospinning process. These include the volumetric feed/flow rate, needle tip-to collector distance, electric field and the needle diameter. The applied electric voltage is one of the crucial factors in the formation of Taylor cone. The applied voltage mainly affects the fiber diameter or sometimes it may lead to bead formation also. [17] The applied voltage mainly affects the elongation/stretching of the drop. [18] The feed rate of the polymer solution is another important parameter; this affects the solidification process of the nanofiber. The slower feed rate is always preferred as it allows the sufficient time for solvent evaporation and stretching of the liquid drop for

formation of bead free nanofiber. [19] The distance between the needle and collector also affects the fiber formation process during electrospinning. If this distance is short, the nanofiber does not have enough time for solidification whereas if the distance is too long, the bead formation possibility increases.

2.2.8 Applications of electrospinning technology:

Since the discovery, various groups have contributed towards the rapid development in the field of electrospinning technology. The current progress is chiefly towards the applications of the NF in various areas as can be seen from the figure 2.5. The electrospun NFs are found to be useful mainly in the nanotechnology areas such as water purification membranes, heterogeneous catalysis, biomedical applications such as drug delivery, tissue engineering. As this process provides versatility for making NFs of polymers, metal oxides, chalcogenide family this technique is also found to be suitable in energy storage applications. In addition to this, the polymer NFs gives high mechanical strength and flexibility which are useful for currently growing flexible electronic devices based research. [1]

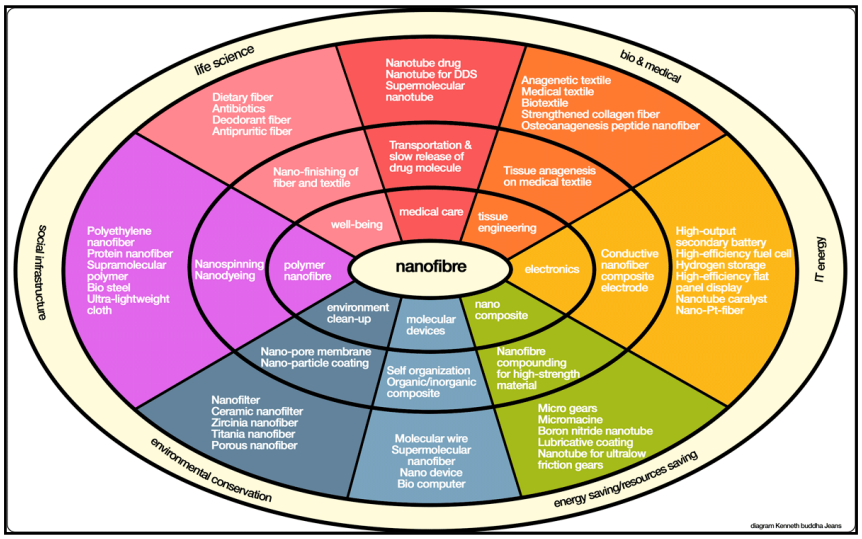

Figure: 2.5 Applications of NF in various fields.

http://buddhajeans.com/2015/03/15/nanotechnology-in-the-textile-and-fashion-business-part-ii/

2.3 Spin Coating:

Spin coating is the widely used technique to deposit thin films of various materials such as polymers, metal oxide suspensions, proteins etc. on smooth and flat surface, [20]

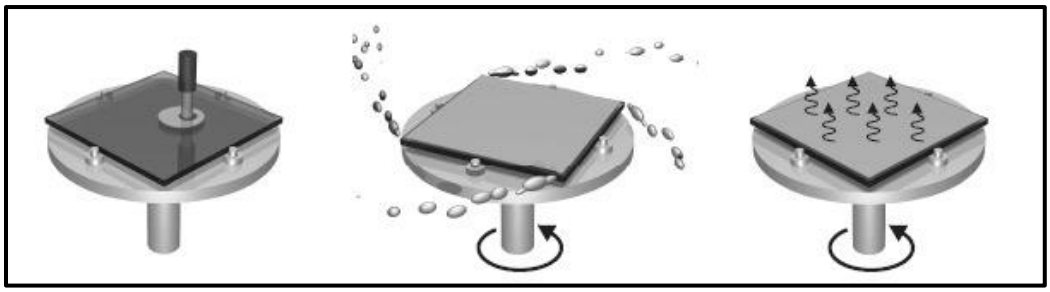

Figure: 2.6 The process of spin coating

Thesis: Ultra-thin Films of a Ferroelectric Copolymer: P(VDF-TrFE)" Dipankar Mandal , Brandenburgische Technische Universität Cottbus, Germany, 2008

This process involves the deposition of viscous solution onto the clean substrate, at the center (as can be seen from the figure 2.6). The substrate holder, then rotated at a fixed rotations per minute (RPM) (1000-6000) depending on the desired thickness of the film. During this process, solution is spread in the outward direction, due to centrifugal force. Excess amount of solution spills out and solvent evaporation takes place during this process. This rapid solvent evaporation increases the viscosity of desired material remaining on the substrate. Hence the adhesion to the substrate is improved and film is formed. This process also provides an advantage of making multilayered structures. In case of programmable spin coater, the speed of rotation can be adjusted using the acceleration; even lowest rpm as 100 is also possible. The film thickness and the uniform coverage of film are mainly dependent on the solution properties such as viscosity, surface tension, solvent evaporation rate etc.

Section II: Characterization Techniques

Introduction: This section covers the various characterization tools used in this thesis for understanding the composition and properties of NFs synthesized by electrospinning. The crystal structure and composition of NFs are mainly obtained by recording X-ray diffraction analysis (XRD) and Fourier transform infrared spectroscopy (FTIR). For morphology and lattice arrangement analysis Scanning electron microscope (SEM) and Transmission electron microscope (TEM) respectively. Further for dielectric properties and ferroelectric properties are NFs are studied. The details of Dynamic mechanical analyzer are also discussed towards end.

2.4 X-ray Diffraction (XRD):

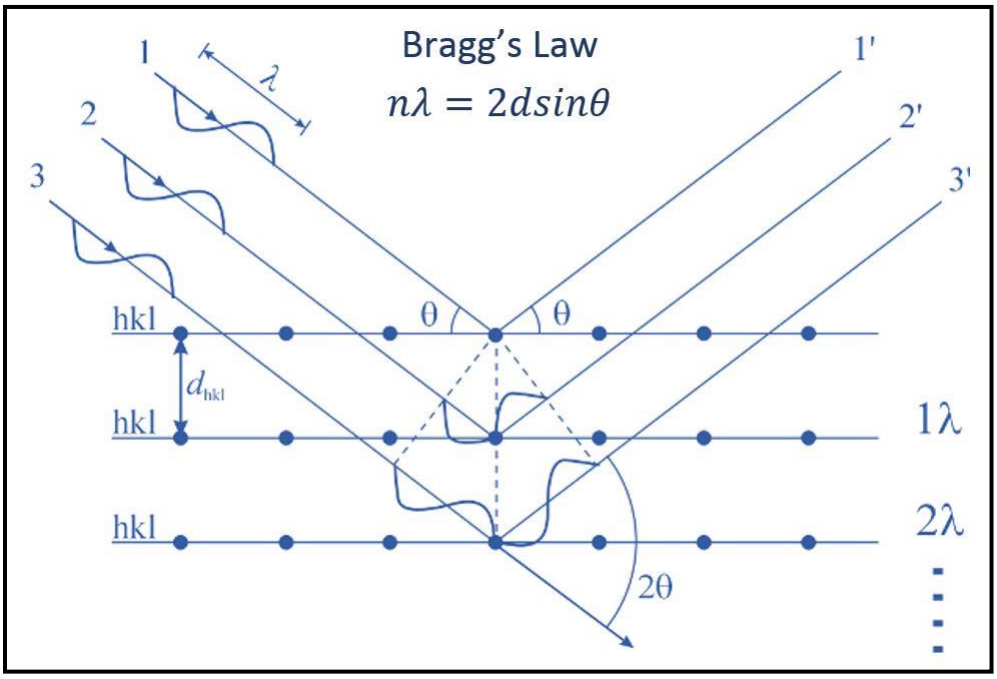

Figure: 2.7 The working principle of XRD

http://www.veqter.co.uk/residual-stress-measurement/x-ray-diffraction

XRD is a versatile and important tool for characterization, particularly in the field of Materials Science. It is a non-destructive technique for the identification of the crystallographic phase and the unit cell dimensions. [21] Interestingly, this

technique can be used for both the bulk and the nano-materials, even in the powder form. It is also used for determination of anisotropic crystal growth as it is a long range order technique. X-rays are the electromagnetic waves with the wavelength in the range of few angstroms. W.L.Bragg and W.H.Bragg first established the relation between wavelength of the incident radiation (λ) and the interplanar distance in any crystal (*d*).

In their study they assumed that these incident monochromatic X-rays constructively interfere with the crystalline sample which possess regular and long range ordered structure. The reflected rays interfere constructively, if the path difference is nλ where n is the integer n = 1,2,3,…

Thus, they mathematically derived the equation which is called as Bragg's law

$$n\lambda = 2d\sin\Theta \text{ where } n= 1, 2, 3,\ldots \text{ (Order of diffraction)}$$

$$\Theta = \text{incident angle}$$

With this Bragg equation, inter-planar spacing can be calculated, if the Θ and λ are known. The constructive interference patterns created, can be converted into XRD pattern. The generated XRD patterns can be used as fingerprints for the particular material. In addition, useful information such as crystalline structure (e.g. cubic, orthorhombic, perovskite etc.), and degree of crystallinity can be obtained as well. Different modes of operation of XRD are available such as, Θ-2Θ scan mode, Θ-2Θ rocking mode and φ scan mode. In case of Θ-2Θ scan mode, the monochromatic beam of X-rays is incident upon the sample, making an angle 'Θ' with the beam direction. The X-Ray source and the detector motion are coupled with each other, so as to have an angle of 2Θ, between the incident beam directions, each time. We thus get the diffraction pattern with intensity recorder by the detector versus the angle 2Θ. The incident X-Ray beam, may reflect in various directions, but will get measured only at one angle. Thus, the precondition is that, angle of incident should be equal to angle of reflectance. The X-ray diffraction shows sharp peak for highly crystalline material whereas broadening occurs due to smaller crystallite size in amorphous, quantum structures and

polymer based samples. The crystallite size can be calculated using, Debye-Scherer's formula as,

$$d = \frac{k\lambda}{\beta cos\Theta}$$ where k= Scherer's Constant ≈ 0.94

β = Full Width at Half Maximum (FWHM) of XRD peak.

The only limitation of XRD is for low atomic number materials. For such cases, sometimes, electron or neutron diffraction is used. In the present thesis, the XRD patterns for all the samples were recorded using Pananalytical Philips X'Pert PRO powder diffractometer. The sources of radiation used was, Cu-Kα (λ = 1.542 Aº).

2.5 Fourier Transform Infrared Spectroscopy (FT-IR) :

The infrared rays are the electromagnetic waves, which have wavelength in the range of 1 μm and 1 mm. These are majorly categorized into, near IR, middle IR and far IR. The middle IR range (Wavelength range 2.5 - 50 μm) is predominantly used in infrared spectroscopy. This spectrum appears when the, the vibrations within the bonded atoms create fluctuations in the dipole moment of the molecule. Thus, it is usually considered that, more the polar molecules more will be the intensity of the IR spectrum for the particular bond vibrations. If the frequency of the IR radiation matches with the characteristic vibrations of the molecule/atom, the IR radiations are then absorbed by the molecule. The spectrum is thus obtained as, intensity of the absorption band corresponding to particular vibration mode. From this spectrum, we can have information about the chemical bonds as well as the composition.

The IR spectrophotometer consists of, source, monochromator and the detector. [22,23] The source is usually, filament which is maintained by the electric current. The monochromator functions as focusing of the IR beam. The detector is usually based on the rise of either temperature or the conductivity variation at a particular frequency.

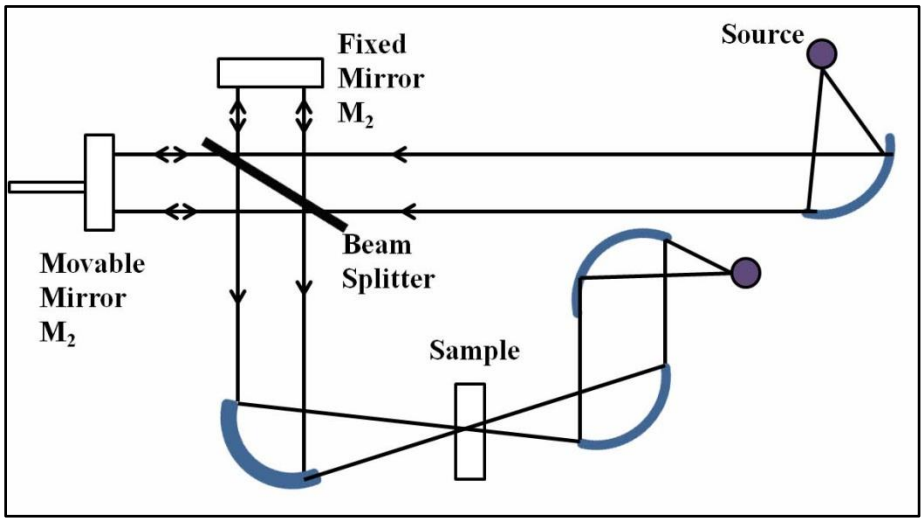

Figure: 2.8 Working Principle of spectrophotometer [22]

Reproduced and reprinted by reference 22: Fundamentals of molecular spectroscopy Book by C. N. Banwell McGraw-Hill, 1994 - Science - 308 pages

The parallel beam of incident radiation is directed from source to the interferometer. B is the beam splitter and M_1, M_2 are the two mirrors. The apparatus designed from the basic concepts of Michelson- Mirror experiment. The beam splitter is made up of suitable transparent materials, which can reflect the 50% of radiations falling on it. The remaining half radiation then goes to the mirrors namely, M_1 and M_2. It is then returned along the same path, and recombined at the beam splitter to a single beam. It is well known that, if the monochromatic radiation emitted by the source is spilt and recombined at beam splitter, the beam shows the constructive or destructive interference. It will depend on the path length from B to M_1 and B to M_2. If these path lengths are identical, or integral multiple of wavelength then constructive interference takes place giving bright beam, while if the difference is a half integral number of wavelength, beam cancels at B. The spectrum is produced in two stages 1) without the sample, the mirror M_2 is moved slowly with approximate distance of 1 cm, while the interferogram is recorded into multi-channel computer. The computer then carries, Fourier Transform of the stored data and produces background spectrum. 2) With sample, the interferogram is recoded in the same

way and Fourier transform data is generated. The ratio of the background and sample spectrum is then plotted as transmittance spectrum. Alternatively, the absorbance can be obtained by simply subtracting, background spectrum from sample spectrum. The FTIR measurements of the samples in the present thesis are carried out using Perkin Elmer Spectrophotometer.

2.6 Transmission Electron Microscopy (TEM) :

The electron microscope mainly consists of a cylindrical tube, of roughly 2 m long. Unlike the optical microscope, electron microscopes uses, thin beam of rapidly moving electrons. [24] The interaction between these moving electrons and the specimen generates the image. We can get the information about composition as well as surface features of the sample through this technique. It can achieve the resolution less than 1 nanometer. The beam of electrons is formed by accelerating the electrons emitted by lanthanum hexaboride (LAB_6) (cathode) at the top of the tube this beam is then passed through scanning coils. With TEM, morphology and information about the atomic plane arrangement can be obtained. As the accelerated electrons in TEM have higher energy compared to scanning electron microscope this technique also provides the information about crystal structures, lattice planes, orientation of crystals, and defects present in the materials.

The Selected area electron diffraction (SAED) can be recorded to study the orientation of lattice planes in given area. The samples are prepared on copper grid which has thin conducting carbon coating. The sample is then placed between the objective and condenser lenses. The transmitted electrons through sample are condensed and falls onto fluorescent screen. The electron beam interacts with the sample and gets diffracted depending on the crystal orientation of sample. The undiffracted beams fall straight on to the screen and generate the bright spot and the diffracted beam generates the contrast. The image of atomic planes is generated through combination of diffracted and undiffracted electrons.

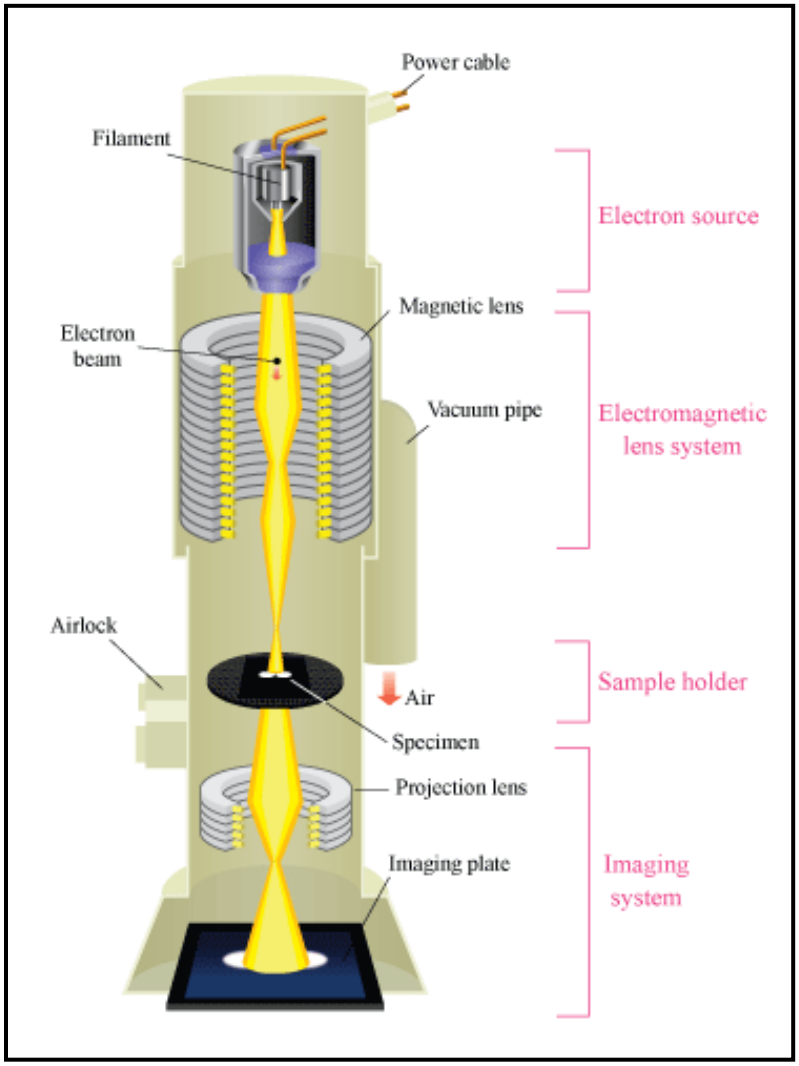

Figure: 2.9 The schematic outline of TEM

http://www.hk-phy.org/atomic world/tem/tem02_e.html

This technique also helps to identify the single crystalline materials when electrons encounter with the specimen various signals such as secondary electrons, backscattered electrons, characteristic X-rays are produced.

The backscattered electrons are used for the purpose of analytical understanding and it also carries the information about Z contrast. It is often used for the identification of distribution of different elements in the sample. The characteristic X-rays are used for the composition identification. There are specialized detectors for the each of the emitted rays. The various amplification

circuits are used in order to amplify the signal, which can be seen as brightness or contrast on the monitor screen. The interaction between the atoms of the specimen and the electron beam leads to formation of image of the specimen, on fluorescent screen. The data is stored in a computer as an image.

2.7 Scanning Electron Microscopy

The SEM is one of the most fascinating tool for the identification of the surface features of nanomaterials. [25] It mainly consists of, the column for the electron beam generation, specimen chamber, vacuum pump, monitor and control panel. The electron gun induces the beam of electron, down towards the specimen in the chamber. To focus this beam, series of electromagnets is used. (As electrons are charged particle they are influenced by the magnetic field.) These are called condenser lenses. Under the electron gun, disc called anode i.e. positively charged electrode is situated. The negatively charged electrons are thus, attracted towards it. In addition to that, the stage on which specimen is mounted is also held at positive potential, The accelerated electron beam can be generated by using Tungsten based filaments which works of thermionic emission or LaB_6 filament which works of field emission. When electron beam hits the specimen, two types of electrons namely, secondary electrons (SE) and backscattered electrons (BSE) are knocked out of it. The secondary electrons come from the surface atoms of specimens which absorbs the energy of the electron beam.

The detector for SE is placed closed to the sample stage. This detector has a positive potential (about +300 V) which generate the Faraday cage where secondary electrons are captured. The detector then uses this information and transforms into the image on the computer screen. The secondary electrons are important, for identification of the surface features. The second types of electrons are backscattered electrons, which actually reflect from deep within the specimen.

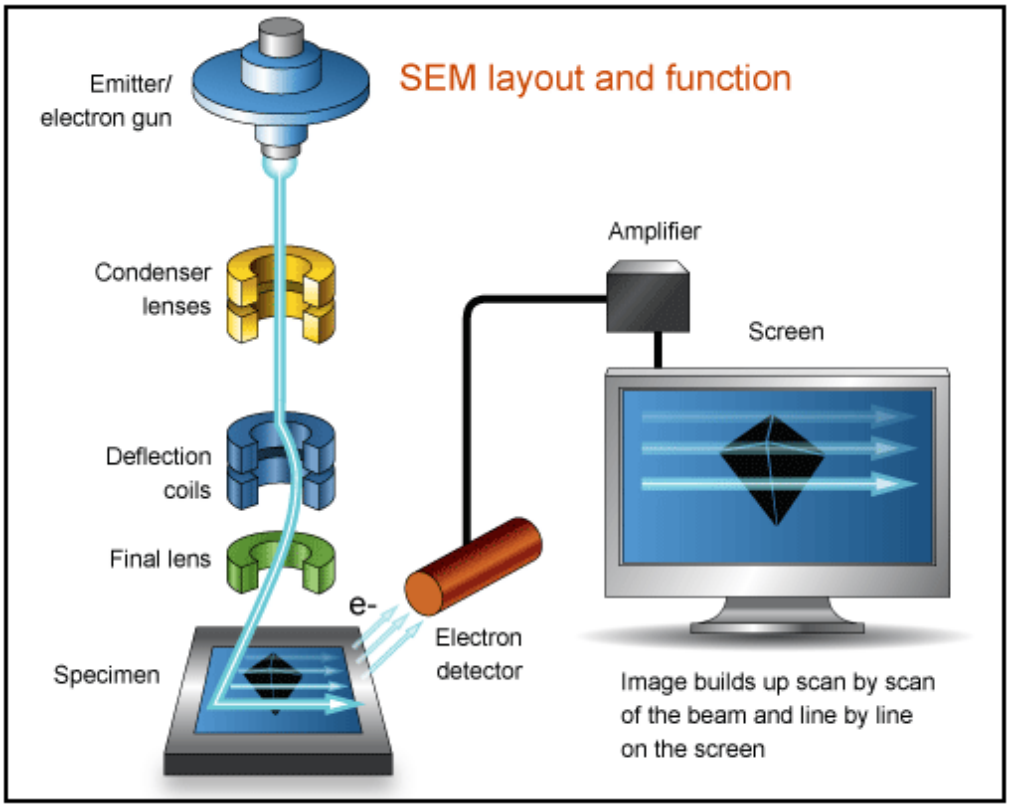

Figure: 2.10 The schematic outline of SEM

http://www.ammrf.org.au/myscope/sem/practice/principles/layout.php

These BSE carries information about the atomic number of atoms present in the sample. Hence to generate the Z contrast based images, BSE are very useful. There is separate detector for their detection. The incident beam also ejects out the characteristic X-rays from samples which are used for quantitative detection of elements present. This X-rays can also be used to generate the elemental mapping over defined area of sample. The electron beam is usually raster scanned on the sampler. It directs the electron beam from left to right direction, until the rectangular area has been scanned and bright image appears on the monitor screen. If many image points are used in a raster scan the real surface profile with minute surface textures can be obtained.

2.8 Dielectric measurement:

Among the metals, semiconductor and insulator classes of materials, insulators are the one of the promising and important materials for commercial and technological growth. These insulators are known as dielectrics which are main component of capacitors. In these materials electrical charges cannot move freely. Dielectric material has the ability to polarize, in the presence of electric field, by creating electric dipoles. There are two types of dielectric materials, namely, polar and non-polar. In the polar family, the centers of positive and negative charges do not coincide, while for non-polar materials it coincides.

2.8.1 Dielectric Polarization:

In dielectric materials under the applied electric field, the positive and negative charges move to opposite sides. This process of partial charge separation without bond breaking produces electric dipoles within the material. This is called as polarization of the dielectric. The dipole moment per unit volume is always the sum of the individual electrical dipoles.

2.8.2 Types of polarization:

Different types of polarization takes place in dielectric materials which respond at different frequency range; namely electronic, ionic, orientation and space-charge polarization. Each of the type is briefly discussed below. [26]

Electronic Polarization:

In the electronic polarization, under the applied electric field the positively charged nucleus and the cloud of electrons displaces with respect to each other in opposite directions. This shift leads to formation of dipole moment within the atom. The shift is proportional to the applied field. The proportionality constant is called as electronic polarizability of molecule. Such polarizations are observed at very high frequency range of 10^{12} - 10^{15} Hz.

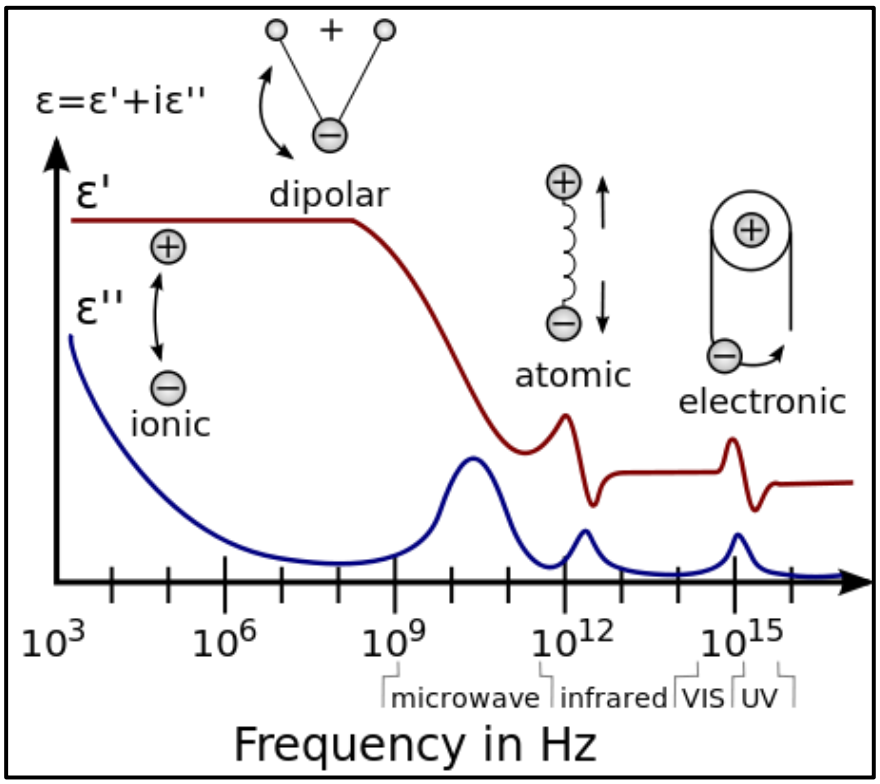

Figure 2.11 Different types of polarization and their frequency dependence

https://en.wikipedia.org/wiki/Dielectric_spectroscopy

Ionic Polarization:

When the electric field is applied to the solid with higher ionic type bond character, cations and anions displaces in opposite directions. This movement of charges results in the formation of dipole moment. Such polarization is called as ionic polarization. Depending on the sign of applied electric field, the dipolar separation will be decided. This polarization is also observed at higher frequency scales.

Orientational Polarization:

In some solids under the applied electric field dipole moments are generated in random directions which are independent from each other. Such dipoles can rotate freely. Hence in such cases the overall dipole moment is greater in certain orientation compared to the other directions. This overall effect leads to

orientational polarization in solids. This helps to understand the origin of dipole moment direction and it be tuned easily by applying reverse electric field. Orientational polarization is comparatively slow process as the dipole takes time to align in presence of electric field. Generally 10^4 -10^6 Hz frequency range is useful for observation.

Space Charge Polarization:

The fourth type of polarization is the space charge polarization. It occurs due to accumulation of charges at the interfaces of the material. The charged ions move in response to applied electric field. This creates the distribution of charges across the interface. Thus, it is also called as interfacial polarization. Total polarization is always the sum of contributions from all types of polarization. This is very slow process.

2.8.3 Dielectric Constant and Dielectric Loss

Dielectric constant:

The capacitance of the condenser is increased if, the space in between is filled by dielectric material. The dielectric constant is then expressed as,

$$\varepsilon = \frac{C}{C_0}$$

Where, ε = relative permittivity or dielectric constant

C = Capacitance when the region is filled with the dielectric medium

C_o = Capacitance without the dielectric medium

Dielectric loss:

Due to conduction processes, power dissipation occurs in dielectric materials. If the polarization lags behind the applied field, the electrical energy loss takes place. It appears to be thermal loss and is proportional to product of dielectric constant and the tangent of the phase angle δ (tan δ).

2.9 Ferroelectric analysis:

One of the fundamental and important characteristic of ferroelectric materials is that, their polarization can be reversed by an applied electric field, which makes it useful for nonvolatile memory applications. This phenomenon is demonstrated using hysteresis loop. [27] This loop is obtained by measuring, the polarization under alternating voltage. The ferroelectric materials show, spontaneous electric polarization and the hysteresis loop is observed at certain temperature which is called as Curie temperature (T_c). Above the T_c, the crystal is non-ferroelectric/non-polar in nature. Figure 2.15 shows the typical PE loop. When the electric field is applied, the ferroelectric domains are aligned in the direction of electric field and overall polarization increases linearly reaching towards saturated polarization (P_s).

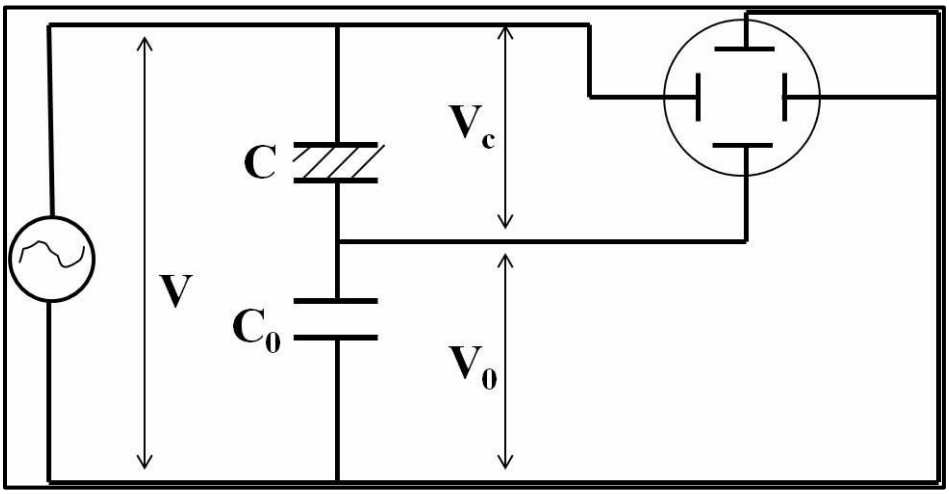

Figure 2.12 The Sawyer-Tower circuit

If the electric field is decreased, few domains switch back normal direction, but the remnant polarization, remains, even when the electric field decreased to zero. In order to completely nullify the remnant polarization, the electric field has to be reversed in the opposite direction; this additional applied reverse electric field is called as corrosive field.

The polarization hysteresis loop is measured using Sawyer-Tower circuit. As it can be seen, the ferroelectric sample is considered as capacitor 'C' which is

connected in series with a standard capacitor 'Co'. Hence the charges on the sample are equal to the standard capacitor. Thus we have,

$$Qs = Qo = CoVo$$

where Qs and Qo are charges on the sample and the standard capacitor. Vo is the voltage drop across the standard capacitor. The Qs can be calculated by measuring Vo. The polarization is obtained as,

$P = \frac{Qs}{A}$ Where A is the area of the electrode

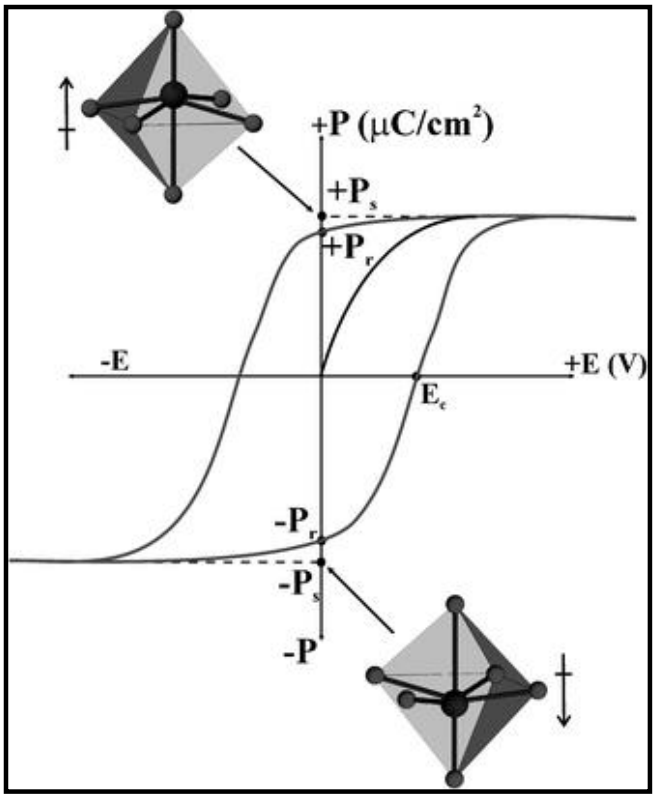

Figure 2.13 The polarization Vs Electric field loop for a typical ferroelectric material [28]

Reproduced by the permission from reference 28: ***Chem. Soc. Rev.***, 2006,**35**, 710-717

2.10 Dynamic Mechanical Thermal Analyzer (DMTA):

The Dynamic mechanical thermal analyzer is an essential instrument for the understanding of structure-property relationship, in macromolecules with varying temperature and applied mechanical strain. In general, it is used to study the viscoelastic behaviors.[29] DMTA, essentially help in understanding relaxation mechanisms in polymers, its mechanical behavior at low to high temperature range as well as molecular motions of the materials under varied stress and frequency. In the measurement, sinusoidal strain or stress is applied to the sample and response of the sample is then monitored as function of frequency or temperature. An interesting feature of this instrument is the availability of multiple geometric fixtures such tensile, compressive etc.

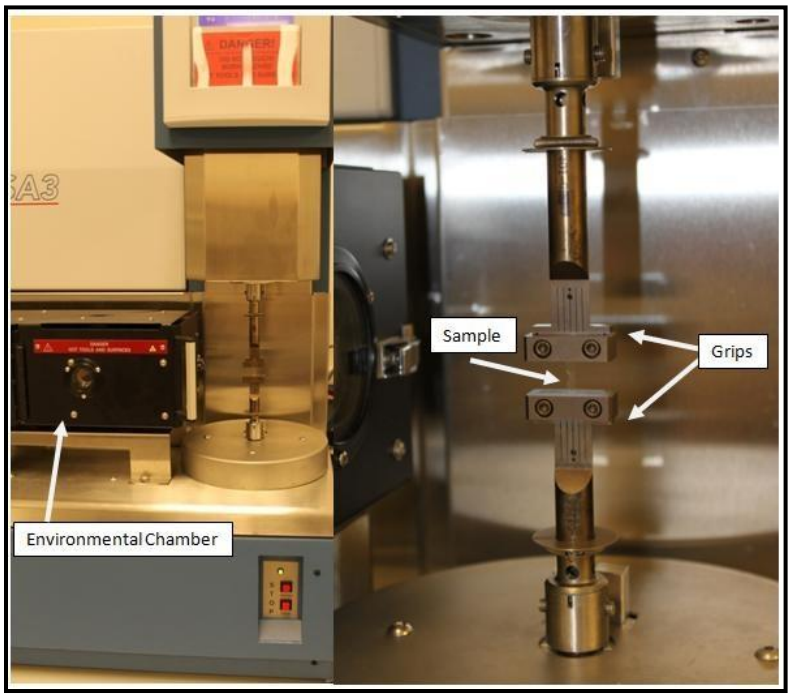

Figure 2.14 The DMTA instrument with tensile fixture in connection

https://en.wikipedia.org/wiki/Dynamic_mechanical_analysis

The stress applied on the viscoelastic materials is always out of phase with the strain generated. This occurs due to several phenomenon such as polymer relaxations and molecular level mobility of polymer chains. The stress applied can be expressed into elastic and viscous modulus which is associated with storage

modulus and loss modulus respectively. The ratio of stress modulus and strain modulus is called as the complex modulus. The data obtained from DMTA consists of real and imaginary parts. The real part gives information about materials ability to store potential energy and is related to Young's modulus. While, the imaginary part is associated with energy dissipation in the form of thermal energy which is related to polymer relaxations, molecular chain mobility, and polymer phase transitions etc. The DMTA gives us the glass transition temperature, which is an essential parameter for the understanding of the mechanical behavior of the material.

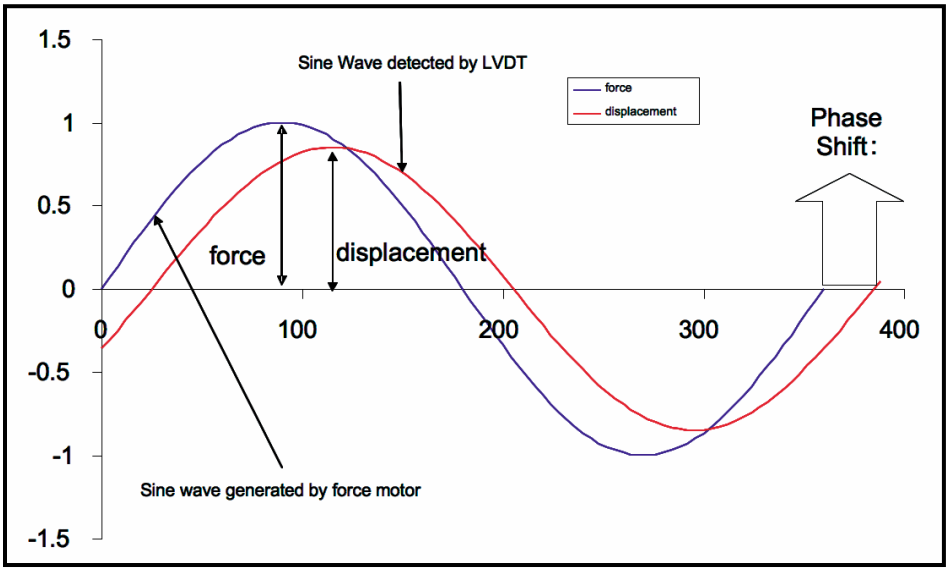

Figure 2.15 The relationship of the applied stress to strain, with the resultant phase lag and deformations.

http://www.perkinelmer.com/CMSResources/Images/44-74546GDE_IntroductionToDMA.pdf

The typical values for dynamic modulus of the polymers range from 100-1000 Pa based on the class of the polymer, at a given temperature and the frequency. The figure 2.15 shows the typical DMTA instrument. In our experiment, we have used the tensile fixture of the DMA, for the application of flexural strain on our flexible devices. The figure 2.15 shows the device under deformation using

tensile fixture. The distance between the grips can be adjusted and the measurements were performed under various curvatures/applied stain.

Section III: Fabrication and measurement of Piezoelectric NGs

Introduction: This section covers the details of nanogenerator fabrication part and the measurement techniques developed for testing the nanogenerator device performance. Towards end the important factors such as output voltage and output current are discussed in brief.

The piezoelectric NGs are the devices which convert the applied mechanical energy into useful electrical energy. The first NG was fabricated using single ZnO NW, where conductive AFM tip was used for the mechanical deflection.[30] Amongst the piezoelectric polymers, PVDF was first used for the NG applications. The single nanofiber was obtained by using near field electrospinning process.[31] The device was then subjected to uniaxial stretching by applying force on one side of the flexible substrate. In case of PZT NF, the interdigitated electrode arrangement is used and the strain is applied using Dynamic mechanical analyzer.[32]

2.11 Electrode Arrangement:

So far there are three different kinds of electrode arrangements are explored for NG fabrication namely a) parallel to the film thickness b) perpendicular to the film thickness and the c) interdigitated patterned electrode arrangement.[33] In the parallel electrode arrangement the, electrodes are usually connected at the ends of the substrate and uniaxial strain sensitivity can be judged. In the perpendicular electrode arrangement, the force/pressure/strain is applied on the top surface of the device. The power output is then calculated, by considering for the overlapping area under the electrode. In interdigitated arrangement the gap between two electrodes is very small which helps in improving the power output per unit area. It has been reported that, the gap between the two electrodes is an essential parameter for piezoelectric output voltage, especially for the d_{31} type of

devices. [34] Thus, depending on the application type, the electrode arrangement can be incorporated.

2.12 Electrical Measurement:

In the case of nanogenerator testing two important signals namely output voltage and output current are studied. This device mainly responds to mechanical vibrations and converts them in useful electrical signals. The output signals generated by the NGs are usually small and difficult to detect. Sometimes it overlaps with the noise in the electrical circuit. It is therefore, essential to differentiate the original signal and the noise. In case of ZnO based NG, often Schottky contact based test is carried out [35] while for PVDF based NG forward and backward connections of the electrical circuits are used as measure of true signal. [36] It is called as switching polarity criteria. It is tested by switching the polarity of electrodes expecting that the sign of output signals will be reversed. Apart from this, if the two NGs are connected in series, the output voltage is the sum of the two, whereas, if they are connected in parallel, the output current is the sum of the two.

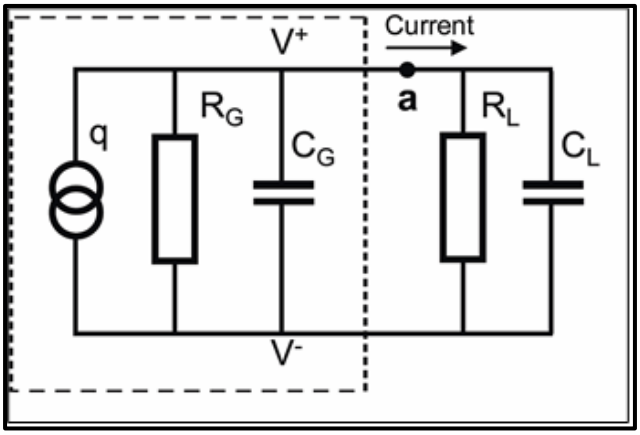

Figure 2.16 The equivalent circuit for the piezoelectric nanogenerator connected to readout circuit with an equivalent load resistor R_L and capacitor C_G. The piezoelectric nanogenerator is modeled as charge generator q. [31]

Reprinted with permission from reference 31: *Nano Letters* **2010** *10* (2), 726-731 Copyright (2003) American Chemical Society

These criteria are applicable to all types of the NGs and can be used as standard tests. Prior to the final measurement, the sealing of the device is done using Polydimethylsiloxane (PDMS) layer for the protection from dust and water. The design for the NG varies widely, but there are certain general considerations for the measurement of the device. When the source impedance and the load resistance match, the power output is enhanced. Most commonly, peak values of the generated open circuit voltage and short circuit are used to calculate power output per unit area. The output voltage and current is usually measured using storage oscilloscope. The figure above shows the equivalent circuit diagram for piezoelectric nanogenerator, where R_L and C_G are the load resistor and capacitor respectively. The 'q' is modeled as the charge generator.[37]

2.13 References

1. Zheng-Ming Huang, Y.-Z. Zhang, M. Kotaki, S. Ramakrishna Composites Science and Technology Volume 63, Issue 15, November 2003, Pages 2223– 2253
2. A. Greiner and J. H. Wendorff, *Angewandte Chemie*, vol. 46, no. 30, pp. 5670-5703, 2007.
3. G. M. Bose, Recherché surla cause et sur la v7ritable th7orie de l87lectricit7, Wittenberg, 1745.
4. J. F. Cooley, US 692,631, 1902.
5. W. J. Morton, US 705,691, 1902.
6. A. Formhals, US 1,975,504, 1934.
7. W. Simm, K. Gosling, R. Bonart, B. von Falkai, GB 1346231, 1972.
8. M. Jacobsen, Chemiefasern/Textilind. 1991, 36 – 41.
9. E.Boland, G. Wnek, D. Simpson, K. Pawlowski, G. Bowlin, Journal of Macromolecular Science, Part A. 38 (2001) 1231-1243.
10. Dan Li, Yuliang Wang, and, and Younan Xia, *Nano Letters* 2003 *3* (8), 1167- 1171.
11. C. Chang, K. Limkrailassiri, L. Lin, , Applied Physics Letters. 93 (2008) 123111.
12. Z. Sun, E. Zussman, A. L. Yarin, J. H. Wendorff, A. Greiner, Adv. Mater. 2003, 15, 1929 – 1932
13. S. N. Reznik, A. L. Yarin, E. Zussman, L. Bercovici, Phys. Fluids 2006, 18, 062101.
14. J. H. Yu, S. V. Fridrikh, G. C. Rutledge, Adv. Mater. 2004, 16, 1562 – 1566.
15. P. Gupta, G. L. Wilkes, Polymer 2003, 44, 6353 – 6359.
16. R. Yang, Y. Qin, C. Li, L. Dai, Z.L. Wang, , Applied Physics Letters. 94 (2009) 022905.
17. Sener, A.G.; Altay, A.S.; Altay, F., Electrical and Electronics Engineering (ELECO), 2011 7th International Conference on , vol., no., pp.I-324,I-328, 1-4 Dec. 2011

18. Koyal Garg and Gary L. Bowlin BIOMICROFLUIDICS 5, 013403 2011
19. Darrell H. Reneker', Alexander L. Yarin Polymer, Volume 49, Issue 10, 13 May 2008, Pages 2387–2425
20. W. W. Flack, D. S. Soong, A. T. Bell, and D. W. Hess, *J. Appl. Phys.*, 1984, 56, 1199.
21. Elements of X-ray Diffraction, ed. by B. D. Cullity, *Addison Wesley Publishing Co*., 1978.
22. Fundamentals of Molecular Spectroscopy, 4th Ed., *Tata McGraw Hill Publishing Co. Ltd*., 2002.
23. Interpretation of Infrared Spectra: A Practical Approach, Encyclopedia of Analytical Chemistry C. N. Banwell, E. M. McCash, A Book: J. Coates, R.A. Meyers (Ed.), 10815, *John Wiley & Sons Ltd*, 2000.
24. Materials Characterization: Introduction to Microscopic and Spectroscopic By Yang Leng , John Wiley & Sons, 07-Aug-2013 - Technology & Engineering
25. Microscopy Techniques for Materials Science Ashley Reginald Clarke Woodhead Publishing, 01-Jan-2002 – Science
26. Dielectric Phenomenon in Solids Kwan Chi Kao Elsevier Academic Press 525 B Street, Suite 1900, San Diego, California 92101-4495, USA 84 Theobald's Road, London WC1X 8RR, UK
27. Physics of Ferroelectrics: A Modern Perspective K. Rabe, C. H. Ahn, J.-M, Triscone, 2007, 105, 1.
28. Bulk characterization methods for non-centrosymmetric materials: second- harmonic generation, piezoelectricity, pyroelectricity, and ferroelectricity Kang Min Ok, Eun Ok Chi[a] and P. Shiv Halasyamani ***Chem. Soc. Rev.***, 2006,**35**, 710-717
29. Thermal Analysis of Polymers: Fundamentals and Applications, John Wiley & Sons, Inc., Hoboken, NJ, USA. Menczel, J. D. and Prime, R. B. (eds) (2009)

30. Zhong Lin Wang and Jinhui Song, Science 14 April 2006: 312 (5771), 242- 246.
31. Chieh Chang, Van H. Tran, Junbo Wang, Yiin-Kuen Fuh, and Liwei Lin. *Nano Letters* 2010 *10* (2), 726-731
32. Xi Chen, Shiyou Xu, Nan Yao, and Yong Shi *Nano Letters* 2010 *10* (6), 2133- 2137
33. Zhong Lin Wang Published by Georgia Institute of Technology, Atlanta, USA, 2011.
34. Kwi-Il Park , Jung Hwan Son , Geon-Tae Hwang , Chang Kyu Jeong , Jungho Ryu , Min Koo , Insung Choi , Seung Hyun Lee , Myunghwan Byun , Zhong Lin Wang , and Keon Jae Lee Adv. ater. 2014, 26, 2514–2520
35. Joe Briscoe, Steve Dunn Nano Energy, Volume 14, May 2015, Pages 15–29.
36. Jiyoung Chang, Michael Dommer, Chieh Chang, Liwei Lin Nano Energy Volume 1, Issue 3, May 2012, Pages 356–371
37. Joe Briscoe, Nimra Jalali, Peter Woolliams, Mark Stewart, Paul M. Weaver, Markys Cain and Steve Dunn *Energy Environ. Sci.*, 2013,6, 3035-3045

Chapter 3

Enhanced Piezoresponse of Electrospun PVDF mats with a touch of Nickel Chloride Hexahydrate salt

In this work, we demonstrate a highly sensitive dynamic strain sensor using electrospun PVDF nanofibers, wherein the piezoelectric β phase component is enhanced significantly (by 30%) with the addition of a hydrated salt, nickel chloride hexahydrate ($NiCl_2.6H_2O$). The peak to peak piezo-voltage generated for PVDF NC is almost 0.762 V, a factor of 3 higher than that for PVDF. The voltage generated per unit micro-strain developed during the free vibration test for PVDF is 0.119 mV whereas it is 0.548 mV for PVDF NC, exhibiting a non-linearly enhanced performance vis a vis the increase in the β phase component. The fiber mats exhibit a significant dynamic strain sensor response and strain sensitivity when compared with the output of commercial metal foil strain gauge. Furthermore with the generated piezo-voltage a commercial LED could light up. These nanofiber devices can have applications in the field of mechanical energy harvesting systems.

*The content of this chapter has been published in "***Nanoscale, 2012, 4, 752-756***. Reproduced by permission of The Royal Society of Chemistry
http://pubs.rsc.org/en/Content/ArticleLanding/2012/NR/c2nr11841f#!divAbstract

3.1. Introduction

Nanomaterial based pressure and strain sensor technology is now a rapidly evolving area of research and through the related development of piezoelectric nanogenerators it has found a synergistic connection with the field of energy harvesting, a topic of great importance at this time. Nanogenerators indeed offer a very simple and easily implementable solution for mechanical energy harvesting as demonstrated by Wang and Song using ZnO nanowire arrays and by Yong Shi et al. using PZT nanofibers.[1,2] However, fabrication and growth of inorganic nanomaterials can be a cumbersome process and the specific state of the synthesized material can affect the properties and performance of devices in significant ways. PVDF (Polyvinylidene fluoride), a semicrystalline and long chain polymer from the fluoropolymer family, could be the best alternative to inorganic counterparts. It is a chemically stable, mechanically strong and flexible polymer. It has been extensively studied because of its widespread applications in many fields. The processability of this polymer is easier because of its comparatively lower melting point i.e. 177 C. It has a Tg (glass transition temperature) of about 35ºC. One more specialty of this polymer is that it exists in four crystal forms (polymorphs) namely α, β, γ and δ. The α phase consists of TGTG (trans gauche alternatively) conformations, while the β phase consists of the TTTT (all trans) conformation. In the γ phase the conformation is TTTGTTTG while the δ phase is a polar analog of α phase. Amongst these polymorphs, β is the most polar form and is majorly responsible for the piezo, pyro and ferroelectric properties of the polymer.[3–7] There are several methods to obtain the polar b phase of this polymer. These include mechanical stretching,[8,9] poling,[10] casting from solutions,[11] spin coating,[12] electro-spinning[13] and use of additives like clay.[14] The effect of addition of different hydrated salts on the β phase formation and in turn the ferro–piezoelectric properties of spin coated films of PVDF have been reported earlier.[12,15] Among these, electro-spinning stands out as an interesting, attractive and facile approach especially in the context of nanostructures of polymers, polymer

nanocomposites as well as inorganic materials. This method involves simultaneous stretching and poling of the solution to form a one dimensional nanofiber from a viscous polymer solution. The polymer solution drop when subjected to a high electric field gets distorted into a conical shape and when the voltage reaches an adequate value the electrostatic repulsion overcomes the surface tension and the fiber is formed.[16] Depending upon the process parameters during electrospinning and the polymer solution properties, fibers with diameter in the range of 100 nanometers to a few micrometers can be obtained. These fibers have a fairly high surface to volume ratio. In the case of electrospinning of PVDF, the morphology and polymorphism behaviors have been studied.[17–19] Yu and Cebe have shown crystal polymorphism in electrospun composite nanofibers of PVDF with nanoclay.[20] Andrew and Clarke[21] have shown the enhanced ferroelectric phase in PVDF nanofibers with addition of ferrite nanoparticles coated with PEO–silane. Recent literature survey shows the use of piezo and ferroelectric properties of electrospun PVDF for energy conversion,[22] power generation[23] and various types of sensors.[24,25] Although β phase formation by addition of a hydrated salt during electrospinning of PVDF is reported,[26] its piezoelectric response and device application are seldom reported. In this work we explored the piezoelectric properties of electrospun PVDF with addition of a hydrated salt, $NiCl_2.6H_2O$. As a consequence, an increase in the fraction of the β phase PVDF was noted. Furthermore this aspect was utilized for the strain sensor and thereby energy harvesting application. The electrospun mats showed a remarkable enhancement in response to strain. The piezoresponse of these mats has also been utilized for efficient capacitor charging and lighting an LED.

3.2. Experimental Section

3.2.1. Materials and synthesis

The PVDF Solef (grade 1008 weight average molecular weight of 1,00,000 g mol^{-1} was obtained from Solvay (Belgium). The solvent dimethylformamide

(DMF) and hydrated salt (nickel (II) chloride hexahydrate, $NiCl_2.6H_2O$) were procured from Merck. Electrospinning was used to fabricate the PVDF nanofibers. For preparation of the solution 2.5 g of polymer was dissolved in 10 ml of DMF at 50ºC and it was continuously stirred simultaneously until a homogeneous, viscous and transparent solution was formed. The effect of hydrated salt concentration on the fiber properties and piezoresponse was examined for a concentration ranging from 0.1 to 1.0 wt%. It was found that a concentration of 0.5 wt% resulted in the highest β content and the best piezo-response. Increase in the salt concentration above 0.7 wt% led to gelation, making the solution unsuitable for electrospinning. Further detailed study was therefore carried out for 0.5 wt% of hydrated salt.

3.3 General Characterization:

The fibers were coded as PVDF and PVDF NC for further analysis. Mettler-Toledo Seven Multi (USA) was used to measure the conductivity of the polymer solutions. The viscosity was measured with Brookfield viscometer. The measurements were done at room temperature. Electrospinning was conducted at 15 kV by keeping a 15 cm distance between the needle tip and the ground collector plate with controlled solution feed rate at 0.9 mL/h. The fibers were collected on the flat plate covered with aluminum foil. The surface morphology and average fiber diameter of the fibers were examined using a scanning electron microscope (Quanta 200 3D). All the samples were sputtered with gold prior to the imaging. For crystal structure analysis X-ray diffractograms (XRD) were recorded using powder XRD (PAN analytical Xpert 1712) with Cu-Ka radiation (wavelength 0.154 nm) operated at 40 kV and 30 mA. The samples were scanned in the 2Ɵ range of 2 to 40. The FTIR spectrum of the fibers was obtained in attenuated total reflectance (ATR) mode in the range of 4000 to 400 cm^{-1} at the resolution of 4 cm^{-1} using a spectrophotometer (GX Perkin-Elmer). The recorded spectrum was an average of 16 scans.

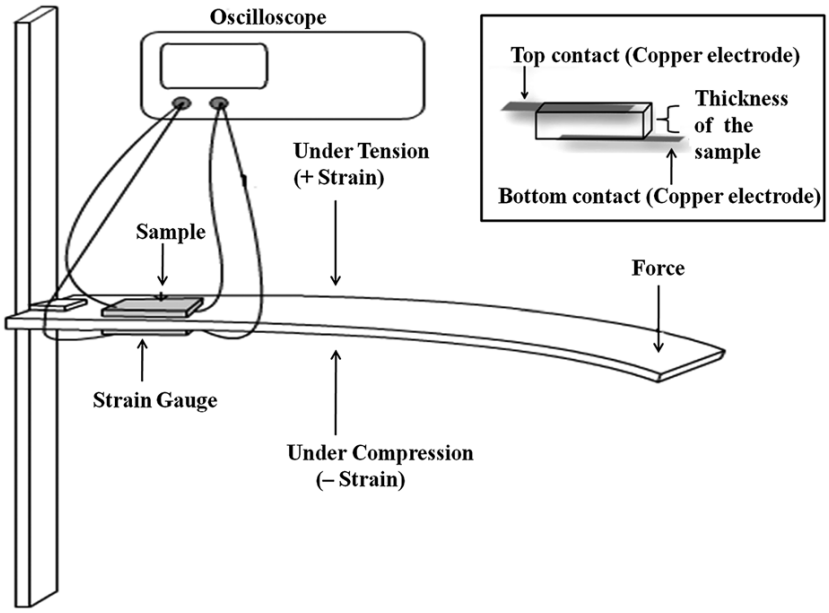

Figure 3.1 Experimental arrangement for dynamic strain measurement and electrode arrangement inset.

The electrospun mats consisted of randomly oriented fibers and the mat thickness was about 0.1 mm. The area for each sample was kept constant as 100 mm^2. The experiments of electrospinning and strain measurements were carried out at room temperature and 60% humidity. The presented results represent an average over 5 samples. As shown in Figure 3.1, the experimental arrangement for dynamic strain measurement mainly consists of a stainless steel scale, oscilloscope and a commercially available metal foil strain gauge. Initially the steel scale of 15 cm was clamped onto a table bench. The strain gauge was pasted on the scale near to the fixed end. A suitable adhesive was applied to affix the gauge for proper transfer of the strain. The bare copper wires were soldered to the terminals of the strain gauge for proper connectivity. The electrodes were attached to the electrospun mat on the two surfaces as shown in Figure 3.1 inset. The Wheatstone bridge circuit was used for the measurement of strain with one of the arms as strain gauge and others with matching fixed resistors. The Wheatstone bridge signal was further amplified with dedicated strain gauge amplifier circuit with a gain of 100. The amplified strain gauge signal was connected to a digital storage oscilloscope. The measurement of the

strain values was done using Whetstones bridge equation. The sample and strain gauge were pasted back to back surface one above the other at fixed end of the scale. The dimension of the each sample was about 10 x 10 mm^2 with the thickness of about 0.1mm. For electrical contacts the sample was sandwiched between two conductive copper tapes. The length and dimensions of the copper electrodes were exactly equal. The signal of the sample was given to oscilloscope for measurement and recording of data. The force was applied to the free end of the scale which generated mechanical vibrations along the length of the scale. The piezoresponse was recorded using storage oscilloscope.

3.4 Results and discussion:

Figure 3.4.1(a) and (b) show the scanning electron micrographs for the PVDF and PVDF NC fibers. In the case of PVDF a few beads were noted in addition to the fibers whereas with the addition of $NiCl_2.6H_2O$ the population of beads was found to decrease significantly. Also a significant change in the distribution of fiber diameters was noted. Such a morphological improvement can be credited to the rise in conductivity values of the polymer solution. The conductivity was found to increase from 2.8 mS cm^{-1} for PVDF to 188 mS cm^{-1} for PVDF NC. The high charge density of the electrified jet, (electrically charged liquid) forms the bead-free, smooth and uniform solid fibers, from the polymer solution containing the salt.[27]

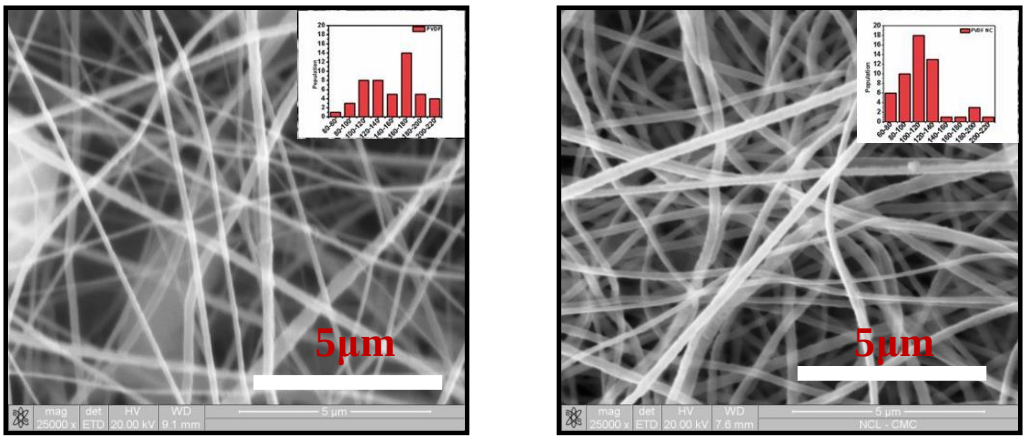

Figure 3.4.1 SEM images for the (a) PVDF and (b) PVDF NC nanofibers

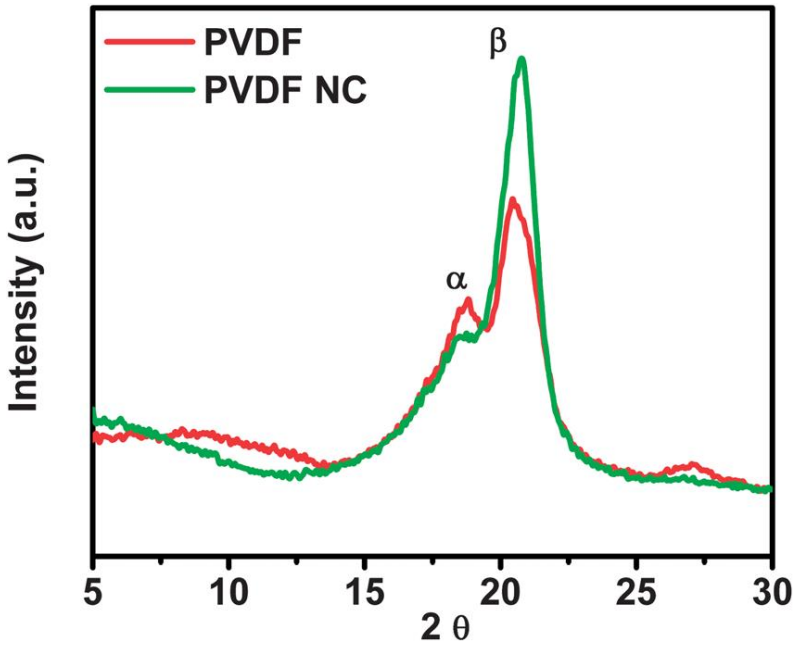

Figure 3.4.2 XRD patterns for PVDF and PVDF NC.

Figure 3.4.2 compares the XRD of PVDF and PVDF NC nanofibers. As seen from the figure, the basic pattern exhibits two prominent peaks, at $2\Theta \approx 18.4$, correspondingto the (020) reflections of the α-phase, and 20.2 corresponding to the (110) reflections of the β phase.[7] The XRD patterns thus reveal the coexistence of both α and β phases in both the samples. The intensity ratio I_β/I_α corresponding to β and α components is dramatically enhanced from 1.45 for PVDF to 2.53 for PVDF-NC. This establishes considerable enhancement of the β phase in PVDF NC due to addition of the salt. In the electrospinning process when the droplet of the viscous polymer solution is subjected to an electric field, its elongation takes place and it undergoes solidification. The polymer chains from the solution get oriented along the applied electric field and hence polarization takes place concurrently. During electrospinning the favored arrangement of the polymer chains through the stretching of the solution droplet also creates a certain preferential orientation of the dipolar moments. The elongation forces, stretching and simultaneous poling during the process promote the formation of the polar β phase. The presence of the β phase in PVDF thus can be attributed to the solidification during electrospinning.[18,28] Addition of NC can further enhance β phase formation due to ionic interactions

of the polymer with the hydrated salt and the polar solvent. The hygroscopic nature of the salt helps in the hydrogen bonding between the water of crystallization and PVDF chains.[29]

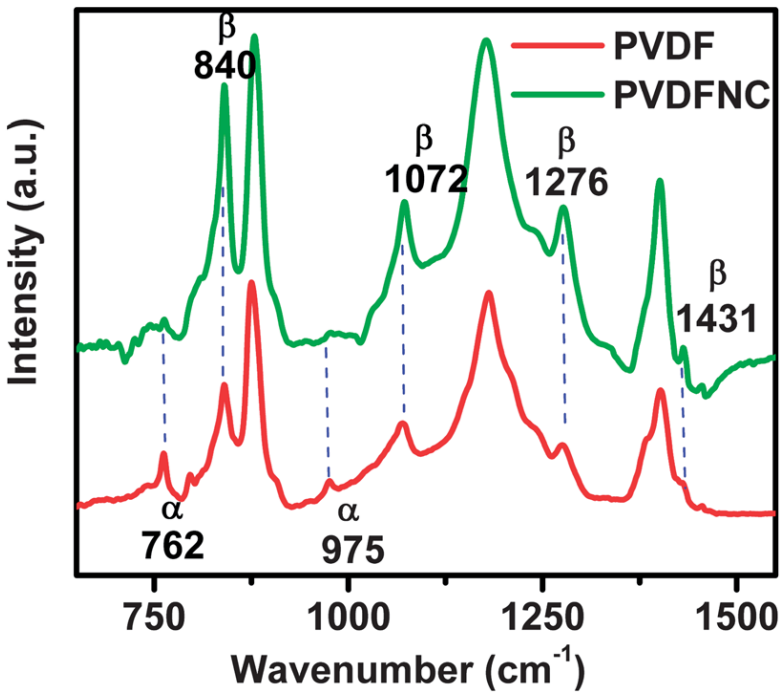

Figure 3.4.3 FTIR (ATR) spectra for PVDF and PVDF NC.

The presence of the β phase in electrospun mats was further investigated by FTIR spectroscopy in the ATR mode. Figure 3.4.3 shows the ATR spectra for PVDF and PVDF NC nanofibers. The characteristic absorption bands designated for the a phase of PVDF at 764 cm^{-1} [CF_2 bending and skeletal bending of (C(F)–C(H)–C(F))], 796 cm^{-1} (CH_2 rocking) and 975 cm^{-1} and those for the b phase at 840 cm^{-1} (CH_2, CF_2 rocking and asymmetrical stretching), 1276 cm^{-1} , 1431 cm^{-1} are clearly visible in the spectra.[30]It is also noted that the intensity of the peaks corresponding to the α phase is suppressed and that for peaks corresponding to the β phase is enhanced for PVDF NC fibers. The fraction of the b phase, F(β) was calculated using the following equation,

$$F(\beta) = \frac{A_\beta}{1.26\,A_\alpha + A_\beta}$$

Where A_β is the intensity of the peak at 840 cm1 in the FTIR spectrum and $A_\alpha$is intensity of the peak at 765 cm^{-1} in the FTIR spectrum.[31] The fraction of the β phase i.e. F(β) for PVDF is 0.64 whereas it is 0.92 for PVDF NC. This fraction calculation of the β phase is clearly seen to be substantially enhanced, in conformity with the XRD data. Dynamic strain sensing of both the fiber mats was determined using a free vibration damping test.

Figure 3.4.4 shows the peak to peak piezoelectric voltage generated at a strain of 950 $\pm$ 30 m^3 as a function of salt concentration. As can be seen the curve is non-monotonic with a maximum at about 0.5 wt% of $NiCl_2.6H_2O$. A higher concentration than 0.5% leads to a decrease in the piezo voltage. The probable reason behind this decrease could be the excess water content in the salt. It has been shown that excess water can notably affect the ferroelectric β phase and in turn the electrical properties of the spin coated PVDF films.[12,15]

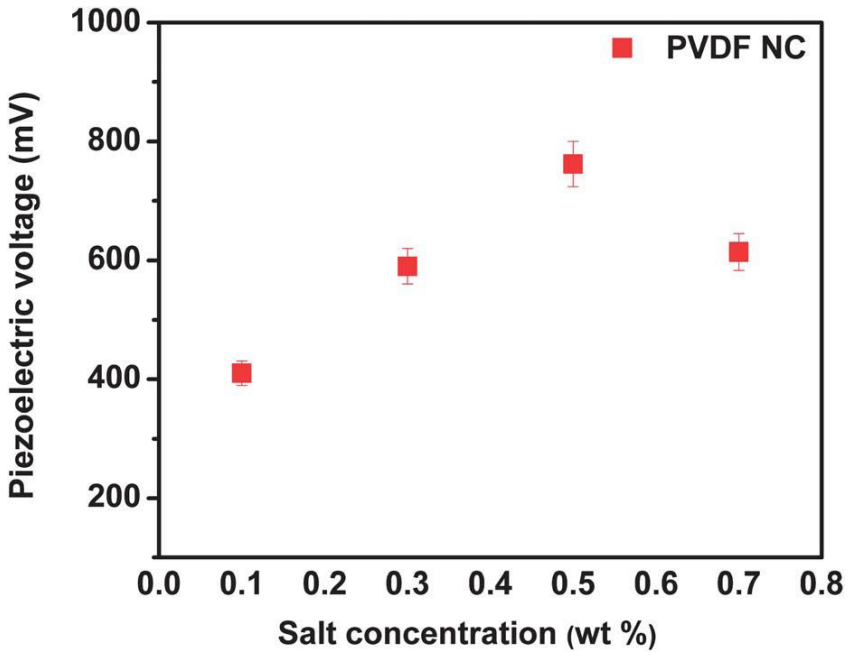

Figure 3.4.4 Effect of variation of the piezoelectric voltage with varying salt concentration

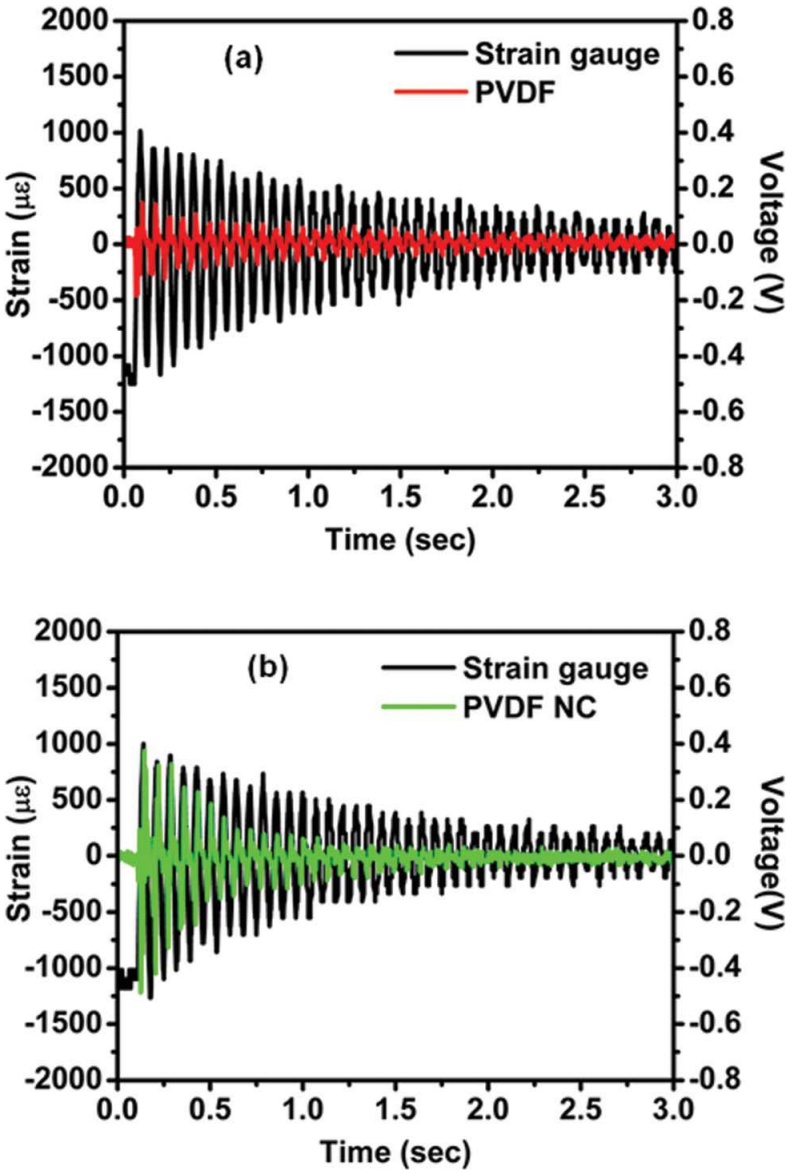

Figure 3.4.5 Dynamic strain sensor responses for (a) PVDF and (b) PVDF NC

Figure 3.4.5 shows variations of piezo voltage (electrical potential generated during the free vibrations) and strain with respect to time over a cycle. When the strain is applied on the fiber mats, piezoelectric charges are generated which build up the potential difference, and the corresponding peak is observed in the positive direction. The peak in the negative direction is observed when the charges are released. The positive and negative peaks in the voltage thus correspond to the compression and tension in the electrospun fiber mat

respectively. The piezo voltage generated can be realized with a standard equivalent RC resonance circuit. It can be seen that the voltage rises proportionally with increase in the applied strain for both the samples. But in the case of PVDF NC the generated peak to peak voltage reaches almost 0.762 V whereas it is maximum 0.296 V for PVDF. This shows that the strain sensitivity of PVDF NC fibers is much higher compared with PVDF. This remarkable increase in PVDF NC fibers can be attributed to the higher β content.

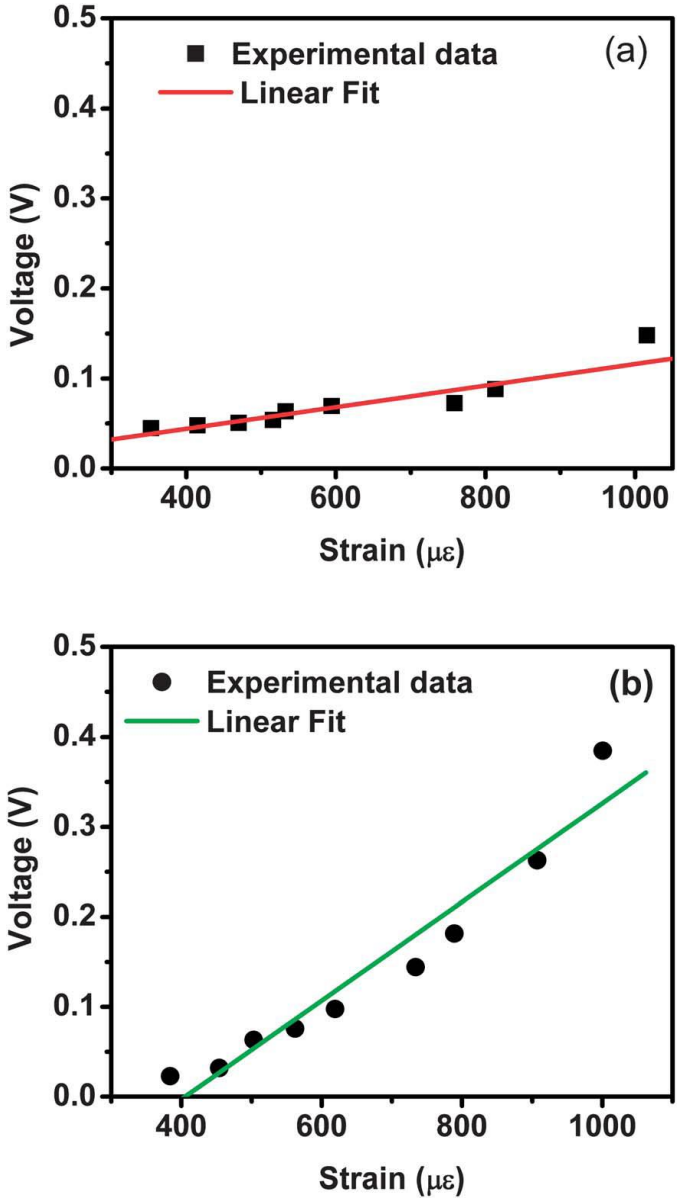

Figure 3.4.6 Voltage vs. strain plots for (a) PVDF and (b) PVDF NC.

Figure 3.4.6 presents the plot of generated voltage vs. strain for PVDF and PVDF NC electrospun mats. The linearity in the readings of both the samples is evidence for the sensor's performance with a low signal to noise ratio. It can be seen that the PVDF NC sample exhibits higher voltage values than those exhibited by PVDF over the range of applied strain. The voltage per unit strain developed during the free vibration test for PVDF was 0.119mV/m^3 whereas it was 0.548mV/m^3 for PVDF NC. This not only reflects an excellent strain sensitivity of the sensor for PVDF NC fiber mats but also a non-linear dependence of the response on the fraction of the β phase in the electrospun mats.

The voltage generated by the strain sensor was used to charge a capacitor. A full wave bridge rectifier was used to convert AC voltage outputs to DC signals. The following full wave bridge rectifier circuit was used for charging of the capacitor and lighting of the LED.

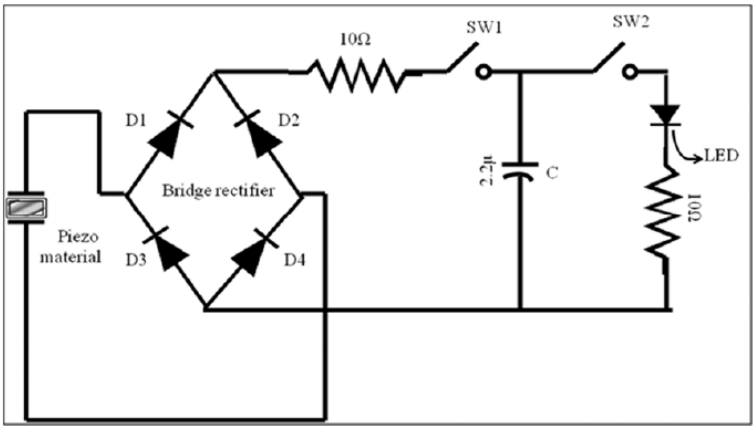

Figure 3.4.7 Circuit diagram for Charging of capacitor and lighting LED

The AC voltage generated by piezo device is converted into DC voltage by using a bridge rectifier circuit and is used for charging the capacitor. The above figure shows the circuit used for charging of the capacitor. The switch SW1 is closed and switch SW2 is kept open initially during charging of the capacitor. Then the charged capacitor is connected with LED by closing switch SW2 to

light it. It takes about 6 minutes to charge the capacitor to a voltage required for lighting LED.

The Wheatstone bridge equation, for single element is used calculating the strain values.

$\varepsilon = \frac{\Delta R/R}{GF}$ Where R = Resistance and GF = gauge factor (GF ε = 4Vr)

$$\varepsilon = \frac{4Vr}{GF\ (1 + 2Vr)}$$

$$Vr = \frac{Vout}{Vin}$$

Where Vout = output voltage and Vin = Excitation voltage given to the bridge

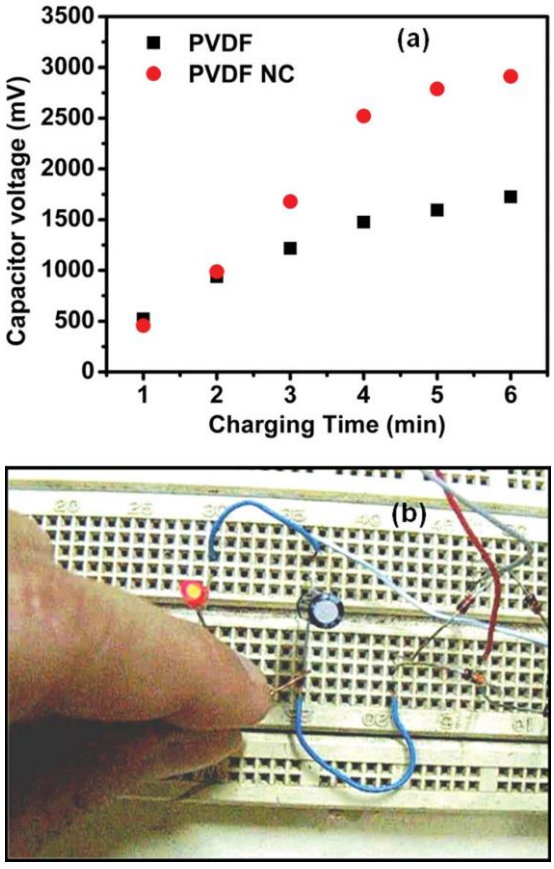

Figure 3.4.8 (a) Plot of capacitor voltage–charging time. (b) Image of the LED.

Figure 3.4.8(a) shows the capacitor voltage versus charging time. The voltage generated across the 2.2μF capacitor was measured after 6 minutes of continuous vibrations. It was found that for PVDF nanofiber mats the voltage generated was 2 V whereas in the case of PVDF NC nanofiber mats it was 2.9 V. The commercial red LED (3 mm) was lit up as shown in Fig. 3.4.8(b). Before concluding it is useful to mention that by adding a low boiling point solvent i.e. acetone into the PVDF–DMF system we could obtain bead free fibers without salt addition allowing us to check whether the beads content has any bearing on the piezoresponse. Indeed it was found that the response is enhanced by about 44% by eliminating the beads, but addition of the salt (0.5 wt %) which also eliminates the beads enhances the response by 157%.

3.5 Conclusion

We have demonstrated a flexible dynamic strain sensor based on PVDF nanofibers modified with addition of a small amount of a hydrated salt. The strain sensitivity of the sensor as determined by the voltage per unit strain developed during the free vibration test was 0.119 mV per m^3 for PVDF whereas it was 0.548 mV per m^3 for PVDF NC. The enhanced performance of PVDF NC was attributed to the observed increase in the piezoelectric b phase fraction from 0.64 (PVDF) to 0.92 (PVDF NC). Interestingly, the enhanced performance increases non-linearly with the fraction of the β phase. These sensors can be used as a reliable and alternative source to conventional resistance based foil strain gauges in a majority of smart structures in health monitoring, biomedical applications and in several electronic devices for energy harvesting applications.

3.6 References

1. Z. L. Wang and J. Song, Science, 2006, 312, 242.
2. X. Chen, S. Xu, N. Yao and Y. Shi, Nano Lett., 2010, 10, 2133.
3. T. Furukawa, Y. Uematsu, K. Asakawa and Y. Wada, J. Appl. Polym. Sci., 1968, 12, 2675.
4. N. Muruyama, J. Polym. Sci., Part B: Polym. Phys., 1975, 13, 929.
5. E. Fukada, Jpn. J. Appl. Phys., 1969, 8, 960.
6. P. Calvert, Nature, 1975, 256, 694.
7. A. J. Lovinger, Science, 1983, 220, 1115.
8. J. B. Lando, H. G. Olf and A. Peterlin, J. Polym. Sci., Part A-1, 1966, 4, 941.
9. V. Sencadas, R. Gregorio and S. Lanceros-endez, J. Macromol. Sci., Part B: Phys., 2009, 48, 514.
10. G. T. Davis, J. E. McKinney, M. G. Broadhurst and S. C. Roth, J. Appl. Phys., 1978, 49, 4998.
11. M. Benz, W. B. Euler and O. J. Gregory, Macromolecules, 2002, 35, 2682.
12. S. Chen, K. Yao, F. Tay and C. L. Liow, J. Appl. Phys., 2007, 102, 104108.
13. J. Doshi and D. H. Reneker, J. Electrost., 1995, 35, 151.
14. L. Priya and J. P. Jog, J. Polym. Sci., Part B: Polym. Phys., 2002, 40, 1682.

15. X. Li, C. Shunting, K. Yao and F. E. Hock Tay, J. Polym. Sci., Part B: Polym. Phys., 2009, 47, 2410.

16. Y. Dzenis, Science, 2004, 304, 1917.

17. W. A. Yee, M. Kotaki, Y. Liu and X. Lu, Polymer, 2007, 48, 512.

18. J. Zheng, A. He, J. Li and C. Han, Macromol. Rapid Commun., 2007, 28, 2159.

19. A. Baji, Y. Mai, Q. Li and Y. Liu, Nanoscale, 2011, 3, 3068.

20. L. Yu and P. Cebe, Polymer, 2009, 50, 2133.

21. J. S. Andrew and D. R. Clarke, Langmuir, 2008, 24, 8435.

22. C. Chang, V. H. Tran, J. Wang, Y. K. Fuh and L. Lin, Nano Lett., 2010, 10, 726.

23. J. Fang, X. Wang and T. Lin, J. Mater. Chem., 2011, 21, 11088.

24. D. Mandal, S. Yoon and K. J. Kim, Macromol. Rapid Commun. 2011, 32, 831.

25. Y. Wang, J. Zheng1, G. Ren, P. Zhang, C. Xu and Y. Wang, Smart Mater. Struct., 2011, 20, 045009.

26. S. Yoon, A. A. Prabu, S. Ramasundaram and K. J. Kim, Adv. Sci. Technol., 2008, 60, 52.

27. D. Li and Y. Xia, Adv. Mater., 2004, 16, 1151.

28. J. S. Andrew and D. R. Clarke, Langmuir, 2008, 24, 670.

29. 29 X. He and K. Yao, Appl. Phys. Lett., 2006, 89, 112909.

30. J. Humphreys, E. L. V. Lewis, I. M. Ward, E. L. Nix and J. C. Mcgrath, J. Polym. Sci., Part B: Polym. Phys., 1988, 26, 141.

31. R. Gregorio and M. Cestari, J. Polym. Sci., Part B: Polym. Phys., 1994, 32, 859.

Chapter 4

A High Performance All Organic Flexural Piezo-FET and Nanogenerator *via* Nanoscale Soft-Interface Strain Modulation

Flexural strain fields are encountered in a wide variety of situations and invite novel device designs for their effective use in sensing, actuating, as well as energy harvesting (nanogenerator) applications. In this work we demonstrate an interesting all-organic device design comprising an electrospun P(VDF-TrFE) fiber-mat built directly on a conducting PANI film, which is also grown on a flexible PET substrate, for flexural piezo-FET and nanogenerator applications. Orders of magnitude stronger modulation of electrical transport in PANI film is realized in this device as compared to the case of a similar device but with a uniform spin-coated P(VDF-TrFE) film. We find that in the flexural mode of operation, the interaction between the laterally modulated nanoscale strain field distributions created by the fibers and the applied coherent strain field strongly influences the carrier transport in PANI. The transport modulation is suggested to occur due to strain-induced conformational changes in P(VDF-TrFE) leading to changes in carrier localization–delocalization. We further show that the fiber-mat based device system also works as an efficient nanogenerator capable of delivering power for low power applications.

*The content of this chapter has been published in "***Phys. Chem. Chem. Phys.***, 2014,**16**, 22874-22881. Reproduced by permission of The Royal Society of Chemistry http://pubs.rsc.org/en/content/articlelanding/2014/cp/c4cp02155j#!divAbstract

4.1. Introduction

Currently there is considerable research emphasis on the development of innovative, flexible or wearable device concepts in view of their portability, light weight, shock resistance, and low cost.[1–9] Functional organic semiconductors clearly offer a natural material platform in this arena with an added advantage of solution-based low temperature processing. It is further desirable that such flexible device platforms are mechanically (or solar) self-powered eliminating the need for a battery or related wiring. Piezoelectric materials, which can generate electrical power locally through stress or flexing, are a great proposition in this regard. Amongst the available modes of mechanical energy harvesting, flexural strain is the form that is encountered in a variety of situations and invites novel device concepts for use in sensing, actuating, as well as energy harvesting (nanogenerator) applications.[10–15] Using piezoelectric materials in novel ways Z. L. Wang and co-workers conceptualized, designed, and promoted the idea of nanogenerators, which has been attracting great interest and attention. Some key interesting contributions from other groups have also fueled the research in this area further.[16,17] Much of the research on nanogenerators or piezo-FET type systems is however still focused on inorganic semiconducting piezoelectric materials such as 1D ZnO nanostructures with a limited number of examples of devices based only on organic materials (polymers).[18–22] In the present work we have chosen to integrate two interesting functional organic materials, namely the well-known semiconducting polymer Polyaniline (PANI) and the piezo (ferro) electric polymer poly(vinylidenefluoride-co-trifluoroethylene) or P(VDF-TrFE), to demonstrate an all-organic piezo FET on a flexible PET substrate. Polyaniline (emeraldine salt) has captured the attention of the scientific community over the last three decades due to its easy synthesis protocol, good transport properties, and environmental stability. [23–27] The P(VDF-TrFE) polymer is known for its highly ferro- and piezoelectric properties, [28] and has been used in many device applications such as field effect transistors, non-volatile memory devices, and energy storage.[29–31] Here we demonstrate an interesting all-organic device design comprising an

electrospun P(VDF-TrFE) fiber-mat built on a conducting PANI film which is also grown on a flexible PET substrate. Orders of magnitude stronger modulation of electrical transport in PANI film is realized in this device as compared to the case of a similar device but fabricated with a uniform spin-coated P(VDF-TrFE) film. We find that in the flexural mode of operation, the interaction between the laterally modulated submicron strain field distributions created by the fibers and the applied coherent strain field strongly influences the carrier transport in PANI. Transport modulation is suggested to occur due to strain induced conformational changes in P(VDF-TrFE) leading to changes in carrier localization–delocalization. We have also examined the nanogenerator potential of the device.

4.2. Experimental Section and Characterization

Figure 4.1a–c shows the schematic of electro-spinning (ES) of P(VDF-TrFE) nanofibers (NFs) onto the Polyaniline film grown on the flexible PET substrate. Figure4.1c shows the process of application of flexural strain on the PANI film under different strain conditions. Briefly, the PANI film was deposited by the drop spreading method on the PET substrate.

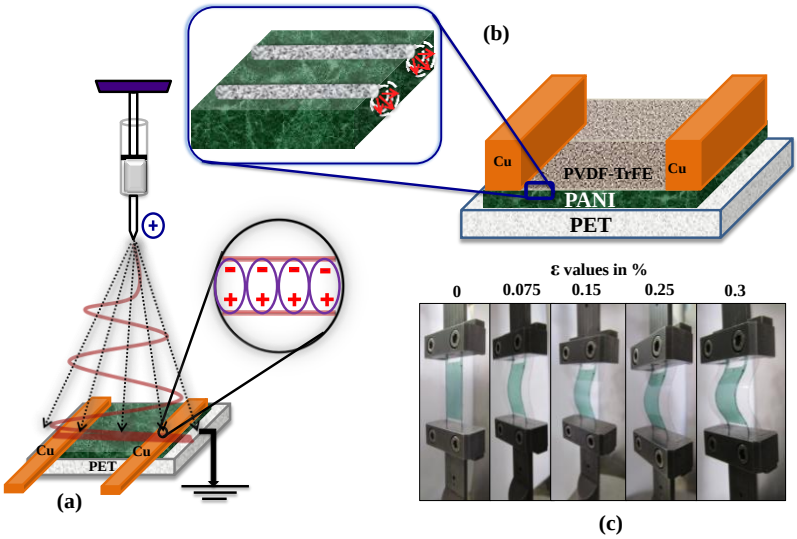

Figure 4.1 (a) Electrospinning set-up and process, (b) device configuration and (c) application of flexural strain on PANI film using DMA.

Subsequently the P(VDF-TrFE) fiber mat was grown directly on this conducting PANI film (serving as the bottom electrode for electro-spinning (ES)) which was provided with two copper strip contacts as shown. This direct ES growth of P(VDF-TrFE) on PANI ensured a good interface between the channel and the modulator. Also, the biasing strips direct the fiber growth in the direction perpendicular to the strip.[32,33] The flexural strain response was first recorded only for the PANI film on PET followed by the measurements on the PANI/P(VDF TrFE) ES heterostructure also grown on PET. The strain-FET device characteristics were studied. For electromechanical measurements, a dynamic mechanical analyser (DMA) was used.

4.3 Results and Discussion:

4.3.1 WAXS and FT-IR spectra of PANI film

The wide angle X-ray scattering (WAXS) pattern for the PANI film figure 4.2(a) matches well with the earlier report by Pouget et al.[34] Correspondingly; the Cl to N ratio is confirmed to be near 0.5 leading to maximum doping in PANI and its high conductivity. The FTIR spectrum figure 4.2b for the PANI film showed the signature bands at 1561 cm^{-1} and 1474 cm^{-1} representing the C–C stretching of quinonoid and benzenoid rings, respectively, which are the building blocks of the desired conducting emeraldine salt phase of PANI. [35]

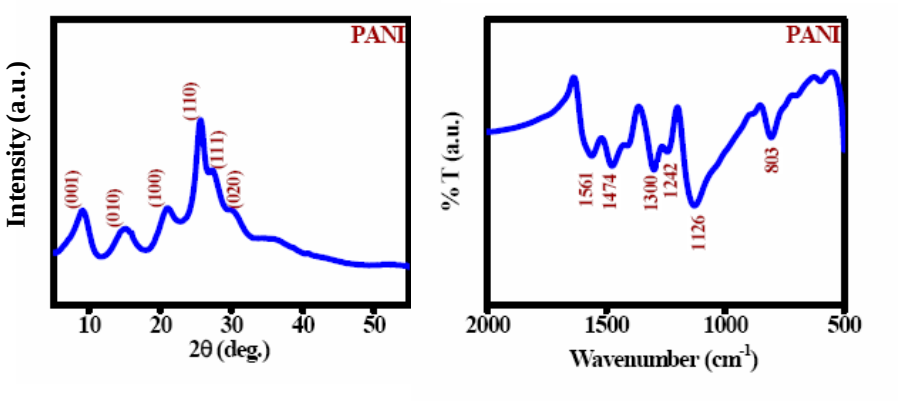

Figure 4.2 (a) WAXS of PANI film, inset shows optical image PANI nanofibers grown on PET (b) FTIR of PANI film

4.3.2 SEM of PANI film and AC conductivity and XRD pattern of P(VDF-TrFE) nanofibers.

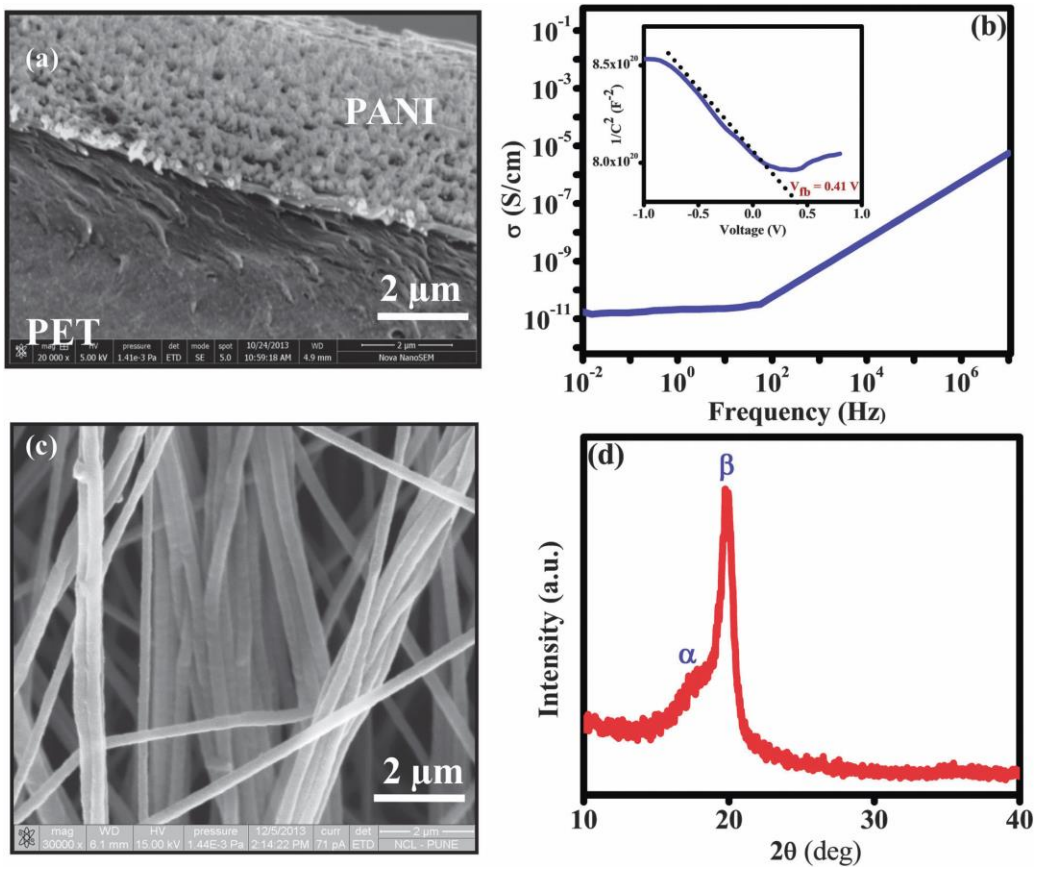

Figure 4.3 (a) SEM image of PANI film, (b) room temperature AC conductivity data of PANI film (inset shows the Mott Schottky plot for PANI), (c) SEM image of P(VDF-TrFE) nanofibers, and (d) powder X-ray diffraction pattern for P(VDF-TrFE) nanofibers.

Figure 4.3(a) shows the FE-SEM image of the PANI film grown on PET. It displays a dense network of oriented nanofibers of Polyaniline on a support layer. This characteristic of PANI film growth is similar to previous reports.[36] The transparent thin film deposited by this protocol adheres very strongly to the substrate. The green colour of the uniform film implies that it is in a highly conductive emeraldine salt state. The value of conductivity obtained by Van der Pauw measurement is 0.5 Scm^{-1}. [37,38] Figure 4.3b shows the AC conductivity of

the PANI film on the PET substrate which was recorded at room temperature using an impedance analyzer as a function of the frequency between 10^2 Hz and 10^7 Hz. The plot is on the logarithmic scale. The conductivities show a nearly frequency independent component up to 100 Hz and pronounced frequency dependence above 100 Hz.

As mentioned in the previous reports, protonic acid doping of PANI results in the formation of polarons leading to an increase in the conductivity. This increase in the AC conductivity at higher frequencies is attributed to contributions from hopping of polarons along smaller distances in the polymer chains. [39–41] The inset of Figure 4.3b shows the Mott Schottky plot, i.e. $1/C^2$ vs. voltage (V) for the Polyaniline film grown on ITO coated PET. The ITO served as the bottom electrode and Cu tape was used as the top electrode. The measurement was performed using the Keithley-4200 semiconductor parameter analyzer. The negative slope of the Mott–Schottky plot shows p-type behaviour of PANI due to hole delocalization through the polymeric chain with linear repeat of quinonoid and benzenoid groups.[42] The value of flat band potential is found to be about 0.5 V and the calculated carrier density was about 1.9 X 10^{15} cm^3. This value depends on the polymeric conformations and growth conditions as well. [43] Figure 4.3c shows the SEM image for the P(VDF-TrFE) NF coating. It shows smooth, bead-free and uniform fibers. These fibers were collected on the top of PANI film with a 1 cm gap between the Cu tape electrodes, placed 10 cm away from the needle. It is reported that spatial orientation of electrospun fibers can be achieved by using such a ‘‘gap’’ method in the conventional collector and the nanofibers are stretched across the gap due to electrostatic interactions to form a fairly parallel array.[32,33,44] The fibers are indeed seen to be generally electro-statically aligned across the electrode gap (the electrodes being placed along the vertical direction in the picture frame). The average fiber diameter of P(VDF-TrFE) NFs is 250–300 nm. It is useful to mention here that other methods have also been used to obtain oriented fibers such as the rotating drum/disk collector method and the near-field electrospinning method. Figure 4.3d shows the X-ray diffraction (XRD) pattern for

the electrospun P(VDF-TrFE) NF. The sharp and intense peak at 2Θ = 20.71 confirms the formation of the desired polar β phase of the polymer. The polar character of P(VDF-TrFE) which exhibits good piezo (ferro-) electric behaviour arises due to the electrical dipoles formed between pairs of electropositive hydrogen and electronegative fluorine atoms which are organized in the form of C–H and C–F bonds perpendicular to the polymer backbone in the molecular chains of P(VDF-TrFE). The room temperature stable crystalline structure of P(VDF-TrFE) is the all-trans polar beta phase.[45] During electrospinning (ES) the stretching and simultaneous poling of this polymer align the crystallites along the axis of the electrospun nanofibers by an electric field gradient. In P(VDF-TrFE) the structural macroscopic anisotropy arises from the directional orientation of crystalline lamellae and defines the corresponding piezoelectric properties of P(VDF-TrFE) nanofibers (NFs). Moreover the simultaneous stretching and poling during the electrospinning render long range ordering of the dipoles on the molecular level as well as high degree of crystallinity and chain orientation.[46] In addition, the flexo-electricity i.e. size dependent piezoelectricity is stronger at the nanoscale due to stronger coupling of the electromechanical strain gradient and polarization.[47,48]The flexural strain dependent variations of the in-plane I–V characteristics of the PANI film on the PET substrate without and with the P(VDF-TrFE) fiber overlayer were measured at room temperature. The tensile testing mode of the dynamic mechanical analyzer (DMA) was used to fix the sample across the fixture. The strain induced in the device with each bending was calculated using the previously reported procedure.[49] Figure 4.4a and 4.4b show the I–V characteristics for PANI and PANI/P(VDF-TrFE) ES devices on PET under 0.075–0.3% flexural strain. In this specific case the strain was applied in such a way that the device side was under positive curvature (convex). For the case of PANI on PET (Figure 4.4(a)), the I–V curves show a linear relationship over the voltage range used establishing the Ohmic nature of the PANI and Cu tape contact. The marginal increment in current with strain essentially reflects the change in the polaronic hopping characteristics due to bond stretching and deformations caused by flexing.

4.3.3 I-V characteristics of PANI and PANI and PANI/P(VDF-TrFE) ES films

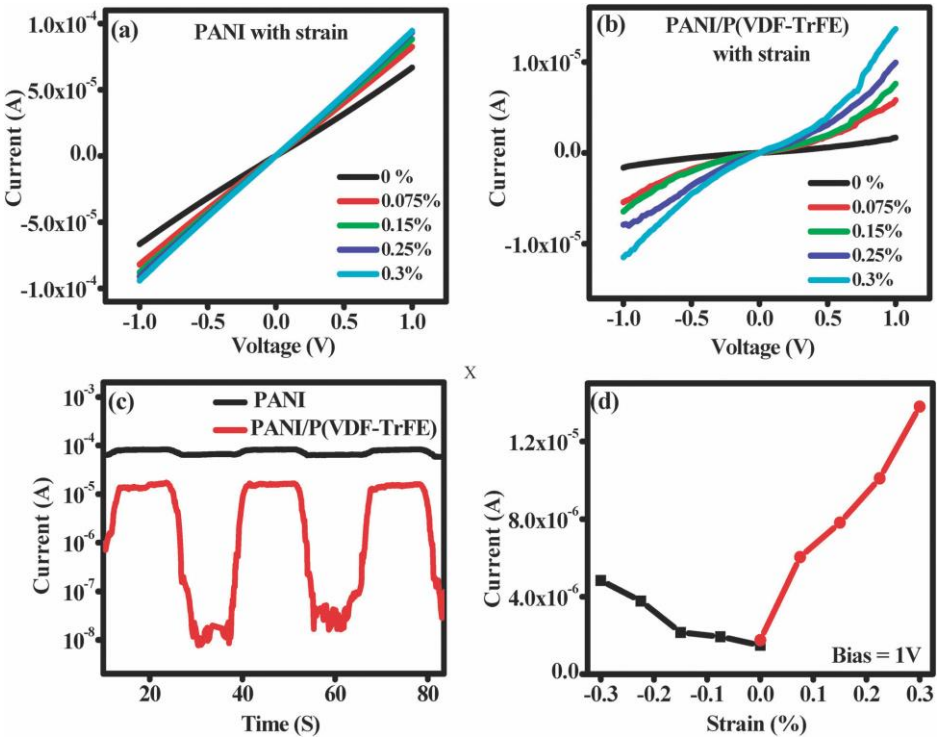

Figure 4.4 (a) Flexural strain dependence of the I–V characteristics of PANI film for positive curvature on the device side, (b) I–V characteristics of the PANI/ P(VDF-TrFE) ES device with applied flexural strain for positive curvature on the device side, (c) comparison of current-time modulation for PANI and PANI/P(VDF-TrFE) ES devices on the log scale, and (d) comparison of the effects of two flexural modes with positive (red line) and negative (black line) curvatures on the device side in the PANI/P(VDF-TrFE) ES device.

It may be noted that the I–V curves exhibit reversibility when the strain is released gradually. The gauge factor given by the slope of (δR/R) vs. applied strain is estimated to be 41. The I–V characteristics for the case of PANI film with the P(VDF-TrFE) nanofiber-mat on the top are shown in Figure 4.4b. Interestingly, the base current of PANI film is found to have decreased considerably by the formation of the P(VDF-TrFE) ES fiber over-layer. Secondly and interestingly, the nature of I–V curves is found to become non-linear with voltage in contrast to the

case of PANI on PET. This non-linearity can be attributed to the modified transport of the PANI film due to in-plane modulated strain fields caused by the electrospun nanofibers. Such modulated strains would locally affect the hopping barriers which can be overcome more easily with increasing voltage, thereby yielding increasing current with increasing voltage. Importantly, the modulation in the electrical characteristics of this device is seen to increase by almost 7 times, i.e. from 20 µA to 148 µA with a gauge factor of 106. Several cycles of bending and relaxation revealed no significant changes in the device performance confirming the flexibility and stability of the device.

We also monitored the current of the device continuously when it was bent and released periodically. We performed these bend-hold-release experiments at higher values of strain (0.7%) at an in-plane voltage bias of 1 V across 1 cm to study the durability of our devices under cycling. In this case, the device was kept for 20 sec in the bent state (ON state) and then brought back to the normal strain-free state (OFF state). Figure 4.4c shows the corresponding modulation in current on the log scale for PANI and PANI/P(VDF-TrFE) ES devices on PET. As noted, upon bending, PANI on PET shows a marginal modulation in current, while the PANI/P(VDF-TrFE) ES device shows a significant modulation. With the very first application of strain the conductivity is seen to increase by about one order of magnitude, but after the release of the first cycle strain the conductivity drops below the original value of the as-prepared device. This can be attributed to the relaxation of embedded stresses in polymeric interface systems. In subsequent cycles, a remarkable change of over two orders of magnitude is realized repeatedly for several cycles of flexural strain application. This shows that electronic transport of the device can be easily and reproducibly tuned by simply controlling the applied strain. Figure 4.4d shows the comparison between strain effects on the current of the PANI/P(VDF-TrFE) ES devices for an applied bias of 1 V due to two complementary flexural modes leading to positive (convex) or negative (concave) curvature on the device side. For the positive (negative) curvature case, the inner surface of P(VDF-TrFE) is under compressive (tensile) strain. These two

modes are depicted in the figure 4.5. Interestingly, an asymmetry is noted in the modulation. We will return to this aspect in the course of discussion.

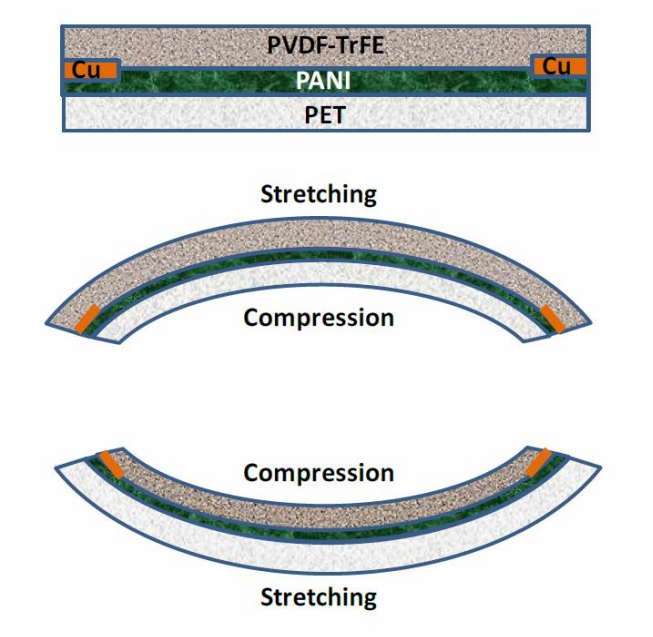

Figure 4.5 PANI/ P(VDF-TrFE) ES device under complimentary flexural modes

4.3.4 I-V characteristics of PANI/P(VDF-TrFE) spin coated films

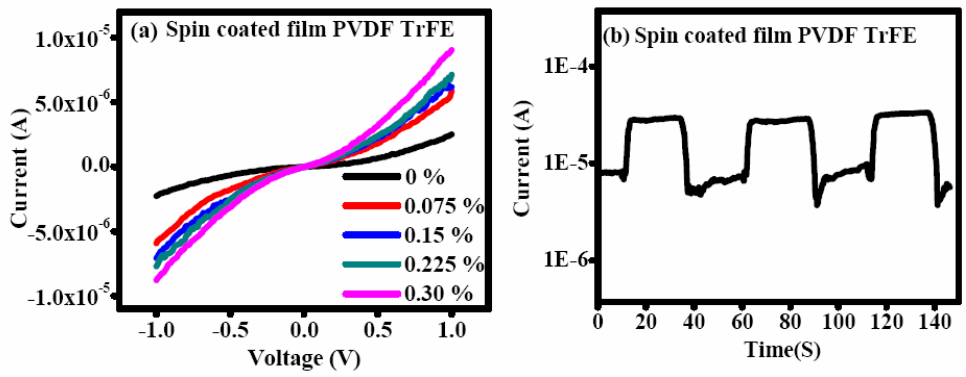

Figure 4.6 I-V for (a) I-Vs for Spin coated P(VDF-TrFE) film on PANI (b) Current-time response for Spin coated P(VDF-TrFE) film on PANI

4.3.5 I-V characteristics of PANI and PANI/PVP ES films

We performed three additional key experiments to bring out some more interesting aspects of the observed effects. First, we performed a study on a spin-coated P(VDF-TrFE) (uniform film) based device instead of the P(VDF-TrFE) electrospun nanofiber based device. As shown in the figure 4.6 (a and b) we found a significantly weaker effect in the uniform film case. Thus, the in-plane submicron modulations caused by fibers are important for a stronger effect.

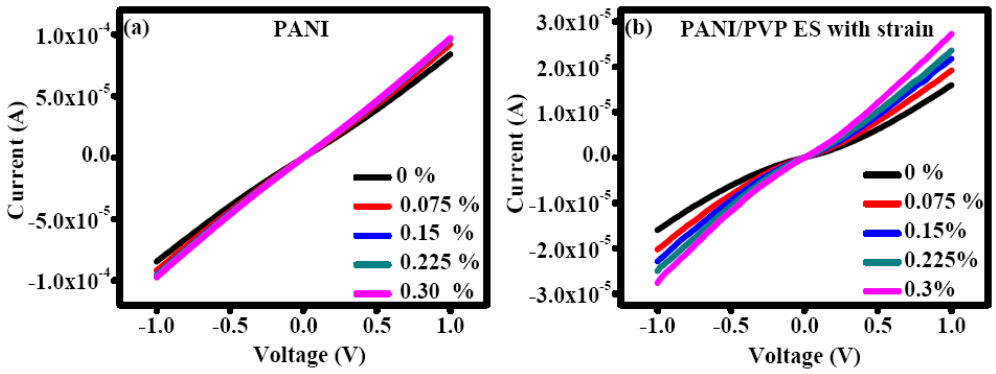

Figure 4.7 I-V for (a) Only PANI Device (b) Only PANI/ PVP ES Device

Second, we replaced P(VDF-TrFE) by a non-piezo/non-ferroelectric polymer polyvinyl-pyrolidone (PVP) and again found a much weaker effect in this case figure 4.7 (a and b). Thus, the submicron scale strain modulations induced by the fibers are alone not sufficient to induce a large effect, but that this strain modulation as well as their piezo/ferro properties concomitantly play a key role.

Third, remembering that the electrospun nanofibers are generally orientated in-plane in the direction perpendicular to the Cu electrodes, we compared the effect of flexural strain applied along two perpendicular in-plane directions, one along the fiber direction and another perpendicular to it. As shown in the figure 4.8 (a and b) the effect was much weaker when the flexing was in the direction perpendicular to the fibers. This is consistent with expectations because such flexural bending does not cause strong in-plane modulation. This shows that bending of fibers (like bending of a beam) has the maximum effect on the carrier transport.

4.3.6 PANI/P(VDF-TrFE) ES device under parallel and perpendicular strain

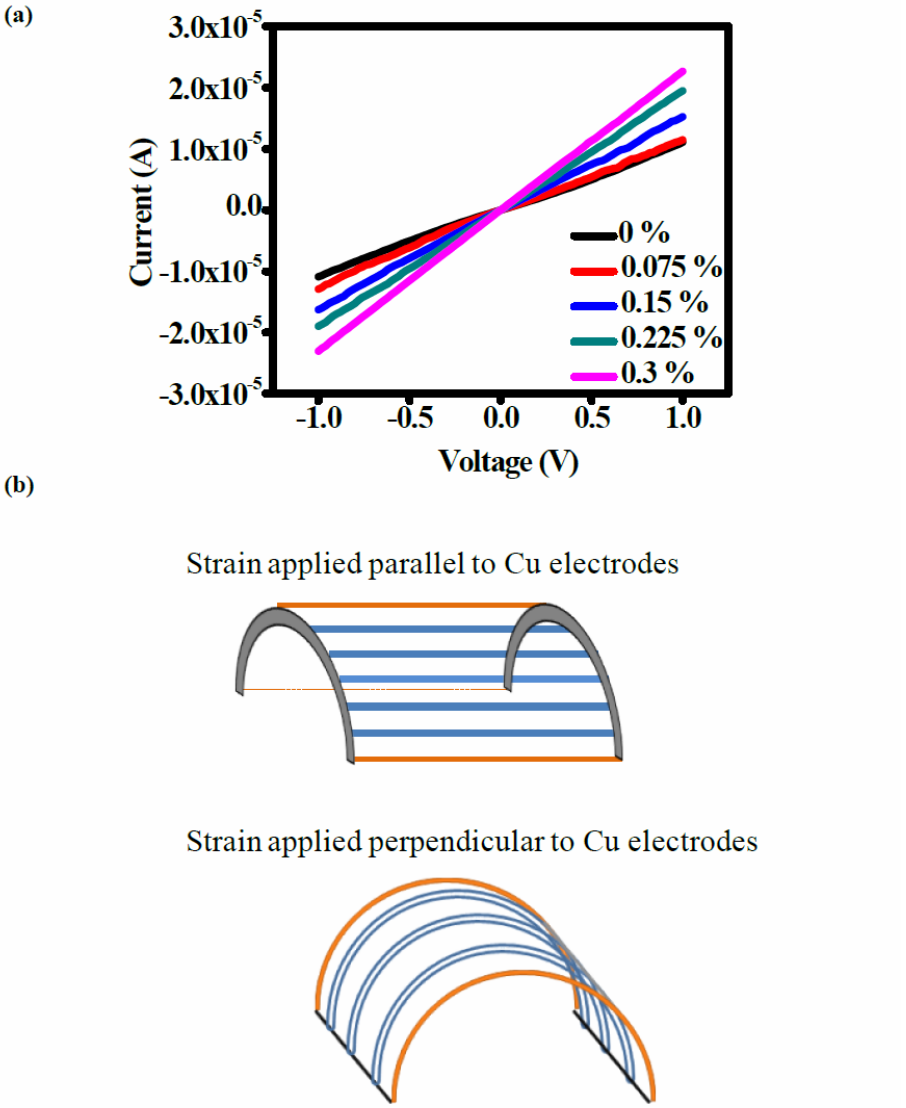

Figure 4.8: I-V for a) tensile axial bending for PANI/P(VDF-TrFE) ES device b) strain applied perpendicular or parallel to the Cu electrodes

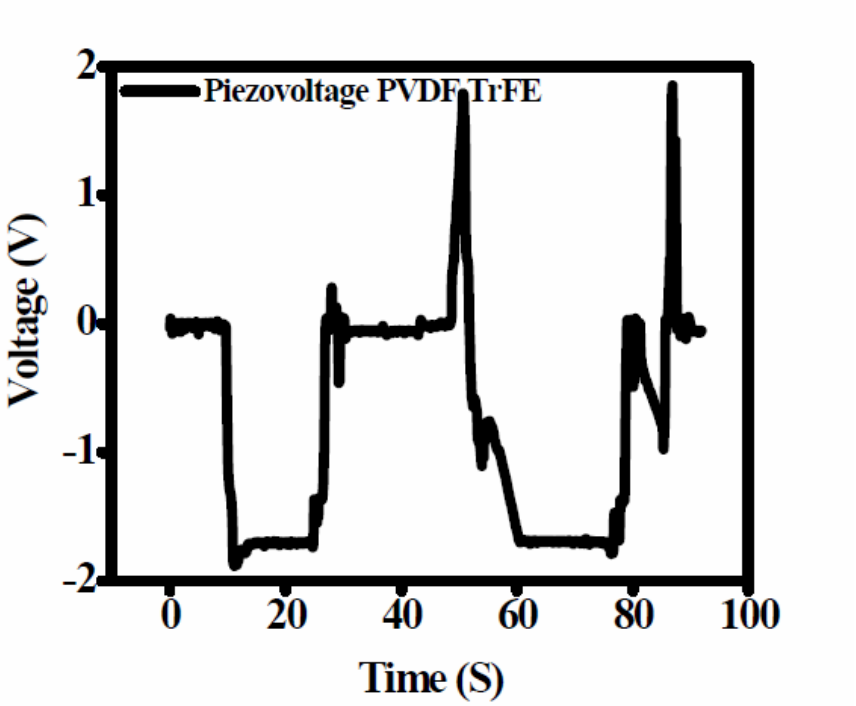

Figure 4.9: Voltage generated for P(VDF-TrFE) NF

Finally we monitored the piezo-voltage generated by the P(VDF-TrFE) fiber mat via periodic bend and release under tensile bending, and the same was found to be 1.75 V for 0.7% strain as shown in the figure 4.9.

4.4 Mechanism

We note that the key ingredients in the problem here are (a) the presence of PANI as a channel layer, whose conductivity depends on chemical doping and strain-induced conformational changes, and (b) the presence of a juxtaposed piezo (and ferro-) electric polymer, whose electric polarization as well as ability to control carriers in PANI depend on bond orientational ordering/disordering, and the fiber-induced strain modulation in the device ground state. It must be remembered that the application of strain onto a soft solid can manifest itself completely differently as compared to its influence on an inorganic solid. This is because polymer chains can move, entangle or de-entangle, twist or undergo bond distortions to reduce the strain-induced mechanical energy input. This leads to significant influences on

carrier transport in these systems especially because of their small bandwidths as compared to inorganic semiconducting or metallic systems. The transport in PANI in the (semi)conducting emeraldine state is of p-type and the conductivity depends both on the carrier density and hopping probability. Changes in conformations can influence both but mainly the latter. The proximity of another molecule such as P(VDF-TrFE) can also influence both but due to different reasons. In particular, the specific nature of bond ordering in P(VDF-TrFE) at its interface with PANI can influence the carrier delocalization, while the electronic polarization supported by the specific bond order can affect the hopping integral. Doping induced changes in the conductivity in the case of conjugated polymers have also been reported in the literature. [50]

We can identify our case with the conditions representative of electrostatic interaction of a conjugated polymer (PANI) with P(VDF-TrFE) via the molecular orientation effects at the interface.(figure 4.10a) Polymers above their Tg are viscoelastic in nature; hence at room temperature they can easily deform or relax. Under the application of mechanical strain, conformational changes occur, which have been reported earlier in the literature using solid state NMR. [51–53]. These conformational changes are termed as dipolar reorientation or dipole flip-flop motion. [19,28,54] It should be remembered that flexural strain is an interesting mode of strain application whereby the strain is imparted through bending deformation. Bending of a soft polymer solid occurs via bond rotations (which are easy on energy as compared to bond stretching or bond angle distortions) as shown in the figure 4.10b. Rotation of even a single bond can change the line profile of an extended molecule. Under the application of flexural strain, the polarization in P(VDF-TrFE) increases leading to electrostatic interactions between electronegative fluorine and hydrogen of PANI.

4.4.1 Molecular interface interaction of PANI/P(VDF-TrFE) device under flexural strain

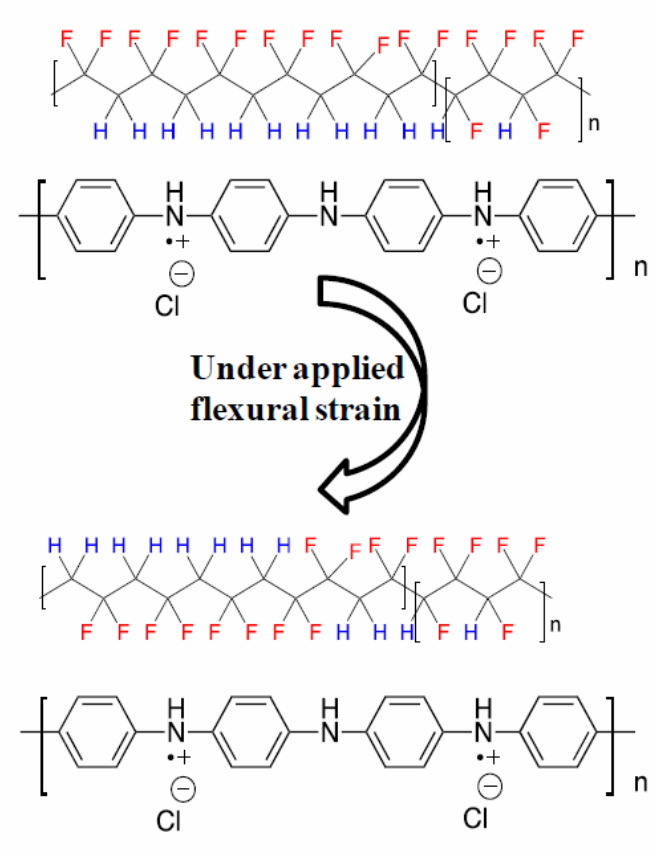

Figure 4.10: (a) Molecular interface interactions without and with applied flexural strain for PANI/P(VDF-TrFE). Note that the Figure suggests that under applied strain more number of F ions will get directed towards PANI by C-C bond re-orientation under strain.

This helps delocalize the carriers in PANI. Due to this interaction nitrogen becomes electron donating and the electron cloud gets pulled by an adjacent benzene ring leading to efficient delocalization. It may be noted that one cause of the considerable modulation observed under the application of flexural strain in the PANI/P(VDF-TrFE) ES device is the significant drop of PANI conductivity upon the growth of electrospun fibers thereupon. This can occur due to two reasons.

First, the nanofibers would produce strong submicron-scale local strain modulation on the film surface influencing its conductivity by local conformational changes.

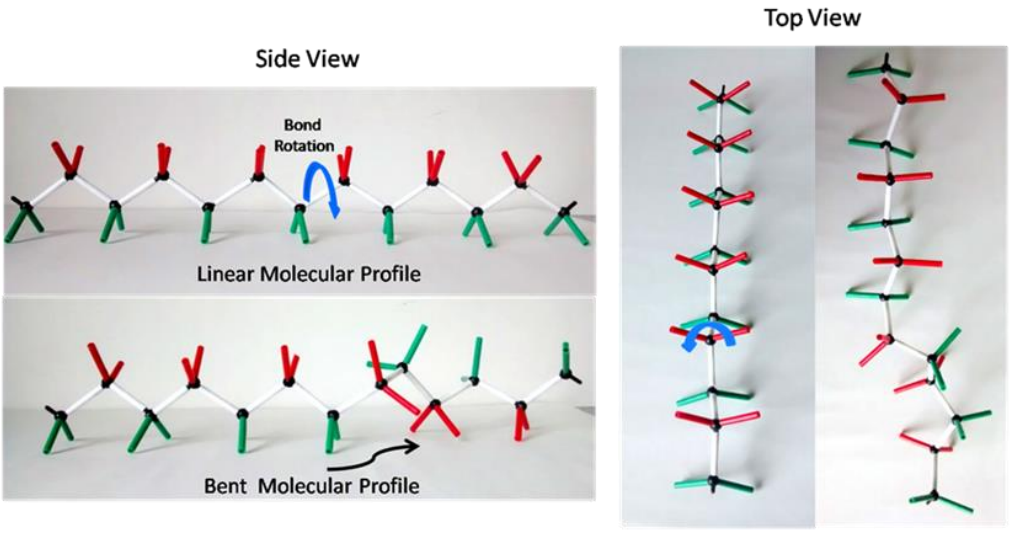

Figure 4.10: (b) Model picture for molecular profile for the case of PVDF

This would certainly not occur for spin coated P(VDF-TrFE). Second, the electrospinning process orients the molecular chains preferentially along the fiber axis, thereby concurrently inducing cross-sectional orientational ordering of the C–F and C–H bonds. The direction of the external electric field at the film surface is such that the negative pole of polarization directs away from the surface. Thus the C–H bonds tend to orient towards the interface with PANI. This causes enhanced localization of carriers, thereby decreasing the conductivity. Once again, the spin-coated P(VDF-TrFE) does not cause such conductivity decrease, highlighting the significance of electrospinning induced strong submicron strain modulation and related polarization effects. We can thus also appreciate why only mild changes are noted on electrospun PVP (the non-piezoelectric polymer), since in this case strain modulation is present but without strain induced polarization effects. As stated earlier, we also compared the effects of two opposite flexural modes (positive and negative curvatures on the device side). In Figure 4.4d an asymmetry is noted between the two cases. This reveals the influence of the differing strain induced conformational changes in a polymeric soft-solid on the carrier transport. This

difference arises from the clear reversal of strain states at the PANI/P(VDF-TrFE) interface, which can populate the density of specific C–H and C–F bonds directed towards the interface differently, leading to an asymmetry.

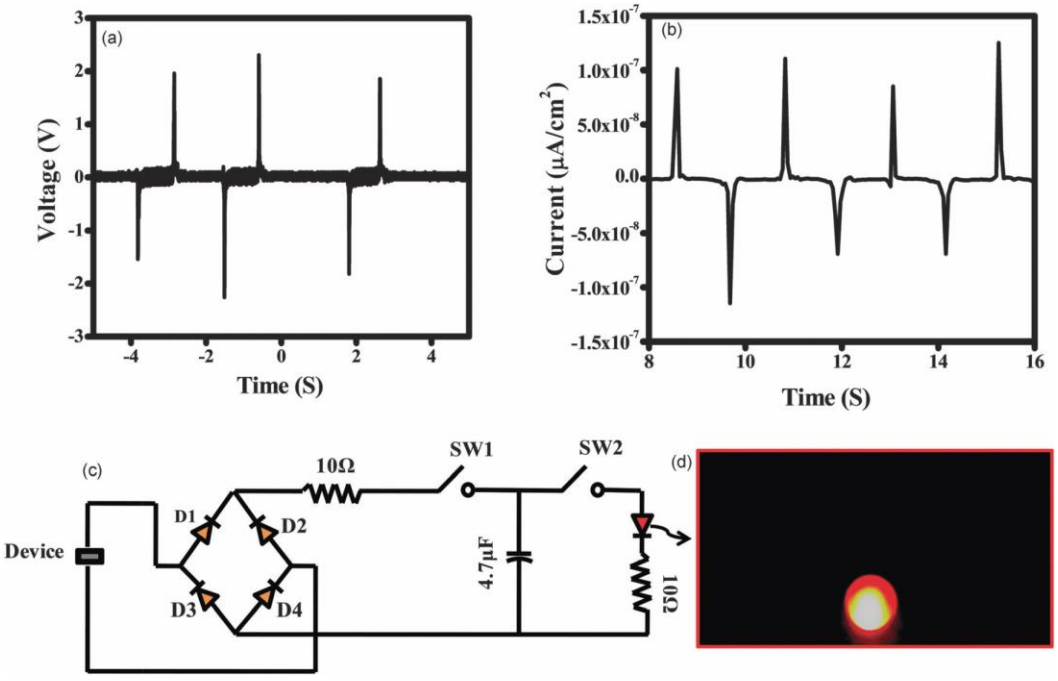

Figure 4.11 (a) Voltage output of the PANI/P(VDF-TrFE) ES device, (b) current output of the PANI/P(VDF-TrFE) ES device, (c) bridge rectifier circuit, and (d) image of a commercial LED lit with our device.

Now we discuss the nanogenerator characteristics of our device, which basically look for the power that can be generated. We calculated the areal power density of our device by taking the product of peak V_{oc} and peak J_{sc} divided by the area. Prior to measurements we varied the load resistances from 100Ω to 10 MΩ as the power density of the device does depend on load matching [3, 4, 5]. It was found to have maximum power density of 0.25μW/cm^2 at a load of 10 MΩ. All the further measurements were done under the same load of 10 MΩ.

In Table 4.1, the performance of our device is compared with other recent studies, which are based only on the piezoelectric polymeric systems, but do not involve a

hetero-structure case, as in our work. Our results are clearly competitive with these other reports. The power generated by our device was further used to light up the commercial red LED using a full wave rectifier bridge circuit (Figure. 4.11c and d). Despite the energy consumption in the diodes, it took less than 3 minutes to charge a 4.7 mF capacitor to light up a commercial red LED.

Piezo-Voltage (V)	Piezo-Current	Material & Morphology	Journal Name & Publication Year
0.03	3 nA/cm^2	Single PVDF NF[18]	*Nano Lett. 2010, 10, 726-731*
0.02	0.2 nA/cm^2	PVDF nanofibers[55]	*ACS Nano 2010 , 4 ,* 3647
1	0.3 µA/cm^2	Porous PVDF film[56]	*Nano Lett. 2011 , 11 , 5142*
0.4	-	PVDF-TrFE nanofibers[19]	*Macromol.Rapid.Commun. 2011, 32, 831–837*
3	0.3 µA/cm^2	PVDF-TrFE film[57]	*ACS Nano 2013, 7,3130-3138*
1	30 nA/cm^2	PVDF-TrFE nanofibers[22]	*Nature Comm, 2013, 4, 1633*
0.6	-	PVDF-TrFE film[58]	*Adv. Mater. 2014, 26, 765–769*
2.5	0.1µA/cm^2	PVDF-TrFE nanofibers	This work

Table 4.1: Comparison of Performance Parameter of our nanogenerator with the literature

4.5 Conclusions

In conclusion, we have designed and tested an all-organic device design comprising an electrospun P(VDF-TrFE) fiber-mat built directly on a conducting PANI film grown on a flexible PET substrate for flexural piezo-FET and nanogenerator applications. Under application of flexural (bending) strain we have observed orders of magnitude stronger modulation of transport in PANI in the case of the electrospun fiber based device, as compared to the case of uniform spin-coated P(VDF-TrFE). The transport modulation is suggested to occur due to strain-

induced conformational changes leading to carrier delocalization. Fairly impressive nanogenerator response is also observed which can easily drive low power applications.

4.6 References:

1. J.Rogers, Z. Bao, K. Baldwin, A. Dodabalapur, B. Crone, V.R. Raju, V. Kuck, H. Katz, K. Amundson, J. Ewing, P. Drzaic, *Proc. Natl. Acad. Sci*. 2001, 98, 4835;
2. J. Lewis, *Materials Today*2006, 9, 38-45.
3. S. Kim, J. Lee, *Nano Lett*. 2010, 10, 2884-2890.
4. S. Park, M. Vosguerichian, Z. Bao, *Nanoscale,* 2013, 5, 1727-1752
5. D. Kim, R. Ghaffari, N. Lu, J.Rogers, *Annu. Rev. Biomed. Eng*. 2012, 14, 113-128.
6. S. Lee, K. Choi, W. Choi, Y. H. Kwon, H. Jung, H. Shin, J.Kim, *Energy Environ. Sci*. 2013, 6, 2414-2423.
7. D. Sun, C. Liu, W. Ren, H. Cheng, *Small* 2013,9, 1188-1205.
8. J. Kim, M. Han, Y. Noh, *Semicond. Sci. Technol.* 2011, 26, 030301
9. S.Forrest, *Chem. Rev*. 2007, 107, 923-925.
10. Z.L. Wang, *Science* 2006, 312, 242-246.
11. Y. Qi, J. Kim, T. D. Nguyen, B. Lisko, P. K. Purohit, M. C. McAlpine, *Nano Lett.* 2011, 11, 1331-1336.
12. C. Dagdeviren, S. Hwang, Y. Su , S. Kim, H. Cheng, O. Gur , R. Haney, F. G. Omenetto, Y. Huang, J. A. Rogers, *Small*,2013, 9, 3398-3404.
13. C. Jeong, I. Kim, K. Park, M. Oh, H. Paik, G. Hwang, K. No, Y. S. Nam, K. Lee, *ACS Nano*, 2013, 7, 11016-11025.

14. S. Xu, Y. Yeh, G. Poirier, M. C. McAlpine, R. A. Register, N. Yao, *Nano Lett.* 2013, 13, 2393-2398.

15. W. Wu, X. Wen, Z. L. Wang, *Science,* 2013, 340, 952-957.

16. K. Park, C. K. Jeong, J. Ryu, K. J. Lee, *Adv. Ener Mater*. 2013, 3, 1539- 1544.

17. K. Y. Lee, D. Kim, J. Lee, T.Y.Kim, M.K.Gupta, and S.W. Kim, *Adv. Funct. Mater*. 2014, 24, 37-43.

18. C. Chang, V. H. Tran, J. Wang, Y. Fuh, L. Lin, *Nano Lett.* 2010, 10, 726-731.

19. D. Mandal, S. Yoon, K. J. Kim, *Macromol. Rapid Commun*. 2011, 32, 831-37.

20. D. Dhakras, V. Borkar, S. B. Ogale, J. Jog, *Nanoscale,* 2012, 4, 752-756.

21. C. L. Sun , J. Shi , D. J. Bayerl , X. D. Wang , Energy Environ. Sci. 2011, 4, 4508-4512.

22. L.Persano, C. Dagdeviren, Y. Su, Y. Zhang, S. Girardo, D. Pisignano, Y. Huang, J. Rogers, *Nature Comm*. 2013, 4, 1633.

23. A.G.Macdirmid, *Angew. Chem. Int. Ed.*2001, 40, 2581-2590.

24. G. Li, Z. Feng, J. Zhong, Z. Wang, Y. Tong, *Macromolecules* 2010, 43, 2178-2183.

25. W. Chen, R. Rakhi, H. Alshareef, *J. Mater. Chem. A* 2013, **1**, 3315-3324.

26. Y.Miao, W. Fan, D. Chen, T. Liu, *ACS Appl. Mater. Interfaces*. 2013, **5**, 4423-4428.

27. M.M. Sk, C. Y. Yue, *J. Mater. Chem. A*.**2014**, *2*, 2830-2838.

28. A.J.Lovinger, *Science*,1983, **220**, 1115-1121.

29. K. Baeg, D. Khim, J. Kim, B. Yang, M. Kang, S. Jung, I.You, D. Kim, Y. Noh, *Adv. Funct.Mater.*2012, **22**, 2915-2926.

30. S. J. Kang, Y. J. Park, J.Y. Hwang, H. J. Jeong, J. S. Lee, K. J. Kim, H. Kim, J. Huh, C. Park, *Adv. Mater.* 2007, **19**, 581-586.

31 S. Han, Y. Zhou, V. A. L. Roy, *Adv. Mater.* 2013, **25**, 5425-5449.

32. W. Yee, A. Nguyen, P. Lee, M. Kotaki, Y. Liu, B. Tan, *Polymer* 2008, **49**, 4196–4203.

33. D. Li, Y. Wang, Y. Xia, *Nano Lett.* 2003, **3**, 1167-1171.

34 J.P.Pouget, M.E.Jozefowicz, A.J.Epstein, X. Tang, A.G.MacDiarmid, *Macromolecules*, 1991,**24**, 779-789.

35. H.K. Chaudhari, D.S. Kelkar, *J. App. Poly. Sci.* 1996, **62**, 15-18.

36. N.Chiou, C. Lu, J. Guan, L.Lee, A.J. Epstein, *Nature Nanotech.* 2007, **2**, 354- 357.

37. J. Chiang, A.G.Macdiarmid, *Synthetic Metals* 1986, **13**, 193-205

38 C. Arenas, G.Sanchez,*Polym Int.* 2011, **60**, 1123-1128.

39. F. Zuo, M. Angelopoulos, A.G.MacDiarmid, A.J. Epstein, *Phy.Rev. B* 1989, **39**, 3570-3578.

40. S.Manjunath, K.Kumar, M. Revanasiddappa, M. Ambika Prasad, *Ferroelectric Letters*, 2008, **35**, 36-46.

41. H. H. S. Javadi, F. Zuo, M. Angelopoulos, A. G. Macdiarmid, A.J. Epstein *Mol.Cryst. Liq.Cryst.* 1988, **160**, 225-233.

42. C. Belabed , A. Abdi , Z. Benabdelghani , G. Rekhila , A. Etxeberria , M. Trari, *Int. J. Hyd. En.* 2013, **38**, 6593-6599.

43. K. Lee, S. Cho, S. H. Park, A. J. Heeger, C. Lee, S. Lee, *Nature* 2006, **441**, 65- 68.

44. D.Li, Y.Wang, Y.Xia, *Adv. Mater*. **2004**, *16,* 361-366.

45. Nanomanufacturing and analysis of novel continuous ferroelectric PVDF and P(VDF-TrFE) nanofibers, Xi Ren, *Ph.D.thesis* University of Nebraska, Lincoln, May, **2007**.

46. J. Chang, M. Dommer, C. Chang, L. Lin, *Nano Energy*, 2012, **1**, 356-361.

47. M.S.Majdoub, P. Sharma, T. Cagin, *Phy. Rev. B*, 2008,**77**, 125424-125429.

48. Y. Wang, K. Ren, Q. M. Zhang, *Applied Physics Letters* 2007, **91**, 222905.

49. J. Zhou, Y. Gu, P. Fei, W. Mai, Y. Gao, R. Yang, G. Bao, Z. L. Wang, *Nano Lett.* **2008**, *8,* 3035-3040.

50. A.J. Heeger,*Reviews Of Modern Physics*, 2001, **73**, 681.

51. Introduction to Physical polymer science, L.H. Sperling, Wiley Inter-science

52. P. Sozzani, M. Galimberti, and G. Balbontin, *Makromol. Chem., Rapid Commun.*,1992, **13**,305.

53. A. L. segre and D. Capitani, TRIP (*Trends in Polym. Sci*.), 1993,**1**, 280.

54. L. Cai, X. Wang, Y. Darici, and J. Zhang, *J. Chem. Phys*., 2007, **126,** 124908.

55. J. Hansen, Y. Liu, R.Yang, and Z.L.Wang*ACS Nano* 2010**, 4** , 3647-3652.

56. S. Cha, S. Kim, H. Kim, J. Ku, J. Sohn, Y. Park, B.Song, M. Jung, E. Lee, B.Choi, J. Park, Z.L. Wang, J. Kim, and K. Kim *Nano Letters* 2011**, 11**, 5142- 5147.

57. G. Ni, Y. Zheng, S. Bae, C. Tan, O. Kahya, J. Wu, B. Hong, K. Yao, and B. Özyilmaz *ACS Nano* 2012, **6**, 3935-3942.

58. J. Lee , K. Lee , M. Gupta , T. Kim , D.Lee , J. Oh , C. Ryu ,W. Yoo , C. Kang, S.Yoon, J. Yoo , and S. Kim *Adv. Mater*. 2014, **26**, 765–769

Chapter 5

High Performance Wearable Organic-Inorganic Hybrid Piezo-nanogenerator Via Interface Enhanced Polarization Effects

In this work, an electrospun fiber based wearable organic-inorganic hybrid piezo-nanogenerator comprising of suitably engineered P(VDF-TrFE) and $BaTiO_3$ based nanostructure is demonstrated. In the case of the device with electrospun mat of piezoelectric β-phase P(VDF-TrFE) and $BaTiO_3$ nano-particulates filled in the inter-fiber open spaces, a power density of $12\mu W/cm^2$ is realized at an applied impact of 0.02 MPa (which essentially corresponds to the finger touch pressure). A similar device, but with $BaTiO_3$ additionally embedded in the P(VDF-TrFE) fibers during their formation, renders a significantly higher power density of $22\mu W/cm^2$ at the same touch pressure. This performance is attributed to the high density of interfaces in such a device and the corresponding enhancement in the dielectric response. It is demonstrated that the power generated from such a hybrid device structure could be used for small scale applications such as charging of a mobile phone.

The content of this chapter has been submitted to Nano Energy,* **2015.

5.1. Introduction

The next generation device systems will be increasingly based on wearable electronics which relies mainly on soft fiber based functional materials because of their several interesting properties such as flexibility, conformability, durability etc. With the rapid progress in the field of nanotechnology, it is now possible to configure the electronic device systems on the surfaces of or inside nanofiber structures of soft materials. This approach has also afforded immense flexibility in nanoscale device design. An important task in wearable electronics is to power such device systems. While thin flexible solar cells, batteries and supercapacitors could be integrated with such systems to deliver and manage the power inputs, a novel approach that is rapidly evolving through the interesting ideas and pioneering contributions of Z. L. Wang and co-workers is the one embodying the concept of nanogenerators and related mechanically self-powering schemes. These concepts primarily use piezoelectric nanostructures to efficiently harvest the mechanical energy for powering low power applications. Other schemes such as tribo-nanogenerators are also shown to be viable for specific application domains. [1] Nanostructures with excellent piezoelectric properties can be easily integrated with polymers for realizing promising applications in various fields such as LEDs, laser diodes, pH, UV, or environmental sensors, speed/weight sensors etc. [2-3] Recently NGs have been shown to be useful to drive electrochemical reactions, [4] electro-degradation of dyes [5] and water splitting for hydrogen generation. [6] Though nanogenerators are conceptually interesting it is highly desirable to increase their output power and efficiency to expand their applications domain. Indeed, such enhanced power along with their flexibility and portability will enable the use of nanogenerators for integrated sensor networks, personal electronics, and implantable biomedical devices etc. Amongst the various self-powered micro/nanosystems, wearable energy harvesting systems provide much better solutions as they can be used for portable and personal electronics, defence as well as bio-medical applications.

Various textile based NG systems have been studied recently using inorganic nanostructures such as ZnO, PZT etc. [7-8]. But the concern with such nanostructures is their brittle character. In order to overcome the same hybrid systems (i.e. combining functional inorganic materials with piezoelectric polymers) have been formulated to have enhanced flexibility along with the desired piezoelectric properties. Wang et al. have demonstrated the use of a hybrid composite PVDF-ZnO to convert biomechanical actions into an electrical output. [9] However, for further effective developments of wearable systems, fiber-based nanostructures are proving to be of great interest due to their light weight nature and quality of comfort afforded. [10] Besides this the high aspect ratio, alignment/orientational/dimensional control and energy conversion efficiency of the synthesized piezoelectric nanostructures strongly affect the performance of the NGs. [11] Recently Tao et al. have shown cloth based flexible nanogenerator using PVDF-$NaNbO_3$ composite *via* electrospinning with power o/p of 2$\mu W/cm^2$. [12] In parallel many groups have worked on lead free perovskite oxide $BaTiO_3$ based polymer nanocomposites using electrospinning due to its interesting properties. [13-17] Herein, we propose and demonstrate a high performance wearable NG using a suitably engineered nanoscale fiber composite of P(VDF-TrFE) and $BaTiO_3$ nanoparticles and fibers. P(VDF-TrFE) is a co-polymer of PVDF which has high mechanical and thermal stability and is well known for its high piezo-ferroelectric properties useful for devices such as non-volatile memory, solar cells, nanogenerators and other flexible electronics applications. [18-20] $BaTiO_3$ is a highly polar material which has high dielectric constant and good piezoelectric properties. Moreover, it can support different types of nanostructure morphologies. [21-23] In our work we have combined both the materials in a novel way on conducting carbon cloth, synthesized in our lab. [24] The P(VDF-TrFE) nanofibers were directly electrospun on such a cloth. It is highly flexible, porous and possesses good electrical conductivity. It has different functional groups (sites) on its surface, which create good surface adhesion with P(VDF-TrFE) nanofibers when directly electrospun on it.

This increases contact area of the device and number of contact points as well. The cloth electrode has additional advantage of substrate flexibility over the rigid planar substrates.

The flexibility and porosity of cloth offers the non-uniform distribution of the applied pressure over the device area. This leads to simultaneous operation of d33 and d31 piezoelectric modes. Two device architectures are examined and compared: a) P(VDF-TrFE) nanofiber mat directly electrospun on carbon cloth followed by BaTiO3 nanoparticle/nanofiber paste incorporated in the inter-fiber spaces; and b) same as a) but with $BaTiO_3$ NP/NFs incorporated also in the P(VDF-TrFE) nanofibers. Our completely sealed device Type (a) consistently produces a peak open-circuit voltage of about 7V and a peak current of 4μA under an applied impact pressure of 0.02Mpa, resulting in a power density of $12\mu Wcm^{-2}$. The device Type (b) with 5 wt% $BaTiO_3$ produces the highest power density of $\approx 22\mu Wcm^{-2}$ under the same experimental conditions.

5.2. Experimental Section and Characterization

Figure 5.1 shows the schematic of steps involved in the device fabrication process. The cloth was heated at 80° in oven for the removal of any water/humidity before using it for the direct electrospinning experiment. For electrospinning, a homogenous and transparent solution of P(VDF-TrFE) (10 wt%) was directly electrospun on the conducting cloth at an applied electrospinning conditions of 10 kV, 10 cm and 0.5 ml/h. For the synthesis of BTO nanofibers by electrospinning barium acetate, tetra-butyl titanate, PVP, ethanol and acetic acid were used as starting materials. [25] For stable sol formation, the ratio of ethanol to acetic acid was optimized. Barium acetate was dissolved in acetic acid by continuously stirring for two hours and TIP was then added into this solution drop-wise under constant stirring.

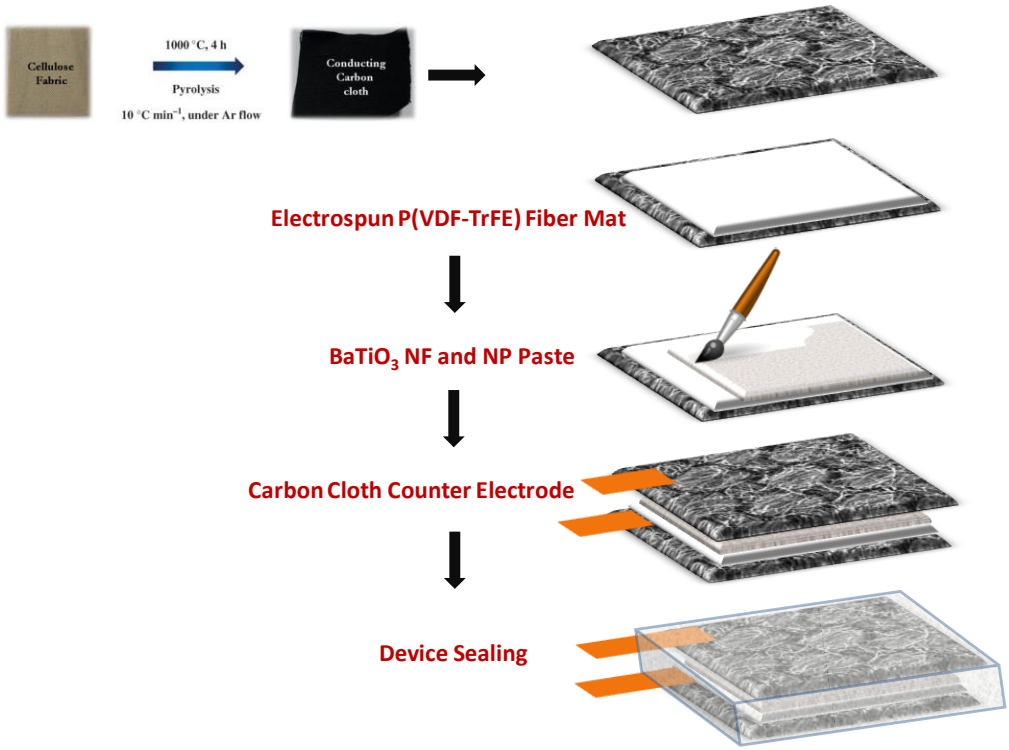

Figure 5.1 Schematic of the device fabrication and sealing

The PVP- ethanol solution was separately prepared and mixed with the above solution to form a viscous and homogeneous solution. This solution was then transferred to the syringe and electrospinning was carried out at an applied voltage of 10kV, distance of 8 cm and with the flow rate of 1 ml/h. The as-synthesized fibers were dried in vacuum oven at 80ºC overnight and then calcined at 750°C for one hour. The BTO NPs were procured from sigma Aldrich. The $BaTiO_3$ paste was prepared by physical mixing of BTO nanofibers and nanoparticles in weight proportion of 100:0, 80:20, 50:50, 20:80, 0:100 respectively for individual cases as shown in Table 5.1. These materials were crushed in the agate mortar for 40 minutes with 0.1 mL Butanol and 0.1 mL Ethanol mixture. The paste was applied on the as-spun P(VDF-TrFE) nanofiber mat. After drying, the counter electrode i.e. the other carbon cloth of the same dimensions was placed onto it.

The devices were further sealed using PDMS for mechanical robustness and dust protection. For the in-situ electrospinning of the composite, P(VDF-TrFE)

/$BaTiO_3$ (NF:NP) the solution was prepared in a mixture of DMF: Acetone solvent with ratio of 60:40. (Volume by volume) Then for the three different cases (1wt%, 5wt% and 10wt %) of the composite with BTO (NF: NP) variations were made. The solution was then sonicated and stirred for 4 hours until it became clear, transparent and homogenous. Further the electrospinning was carried out directly on conducting carbon cloth as electrode (1.5 x 1.5 cm^2) for these composite cases. For the complete fabrication of the device the paste of BTO (NF: NP) was applied and devices were sealed with PDMS after the paste drying. The nanogenerator voltage and current measurements were done using Tektronix Oscilloscope. The as fabricated devices were tested under the pressure equivalent to that of thumb pressure ≈0.02 MPa. For the demonstration of self-powered device (mobile charging unit), the wearable nanogenerator was connected to bridge-rectifier and the piezoelectric output was rectified to the usable DC power. The vibrations were given by using a motor with 40Hz frequency.

5.3. Results and discussion

5.3.1 FE-SEM and TEM images

Figure 5.2 (a-e) shows the morphological features of the P(VDF-TrFE), BTO and the composite nanostructures.Figure 5.2a shows the FE-SEM image of the P(VDF-TrFE) NFs. The image show uniform, smooth and bead-free nanofibers. The diameters of the fibers are in the range of about 500-550 nm.Figure 5.2b shows the FESEM images of as-synthesized BTO NFs. The inset shows the TEM for these nanofibers. The average diameter and length of the electrospun nanofibers are around 150-200 nm and few microns, respectively. The fibers exhibit good surface morphology.

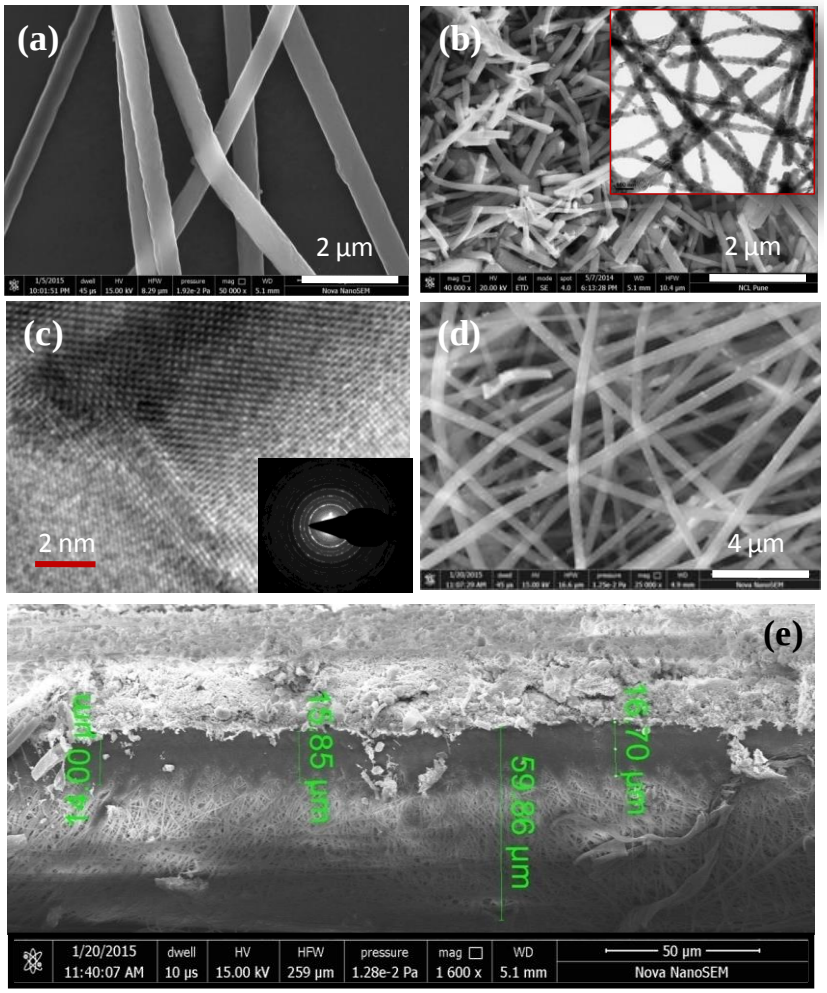

Figure 5.2 FE-SEM images showing the morphological features of a) FESEM of P(VDF-TrFE) NF, b) FE-SEM for BTO NF (inset TEM for BTO NF), c) TEM image for BTO NF, d) FE-SEM electrospun composite P(VDF-TrFE)-BTO NF, e) the cross-section of the fabricated device

The fiber formation majorly depends on the annealing temperature. At higher temperatures, the nanofibers become fragile and have a tendency to form nanoparticles. Hence, optimization of the temperature is an important parameter for both the phase formation as well as morphological features. Figure 5.2c shows the TEM images along with the SAED pattern for the BTO NFs as inset. It shows small uniform grains of approximately 20-25 nm size of BTO connected to form continuous and uniform fiber. The diameter of a typical single nanofiber is around 100 nm. The lattice fringes show the highly crystalline nature of the

nanofibers.Figure 5.2d shows the FESEM image of the composite structure. It shows the uniform distribution BTO (NF:NP) mixture throughout the polymer matrix. This increases the formation of multiple interfaces locally. Figure 5.2e shows the FESEM image of the device after the application of the paste layer on the top. It shows the BTO NF:NP mixture surrounded in the polymer matrix. The cross-sectional image shows the thickness of the device. The overall thickness is around 75µm whereas that of the paste layer (BTO NF:NP) is 15µm. This shows that the BTO nanosystem has percolated through the P(VDF-TrFE) layer and filled up the voids/spaces in between. The BTO NF:NP connected to P(VDF-TrFE) NF at various points increase the number of contact points significantly, thereby increasing the interface density. At a few places the BTO mixture is collected to form agglomerates. The paste is seen to be uniformly spread over the entire area. This increases the interface density as well as fills the gap/separation in between the TrFE NFs by the BTO NF: NP paste. Figure 5.3 shows characterization data for P(VDF-TrFE) NFs and BTO NFs as-synthesized by the electrospinning process. Figure 5.3a shows XRD pattern for the BTO NFs. The presence of the peaks at 2Θ values of 31ºC and 39ºC [(110)/(111) reflections] confirms the formation of tetragonal perovskite phase, which is the polar-ferroelectric phase of $BaTiO_3$. The intensity of the peakshows improved crystallization which mainly depends on the optimization of the sol prepared for the electrospinning process as well as the heating temperature. [26]

5.3.2 XRD, PE loop and dielectric measurement:

Figure 5.3b shows the XRD for P(VDF-TrFE) NFs with characteristic Θ-phase peak at 2Θ value of 20.7°. The inset of the figure shows FTIR data for the P(VDF-TrFE) NFs which also confirms the formation of the βphase. The bands at 845 and 1280 cm^{-1}further confirm the presence of polar β phase which is responsible for all the ferroelectric and piezoelectric properties of this polymer. Electrospinning of P(VDF-TrFE) leads to the formation of polar β phase due to simultaneous stretching and poling during the process. [27]

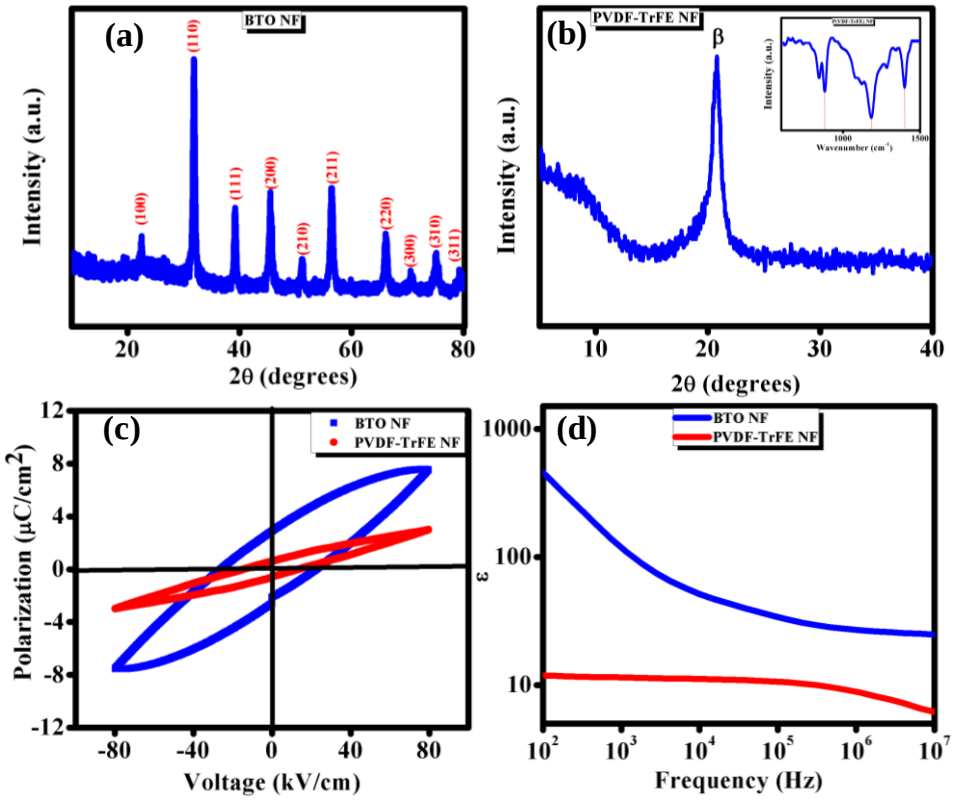

Figure 5.3 a) XRD of BTO NF, b) XRD of P(VDF-TrFE) NF (inset shows FTIR for P(VDF-TrFE)), c) PE loops for BTO NF and P(VDF-TrFE) NF, d) Frequency dependent dielectric constant data for BTO NF and P(VDF-TrFE) NF.

The polar (ferro/piezoelectric) character of P(VDF-TrFE) arises due to electrical dipoles formed between pairs of electropositive hydrogen and electronegative fluorine atoms which are organized in the form of C-H and C-F bonds perpendicular to the polymer backbone in the molecular chain axis of P(VDF-TrFE). [28]

Figure 5.3c and d show the dielectric and piezoelectric properties of the P(VDF-TrFE) and BTO NFs. We made the pellet of BTO NFs for this measurement. Figure 5.3c shows the PE loop at an applied electric field of 80kV/cm. The polarization value for P(VDF-TrFE) NF is 2μC/cm^2. We sandwiched the pellet between two Cu tape as contact electrodes. The value for the polarization is found to be about 6 μC/cm^2 which matches well with the literature. [29] Figure 5.3d

compares the dielectric data for the P(VDF-TrFE) and BTO NFs. The measurement was done using dielectric impedance analyzer in the frequency range of 10^2-10^7. The dielectric constant for BTO NFs is found to be close to 1000 whereas that of P(VDF-TrFE) is 10, which match well with the reported literature. [30] The device measurements were carried under the applied pressure of 0.02MPa (≈ Thumb pressure) on the active area of the device. Figure 5.4a and b show the nanogenerator device data for only P(VDF-TrFE) and BTO NFs cases. Later on, the composition variation was done to test the performance of the hybrid devices.

Nanogenerator	% BTO NF composition	% BTO NP composition
I	100	0
II	80	20
III	50	50
IV	20	80
V	0	100

Table 5.1 shows the devices with composition variation using paste of BTO NFs and NPs for making hybrid devices.

Nanogenerator	Voltage o/p (V)	Current o/p (µA)
I	3-3.5	2-3
II	≈6	3.5-4
III	3-4	1.5-2
IV	4-4.5	2-3
V	3-3.5	2-3

Table 5.2: Voltage and current outputs of the PVDF-TrFE/BTO(NF:NP) paste composition

For all the compositions made, the piezo-voltage generated was in the range of 3-7V as can be seen from Table 5.2 . Particularly, for the device with 80:20 BTO (NF:NP) a highest voltage i.e. 7V and current of 4μA were realized. Figure 5.4 a and b show the nanogenerator data for BTO NF: NP (80:20) composition case. The power o/p with 80:20 ratio produced highest value of 12μW/cm^2 as canbe seen from Figure 5.4e.This is the highest power o/p reported for wearable type of nanogenerators using conducting cloth as electrode. [13,31] (Table 5.3)

Material	Device dimensions	Strain/force/ pressure/ frequency	Current	Peak voltage	Power output
PVDF/NaNbO3 nanofiber nonwoven fabric	**2.5 cm x 2.5 cm**	**1Hz, 0.2MPa,**	**4.4 μA**	**3.4 V**	**2.15 μWcm^{-2}** ***EES , 2013***
3-D structure PVDF monofilament spacer yarn	**15 cm x 5.3 cm**	**0.02 - 0.10 MPa**	**~30 μA**	**~14 V**	**5.07 μWcm^{-2}** ***EES , 2014***
Our data	**1.5 cm x 1.5 cm**	**0.02 MPa**	**~4.5 μA**	**~6 V**	**12 μWcm^{-2}**

Table 5.3: Comparison of our nanogenertaor performance with the literature

5.3.3 Piezoelectric voltage measurement

From the Table 5.1, it is observed that as the concentration of BTO NFs in the paste mixture is increased, the power o/p increases. Particularly, in the case of NGs based on (80:20) composition, almost all the voids of uncovered area is filled with piezoelectric filler. FESEM images also reveal the same fact. Secondly, we have directly electrospun the P(VDF-TrFE) NFs on the conducting carbon cloth. The direct electrospinning increases the number of contact points, due to surface functional groups (active sites) on the cloth. This enhances the adhesion between cloth and nanofibers which in turn contribute in enhancing the o/p of the device.

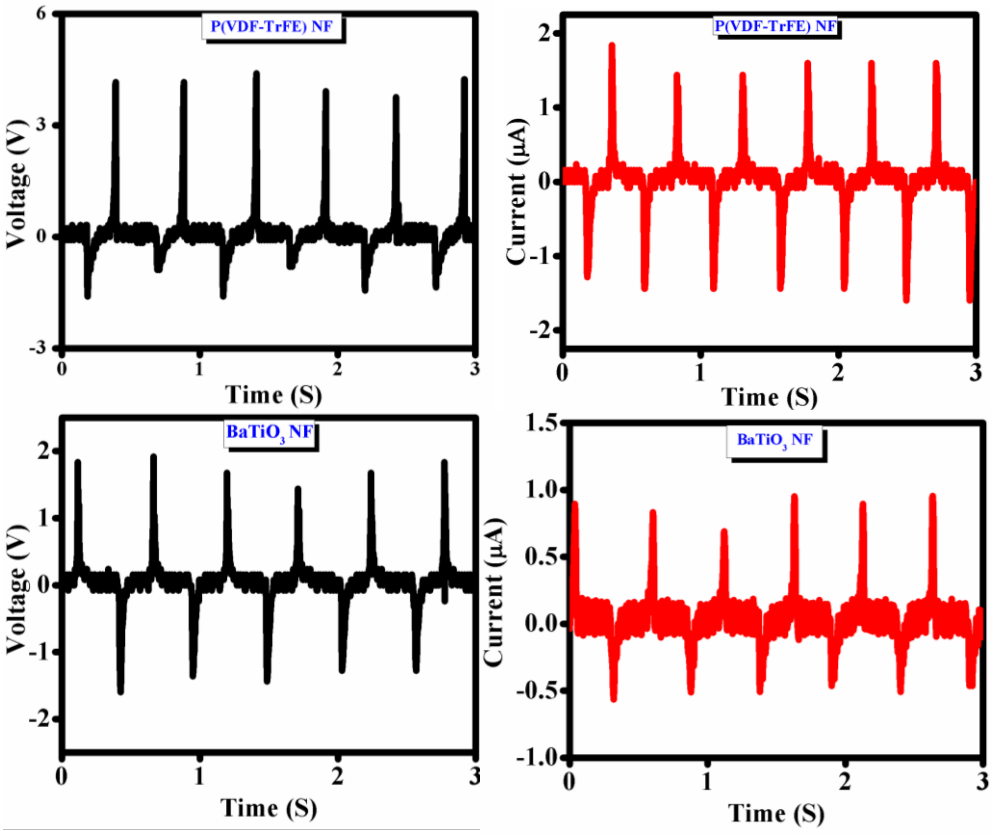

Figure 5.4.Voltage and current output for P(VDF-TrFE) NF and BTO NF

We further used another strategy for obtaining further enhancement in the power output, namely increasing the interface density even more.Towards this end we added the $BaTiO_3$ NF:NP mixture in the P(VDF-TrFE) solution to be electrospun so as to have additional internal interfaces in the system. We made three composites such as 1, 5, and 10 wt% of BTO (NF:NP) composition into the P(VDF-TrFE) solution during electrospinning. The BTO (NF: NP) were properly sonicated before adding into P(VDF-TrFE) solution so as to avoid any agglomeration.Using in-situ composite making process not only enhances the interface density but the aspect ratio and effective shape function of the nano inclusions/fillers affecting strongly and positively the dielectric and ferroelectric properties of the nanocomposites. [32-33] The voltage o/p for all the cases is higher compared to devices without the in-situ composite cases. Figure 5.5 shows that the highest power o/p is realized for the 5 wt% case, the value being 22μW/cm^2.

5.3.4 Piezoelectric voltage measurement for device

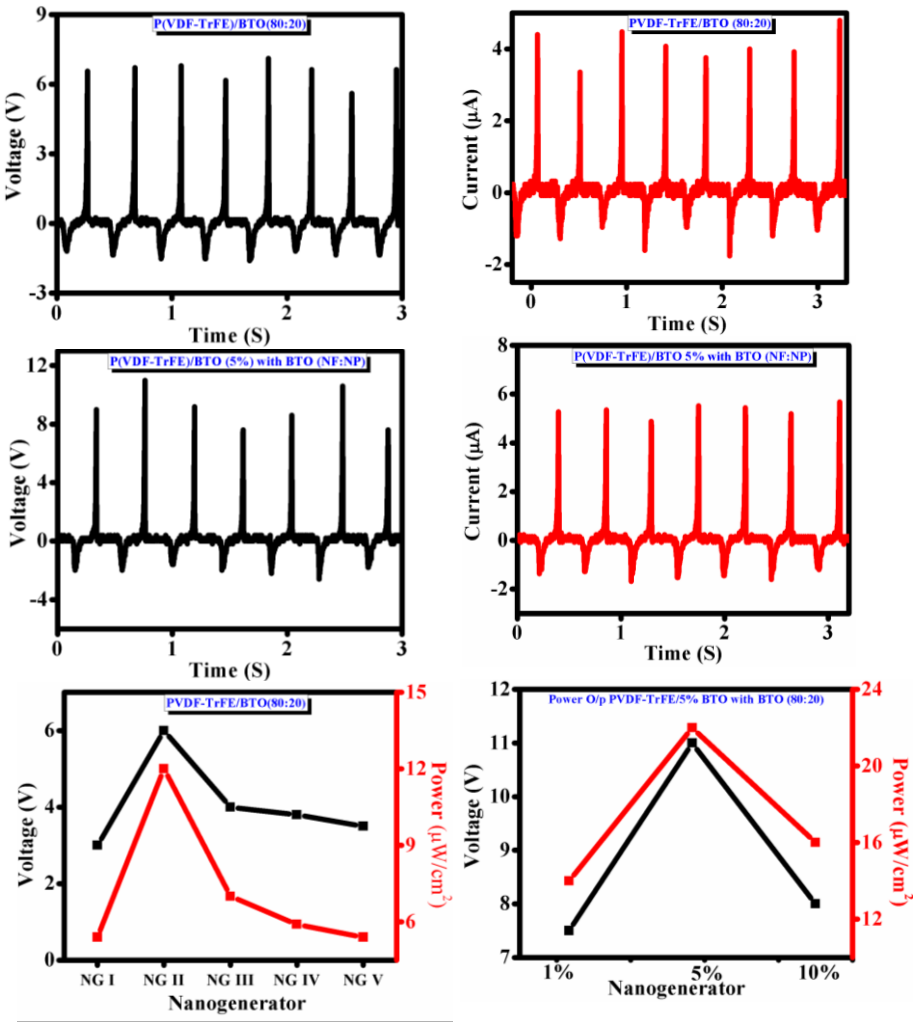

Figure 5.5: Voltage and current output for P(VDF-TrFE)/BTO(80:20) and P(VDF-TrFE)/embedded BTO (5%) with BTO(80:20), and power o/p for different cases of composites.

5.4 Mechanism

Figure 5.4.1 shows the schematic for the suggested origin of high performance of our devices. Interface engineering has been used as general strategy particularly for heterogeneous systems. Here we have used this strategy to modulate the interfaces created between two piezo-ferroelectric materials to enhance the interfacial polarization contribution.

The dielectric properties at the interface mainly depend on 1) ionic and electronic polarization at the interface, which is limited only upto few atomic layers of the interface, and 2) field induced polarization/interfacial polarization which is present at the interfacial regions as classic double layer diffusion process. Tremendous efforts have been made on inducing higher interfacial polarization in polymer nanocomposites by varying the fraction of nano-inclusions. [34-35] Interface has been modified further by surface treatments of the filler used. [36-37] The use of nanofillers with varying aspect ratios has also been explored for the similar effects. [38]

5.4.1 Mechanism

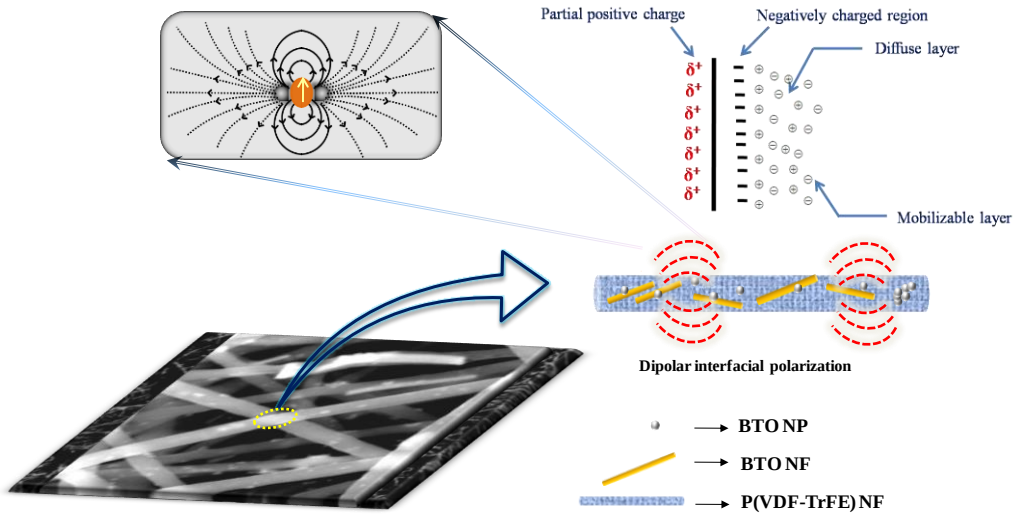

Figure 5.6: Schematic depicting the mechanism for enhanced interfacial polarization effects

In our case, we have synthesized the P(VDF-TrFE) nanofibers using electrospinning. The electrospinning induces higher crystallization as well as polarization in the P(VDF-TrFE).Consider the region near the interface in Figure 5.6.The interface polarization mainly occurs due to space-charge region formed at the interface. [39] A discontinuity at the interfaces of twodissimilar materials leads to the accumulation of electrostatic charges at the interface and formation of a space-charge layer. This leads to a dipolar region or interface polarization. Due to

space charge (polarization) the dipolar region is formed near the interface. At higher concentrations of the filler the interfacial regionscould start overlapping, creating strong local electric fields. This boosts the polarization even further. [40-41] The FESEM image (Figure 5.2d) shows that the in-situ electrospinning process of P(VDF-TrFE)/BTO(NF:NP) forms multiple interfaces within the nanofiber networks. There are three possible interfaces P(VDF-TrFE)/BTO NF, P(VDF-TrFE)/BTO NP and BTO (NF:NF and NF:NP). Multiplicity and high density of such external and internal interfaces are the sites of enhanced polarization effects. In the case of electrospun composites with $BaTiO_3$ NP and NF inclusions within the fibers, the electrical characterization of the devices shows that although devices with 10wt% composite show highest dielectric permittivity, interestingly the device with that of 5 wt% composite case shows highest piezoelectric performance and power output. As the volume fraction of $BaTiO_3$ (NF:NP) increases, the networks of the interfacial regions provide percolation paths for the charges and start overlapping. During this, charges already present in the interfacial regions migrate along the external electric field and accumulate at the end of the nanofibers to build a very high depolarization electric field, resulting in a significant amount of stress. This increases the dielectric loss of the overall system. For the NG case the, stress concentration can lead to breakage points nearby the stress centers which can lead to decreased device performance. In order to understand the particular effect of piezo(ferro)electric polymer and piezo(ferro)electric filler hybrid system, we did two additional experiments. Firstly we fabricated the device with the non-piezo(ferro)electric polymer i.e. PAN and piezi(ferro)electric filler ($BaTiO_3$) with the same experimental conditions. Figure 5.7 shows the data for the device. The device shows the voltage of 1.5-2V and current of 0.8μA under identical conditions of applied thumb pressure. This supports the fact that, although the interfacial polarization and the flexibility of the polymer matrix are the key factors, the stronger polarization of highly piezo(ferro)electric polymer is also an important aspect for the enhanced piezoelectric performance of the device. The flexibility of the PAN gives better support for the device, but the piezo-response from the composite is weak due to

the non- piezo/ferroelectric character of the PAN matrix. Secondly, we replaced the piezo(ferro)electric filler with the non-piezo(ferro)electric filler i.e. TiO_2 keeping the polymer to be ferro/piezo-electric P(VDF-TrFE). The piezoelectric performance of the device improved as compared to the PAN-$BaTiO_3$ case as can be seen in Figure 5.8 due to polarization of P(VDF-TrFE). But it is still low as compared to our piezo-hybrid composite case.

5.4.2 Piezoelectric voltage and current for non-piezoelectric polymer with ferroelectric filler

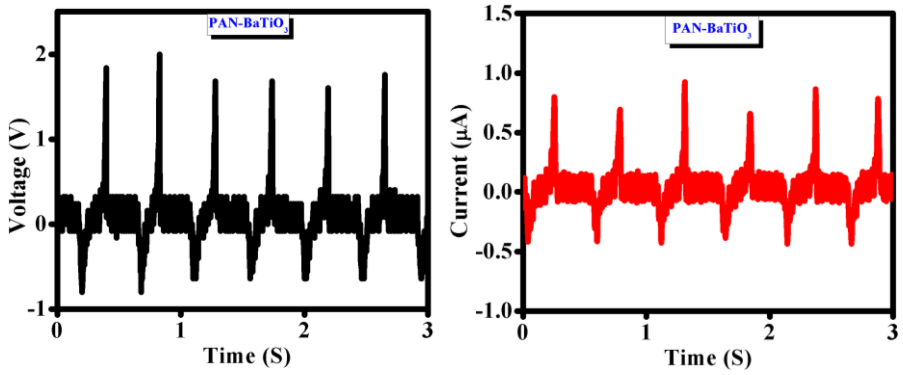

Figure 5.7.Voltage and current output data for PAN-$BaTiO_3$ based NG

5.4.3 Piezoelectric voltage and current for non-piezoelectric polymer with ferroelectric filler

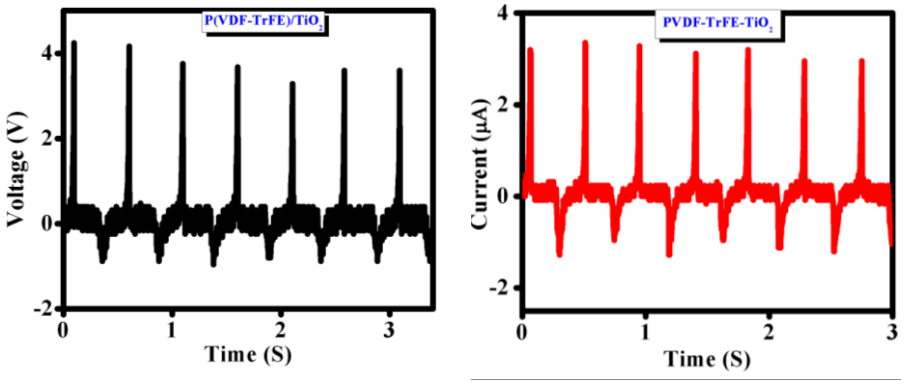

Figure 5.8.Voltage and current output data for PVDF-TrFE-TiO_2 based NG

It is important to highlight on some other interesting points pertaining to the enhanced piezoresponse of our device. The direct electrospinning on the cloth provide additional benefits of enhanced charge collection due to increased number of contact points and surface area as well. For comparison we replaced the carbon cloth with metal foil electrodes i.e. Cu and metal coated thin films i.e. ITO coated PET. The results show that the substrate rigidity lowers the response of the device. Moreover, the conducting carbon cloth has an interesting turbostratic microstructure

5.4.4 FESEM image for cloth

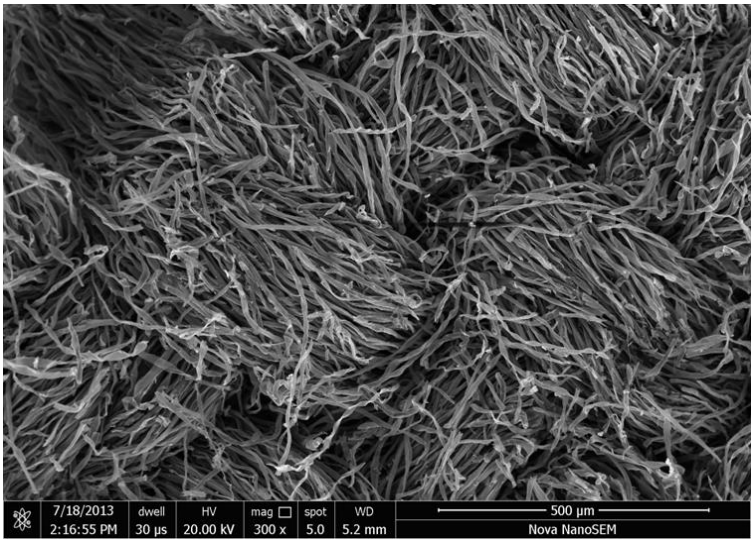

Figure 5.9: FESEM image for cloth

and functional groups that are distinctly different from other ordered forms of carbon, such as graphite, graphene, and carbon nanotubes. It has stronger surface adhesion with the as-electrospun nanofibers. This directly has a positive effect on output voltage of the nanogenerator. Interestingly the flexibility and porosity of the cloth also have an important role on the device performance. The FESEM images Figure 5.9 of the cloth show the circular loop like structures. It has been reported recently, by Weng et al. that, such flexible structures behave differently under applied pressure. [13] As the electrodes are flexible and porous in nature, the pressure applied is non-uniformly distributed onto theactive area of the device.

Now, in our case, the piezoelectric voltage measured is across the thickness of the device. Therefore, many other deformation modes such as compression, twisting, stretching etc.can simultaneously operate. This leads to simultaneous activation of both piezoelectric modes namely, d33 and d31. Additionally, flexoelectric effects and strain gradients withinthe non-uniformly deformed regionsof the electrospun fiber mat as modulated by the conducting cloth morphology can play an interesting role. [42] The results show that it is the synergistic effect of piezoelectric polarization, flexibility, porous nature of the cloth, and enhanced interfacial polarization density, which contribute to the high output power of our device.

Figure 5.10: Images showing the ability of the device to charge a mobile: The image on the left shows the powering of the device with a vibrator (the voltage is also reflected); and the image on the right shows that mobile charging could be initiated.

As a demonstration, the as fabricated device (1.5 x 1.5 cm^2) was exposed the vibrations of 40 Hz frequency, using a commercial vibration motor. (Figure 5.10). When the motor was turned on, the device was vibrated. The AC voltage thus generated was rectified by bridge rectifier and stored in capacitors. The output voltage reached upto 5.4 V with 47µF capacitor. The power generated was used to start the process of charging of a smart phone. This demonstrated the promising application/ potential of our device as a supportive energy source for powering personal electronics using ambient mechanical energy sources.

5.5. Conclusion

In summary, we have fabricated an efficient hybrid wearable nanogenerator by direct electrospinning of piezoelectric P(VDF-TrFE) nanofibers withnanoscale $BaTiO_3$ inclusions onto a conducting carbon cloth, and subsequently filling the interfiber spaces with $BatiO_3$nanoparticulates. This architecture is specifically designed to enhance the interface density per unit volume significantly and thereby harnessing the high polarization at the interface for increasing the power output of the nanogenerator. This increase is further aided by the specific morphology of the supporting conducting cloth which enables multiple directional tensor strain fields to be effective. Amaximum power output of $22\mu W/cm^2$is thus realized. It is shown that our device can succesfully charge a smart phone suggesting its viability as a vibrational energy harvester for mechanical energy.

5.6 References

1. Z. Wang ACS Nano 7 (2013), 9533-9557
2. Z.Wang. Springer, New York 2012
3. W.Wu, C.Pan, Y.Zhang, X.Wen, Z.L.Wang, NanoToday 8 (2013), 619–642.
4. X.Xue, S.Wang, W. Guo, Y. Zhang, and Z. L. Wang Nano Letters 12 (2012), 5048- 5054.
5. Y. Yang, H. Zhang, S. Lee, D. Kim, W. Hwang, and Z. L. Wang Nano Letters 13 (2013), 803-808.
6. M. B. Starr, J. Shi and Dr. X. Wang, Angew. Chem. Int. Ed., 51 (2012), 5962-5966.
7. H. Kim, S. Kim, H. Son, H. Kim, B. Park, J. Ku, J. Sohn, K. Im, J. Jang, J. Park, O. Kim, S. Chax and Y. Park Energy Environ. Sci., 5 (2012), 8932–8936.
8. W. Wu, S. Bai, M. Yuan, Y. Qin, Z. L. Wang, and T. Jing ACS Nano 6 (2012), 6231-6235.
9. M. Lee ,C. Chen , S. Wang , S. Cha , Y. Park , J. Kim , L. Chou , and Z. L.Wang, Adv. Mater.24(2012),1759–1764.
10. Fiber-Based Wearable Electronics: A Review of Materials, Fabrication, Devices, and Applications, Adv. Mater. 2014.
11. Joe Briscoe, Steve Dunn, Piezoelectric Nano Energy, ISSN 2211-2855, http://dx.doi.org/10.1016/j.nanoen.2014.11.059.
12. W. Zeng, X. Tao, S. Chen, S. Shang, L. Chanwong and S. Choy, Energy Environ. Sci., 6 (2013), 2631-2638.
13. S. Shin, Y. Kim, M. Lee, J. Jung, and J. Nah ACS Nano, 8 (2014), 2766-2773.
14. Y. Zhao, Q. Liao, G. Zhang, Z. Zhang, Q. Liang, X. Liao, Y. Zhang, Nano Energy, 11, (2015), 719-727.
15. M. Zhang, T. Gao, J. Wang, J. Liao, Y. Qiu, Q. Yang, H. Xue, Z. Shi, Y. Zhao, Z. Xiong, L. Chen, Nano Energy, 13, (2015), 298-305.

16. S. Siddiqui, D. Kim, L. Duy, M. Nguyen, S. Muhammad, W. Yoon, N. Lee, Nano Energy, 15, (2015), 177-185.
17. K. Kim, J. Chun, S. Chae, C. Ahn, I. Kim, S.Kim, Z. L. Wang, J. Baik, Nano Energy ISSN 2211-2855, http://dx.doi.org/10.1016/j.nanoen.2015.01.004.
18. R. Naber, B. Boer, and P.W.M. Blom, and D. Leeuw, Applied Physics Letters, 87 (2005), 203509- 203509-3.
19. Y. Yongbo T. Reece, P. Sharma, S. Poddar, S. Ducharme, A. Gruverman, Y. Yang & J. Huang, Nature Materials 10 (2011), 296–302.
20. L. Persano, C. Dagdeviren, Y. Su, Y. Zhang, S. Girardo, D. Pisignano, Y. Huang & J. Rogers Nature Communications 4,Article number:1633
21. G. Francis (1973). "Barium Titanate, BaTiO3". Inorganic Syntheses 14: 142–143.
22. M.Lines, A.Glass, Principles and applications of ferroelectrics and related materials, OUP Oxford, 1977
23. N. Setter, D. Damjanovic, L. Eng, G. Fox, S. Gevorgian, S. Hong, A. Kingon, H. Kohlstedt, N. Y. Park, G. B. Stephenson, I. Stolitchnov, A. K. Taganstev, D. V. Taylor, T. Yamada, and S. Streiffer Journal of Applied Physics 100, (2006), 051606
24. M Biswal, A Deshpande, S Kelkar, S Ogale ChemSusChem 7 (2014), 883-889
25. J. Yuh, J. Nino, W. Sigmund Materials Letters 59, (2005), 3645–3647
26. H. Li, H.Wu, D. Lin, and W. Pan J. Am. Ceram. Soc., 92 (2009) 2162–2164
27. D. Dhakras, Y. Gawli, S. Chhatre, P. Wadgaonkar, S. Ogale Phys Chem Chem Phys. 16 (2014), 22874-81.
28. A.Lovinger, Science, 220 (1983), 1115-1121.
29. Y. Song, Y. Shen, H. Liu, Y. Lin, M. Li and C. Nan J. Mater. Chem., 22 (2012), 8063-8068.
30. Y. Wei, Y. Song, X. Deng, B. Han, X. Zhang, Y.Shen, Y. Lin J. Mater. Sci. Technol., 2014, 30 (2014), 743-747.

31. N. Soin, T. Shah, S. Anand, J. Geng, W. Pornwannachai, P. Mandal, D. Reid, S. Sharma, R. Hadimani, D. Bayramol and E. Siores Energy Environ.Sci. 2014,7, 1670-1679.
32. X. Zhang, W. Chen, J. Wang, Y. Shen, Y. Lin, and C. Nan Nanoscale, 6 (2014) , 6701
33. X. Zhang , Y. Shen ,Q. Zhang , L. Gu , Y. Hu , J. Du , Y. Lin , and C. Nan Adv. Mater. 27 (2015), 819–824.
34. Q. Wang, L. Zhu, Journal of Polymer Science B: Polymer Physica 49 (2011), 1421–1429.
35. M. Roy, J. Nelson, R. MacCrone, L. Schadler, C. Reed, R. Keefe, 12(2005) ,629-643.
36. P. Kim, N. Doss, J. Tillotson, P. Hotchkiss, M. Pan, S. Marder, J. Li, J. Calame, and J. Perry ACS Nano 3 (2009), 2581-2592.
37. J. Li, J. Claude, L. Enrique, N. Franco, S. Seok, and Q. Wang Chemistry of Materials 20 (2008), 6304-6306.
38. H. Tang, Y. Lin and H. Sodano , Advanced Energy Materials, 3 (2013) 451–456.
39. L. Gao, J. He, J. Hu, and Y. Li J. Phys. Chem. C, 118, (2014), 831−838.
40. Lewis, T. J.J. Phys. D: Appl. Phys. 38 (2005), 202−212.
41. T. Tanaka, M. Kozako, N. Fuse, Y. Ohki, IEEE Trans.Dielectr. Electr. Insul. 12 (2005), 669−681.
42. C. Chang, V.Tran, J. Wang, Y. Fuh, and L. Lin Nano Letters 10 (2010), 726-731.

Chapter 6

Summary and Future work

In this chapter we present the concluding remarks on the work presented in this thesis and suggest a few new approaches for future work in this interesting field of research.

6.1 Summary

With the limitations on the availability of the fossil fuels and their negative consequences for the environment alternative options such as solar energy, wind energy, tidal energy etc. are currently being focused upon in order to generate mega-giga watts of energy. However there are many functions in modern life which depend on the extensive use of low power electronic, optoelectronic and sensing devices which thrive upon much smaller but distributed and transportable power needs. Such systems require energy harvesting and energy storage alternatives which are low cost, highly efficient and robust. Many such devices are needed for personal and portable electronics, medical care, infrastructure monitoring, environmental protection, defense, as well as security for the technological advancements and betterment of human life. As an example of the vast canvass of such growing device and related small power requirement, the need for the sensor networks itself is increasing and is expected to reach trillion dollars by the year 2020. The power requirements for most of such kinds of sensor systems are in the range of nano to micro watts. Same is the case with novel micro-fluidic devices. The conventional transportable power supply units are the batteries. However these are bulkier and environmentally toxic. Moreover, they have a limited life span and have issues about recycling. Thus, alternative options have to be developed for sustainable and self powered small power systems. Since much of India resides in the village sector with several sensing needs for agriculture it is highly desirable that such small power is harnessed locally.

With the development of the concept of nanogenerator, it is amply demonstrated that reasonable amount of energy can be easily harvested from mechanical sources such as vibrations, wind or solar energy derived mechanical motions or human/animal movements and sufficient power can be generated to power small device systems. Several research groups have contributed to this rapidly developing research area for furthering and improving the self powered nanosystems. The present thesis is a modest attempt towards the development of

some interesting ideas in this respect based on polymer and polymer composites. Our focus has been on developing flexible piezoelectric energy harvesting devices using the electrospinning process.

Piezoelectric polymers have a unique advantage of flexibility over the inorganic and ceramic based systems which can perform similar functions. Besides that, polymeric systems lend themselves to easy synthesis protocols, and large area processability; and can tolerate and sustain fairly high mechanical strains without rupture. The piezoelectric polymers, namely (PVDF and PVDF-TrFE), used in this thesis possess high piezoelectric coefficients which is the prime requirement for the enhanced performance of the piezoelectric energy harvesting systems. The electrospinning process also has several merits over other synthesis methods. Firstly, it forms nanofibers with high surface to volume ratio. Secondly, during the process itself the simultaneous stretching and poling of the polymer chains takes place, which is an essential criterion for dipole orientation in the case of piezo and ferroelectric polymers. Moreover, organic-inorganic hybrid nanostructures can also be obtained using this process. This hybrid approach leads to high interfacial polarization in the nanostructures which can dramatically enhance the power output.

Summary of each topic

1. In our first research work, we demonstrated highly sensitive dynamic strain sensor development using electrospun PVDF nanofibers with the addition of small amount of hydrated salt, $NiCl_2.6H_2O$. The electrospinning process itself favours the formation of the polar β phase which is responsible for the piezo and ferroelectric properties of the PVDF. Furthermore, the addition of salt not only improves the solution properties but also enhances the β phase content by 30%. The piezoelectric voltage generated is about 0.8V. The voltage generated per unit micro-strain developed during the free vibration test for PVDF is 0.119 mV whereas for PVDF with the hydrated salt it is significantly enhanced to 0.548 mV.

2. In the second piece of work, we examined the interesting interface configuration between two functional polymers namely, P(VDF-TrFE) and PANI Polyaniline. The interface effects are used to demonstrate the novel concept of Piezo-FET. It is shown that under the applied mechanical strain, the piezoelectric layer, i.e. electrospun P(VDF-TrFE) generates an electric field which acts as the gate for controlling the current in the PANI layer located underneath. The piezoelectric voltage/ potential difference measured separately is around $1.5 \approx 2$ V. This demonstrates the possibility of using the device effectively as a self powered interface system. The interesting morphology of the P(VDF-TrFE) nanofibers produces non-uniform strain contours on the PANI film which locally affect the strain distribution as compared to the case of a uniform spin coated film. Moreover, the conformational changes in the P(VDF-TrFE) lead to carrier localization-delocalization effect by modulating the conductivity of PANI under the applied strain.

3. In the third research problem, we engineered the interface density in an organic-inorganic hybrid material to enhance nanogenerator power generating functionality for wearable applications. The piezoelectric nanostructures used are namely, P(VDF-TrFE) and $BaTiO_3$. The P(VDF-TrFE) nanofibers are produced using electrospinning, directly on a conducting carbon cloth that is synthesized via simple pyrolysis technique. The $BaTiO_3$ nanofibers are synthesized separately using electrospinning. These nanofibers are then crushed and their thick slurry/paste is made using solvent mixture of 1 butanol and ethanol. The paste is further applied onto the P(VDF-TrFE) nanofiber layer to fill the intermittent porosity within the electrospun fibrous mat. The piezoelectric response of this composite layer is measured rendering a voltage of almost 4 V. Interestingly we further modified the strategy by introducing $BaTiO_3$ nanofibers during the electrospinning process to enhance the interface density which enhanced the power output to 22 $\mu W/cm^2$. The direct electrospinning on the conducting carbon cloth provides an additional advantage of enhanced charge collection due to increased number of contact points and surface area as well. The non-uniform distribution of strain with more flexoelectric effect leads to concurrent occurrence

of parallel and perpendicular piezoelectric modes, namely d33 and d31, as the device undergoes extension, twisting, stretching etc. simultaneously. The power generated from the hybrid device structure is further used for charging of a mobile phone by providing a promising solution for the development of such self-powered electronic devices.

The rapid development in the field of piezoelectric energy harvesting systems reveals a bright future for the vibrational energy harvesting technologies. However, in order to commercialize the nanogenerator technologies, several issues still need to be overcome. In the following paragraphs, we propose a few interesting new approaches for enhancing the power output and energy conversion efficiency of such systems and related application areas.

6.2 Future work

Numerous electronic device systems have been demonstrated in the past few years, particularly for small scale applications. Based on this background, we suggest below a few approaches for possible large scale energy scavenging applications.

1. **Multilayered large scale designs**: The power output of piezoelectric nanogenerators is the major hurdle towards the potential commercialization of this technology. We would therefore like to propose a multilayer large scale design for the NGs using polymer based flexible systems. Some attempts have been made in the past for the layer by layer device design to enhance the piezoelectric power output of the device. Such large area flexible and transparent systems can be used as curtains or flags to harvest wind energy. Similar kind of systems can also be made by making hybrids with CNTs or graphene. Such load bearing structures can be used on the footpaths or at jogging parks to harvest mechanical power.

2. **Bio-compatible stretchable membranes:** As stated earlier the piezoelectric energy harvesting technology enables self powered operation of the sensor

networks, personal gadgets, and healthcare devices by capturing the energy from the mechanical work schedule. We propose to design bio-compatible stretchable membranes using piezoelectric nanostructures of ceramic (such as BSTO i.e. barium strontium titanate) nanofibers produced via electrospinning. These are lead-free ceramics. They are non-toxic and bio-compatible in nature. Additionally, they possess higher piezoelectric coefficients than undoped $BaTiO_3$. Moreover, hybrid systems can be made using these ceramic fibers with addition of PDMS (stretchable matrix) and CNT/Graphene (mechanically strengthening materials). These stretchable matrices can be used as bio-compatible stretchable patches for BP, Sugar, heart beat etc. monitoring.

3. **Nanomaterials growth for Triboelectric nanogenerator (TENG):** Electrospinning produces various interesting nanostructures for variety of applications. With the development of (TENG), the power generation range has been pushed to the level of Kilowatts in the last 3-4 years. This nanogenerator works on the principle of contact electrification and electrostatic interaction. The material selection for this kind of a nanogenerator is usually done on the basis of electronegative series. In addition, the protruding/pointed structures have shown significant effectiveness in producing higher power than the uniform flat surfaces. We propose to produce protruding structures by electrospinning and then further growing needle like pointed structures (caterpillar like) on these to produce 3D hybrid networks so as to enhance the power output of the device.

4. **Nanostructured ceramics by electrospinning for piezo magnetic applications:** Another interesting aspect for potential creative extension of the nanogenerator study is the exploration of the possible coupling of piezoelectric and magnetic properties of the materials. The piezoelectric nanogenerators (PENG) have been used as active sensors in the recent literatures. We propose to use the NGs for the detection of weak magnetic field as well as to implement them in magneto-electric actuators.

We conclude that there are various new directions possible for the scientifically stimulating and technologically useful expansion of research on self powered nanosystem using newer materials, nanoscale architectures, and novel device concepts. We hope that this research could eventually overcome the daunting requirements of global need for widespread but small distributed form of energy for our modern world driven by electrical device systems.

List of Publications

1] RS Devan, **Dipti Dhakras,** TG Vichare, AS Joshi, SR Jigajeni, and YR Ma, *Li0.5Co0.75Fe2O4 + BaTiO3 particulate composites with coupled magnetic-electric properties* ***Journal of Physics D: Applied Physics.,*** **2008**, 41 (10), 105010.

2] **Dipti Dhakras**, Vivek Borkar, Satishchandra Ogale, Jyoti Jog, *Enhanced piezoresponse of electrospun PVDF mats with a touch of nickel chloride hexahydrate salt* ***Nanoscale.,*** **2012**, 4 (3), 752-756

3] **Dipti Dhakras ,** Yogesh Gawli, Sharddha Chhatre, Prakash Wadgaonkar, Satishchandra Ogale, *High performance all- organic flexural piezo-FET and nanogenerator via nanoscale soft-interface strain modulation* ***Physical Chemistry Chemical Physics.,*** **2014** 16 (41), 22874-22881.

4] **Dipti Dhakras,*** Satishchandra Ogale, *High performance wearable organic-inorganic hybrid piezo-nanogenerator via interface enhanced polarization effects,* ***Submitted to Nano Energy,*** **2015.**

5] Yogesh Gawli, Abhik Banerjee, **Dipti Dhakras**, Meenal Deo, Prakash Wadgaonkar and Satishchandra Ogale. *Highly conducting 3D Polyaniline architecture by concurrent inorganic and organic acid doping for superior and robust high rate supercapacitor performance* ***Submitted to JMC A, 2015.***

Patent Submitted

An organic flexural piezo-ferro-FET: 48-NF-2014: 2014-INV-0011 (complete specification)

Poster Award

Dipti Dhakras , Yogesh Gawli, Sharddha Chhatre, Prakash Wadgaonkar, Satishchandra Ogale, , *An all-organic flexural piezo-ferro-FET based on PANI and electrospun P(VDF-TrFE)*

Best Poster Award, National Science Day 2013, National Chemical Laboratory, CSIR, Pune.